NASA SP-8069

NASA SPACE VEHICLE DESIGN CRITERIA (ENVIRONMENT)

THE PLANET JUPITER (1970)

CASE FILE COPY

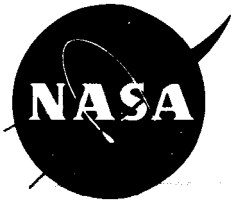

DECEMBER 1971

NATIONAL AERONAUTICS AND SPACE ADMINISTRATION

FOREWORD

NASA experience has indicated a need for uniform criteria for the design of space vehicles. Accordingly, criteria are being developed in the following areas of technology:

Environment
Structures
Guidance and Control
Chemical Propulsion

Individual components of this work are issued as separate monographs as soon as they are completed. A list of the monographs published in this series can be found on the last page.

These monographs are to be regarded as guides to design and not as NASA requirements, except as may be specified in formal project specifications. It is expected, however, that the monographs will be used to develop requirements for specific projects and be cited as the applicable documents in mission studies, or in contracts for the design and development of space vehicle systems.

This monograph was prepared under the cognizance of the Goddard Space Flight Center with Scott A. Mills and Mason T. Charak as program coordinators. The principal author was Neil Divine of the Jet Propulsion Laboratory. Valuable contributions were also made by A.J. Beck, C.A. Haudenschild, F.D. Palluconi, and R.A. Schiffer of the Jet Propulsion Laboratory. J.W. Warwick of the University of Colorado served as a consultant in the preparation of the fields and particles sections.

Comments concerning the technical content of these monographs will be welcomed by the National Aeronautics and Space Administration, Goddard Space Flight Center, Systems Reliability Directorate, Greenbelt, Maryland 20771.

December 1971

CONTENTS

THE PLANET JUPITER (1970)

1. INTRODUCTION

Both qualitative and quantitative descriptions of Jupiter are needed to properly design spacecraft for the investigation of that planet and its environment. Although different data are needed for atmospheric probes, orbiters, and flyby missions, the paucity of present data permits inclusion of pertinent information for all three types of missions in one monograph.

This monograph is based primarily on data obtained through 1970 but includes some material published during the first half of 1971 and conclusions of the Jupiter Radiation Belt Workshop held at the Jet Propulsion Laboratory in July 1971. All the information of Jupiter has been derived from data obtained at the angular and spectral resolutions possible with Earth-based instrumentation or with sensors on aircraft, rockets, and balloons. The observations were made primarily in the visible, near visible, infrared, and radio portions of the electromagnetic spectrum. The information was assessed for the potential effects of Jupiter's environmental properties on spacecraft performance. The assessment was done independently for the three types of missions under consideration and formulated for overall spacecraft as well as for subsystem design. Many of the environments presented, including physical properties, gravity field, charged particles, and atmospheric structure, are also important for mission planning.

For flyby spacecraft, the effects of electric and magnetic fields and charged particles on electronic components are important as well as the effects of electromagnetic radiation on light, heat, and radio-wave sensitive subsystems and the hazards of meteoroids on structural integrity and exposed surfaces. An orbiter spacecraft suggests similar environment-design interaction plus the effects of prolonged or repeated exposure on survival capabilities. In the case of atmospheric-entry probes, the effects of static, transport, and dynamic properties of Jupiter's atmosphere on pressure and temperature-sensitive electronic and structural components are important for design consideration. In table I the relative design importance of various aspects of Jupiter's environment on the subsystems of an entry probe are given.

References 1, 2 and 3 describe the electromagnetic, magnetic field, and meteoroid environments which are applicable to the design of spacecraft which will travel to and encounter the environment of Jupiter. Pertinent symbol definitions, mathematical formulations, and glossary are contained in appendices A through E.

2. STATE OF THE ART

2.1 Physical Properties

The physical properties considered here are the planetary mass, radius, shape, mean density, and rotational quantities. Related discussions of the orbital elements are given in Melbourne et al. (ref. 4). Photometric properties are discussed in section 2.5 of this monograph.

TABLE I

IMPACTS OF JUPITER'S ENVIRONMENTS ON
THE DESIGN OF ATMOSPHERIC PROBE SUBSYSTEMS*

ENVIRONMENTAL PARAMETERS	SUBSYSTEMS												
	Structure	Propulsion Subsystems (Acceleration & Deceleration)	Guidance Subsystems	Attitude Control Subsystems	Heat Shield Subsystems	Other Thermal Control Subsystems	Power Supply Subsystems	Scientific Experiments	Radio-Frequency Subsystems	Command, Telemetry & Data Handling Electronics	Other Electronic Devices	Optical Devices	Mechanical Devices
Physical Properties			S	S		W	S		W	S		S	
Gravity Field	W	W	W	S	S	W	W				W		S
Magnetic Field and Magnetosphere		W		W				W	S	W	W		
Electric Fields		W		W					W	W	W		
Electromagnetic Radiation		W	S	S		S	S	W	S	W	W	S	
Satellites & Meteoroids	S	S	S	W	S	W	S	S	W	W		W	S
Charged Particles		W	W	W		W	S	S	S	S	S	W	W
Magnetosphere Transfer Properties		W		W		W	S		S	W	W		W
Atmospheric Structure	S	S	S	S	S	S	W	S	W	W		W	S
Cloud Properties			S	S	W	W		S	W	W		W	W
Atmospheric Motions	S	S	W	S	S	S		S	W			W	S
Atmospheric Transfer Properties	W	S	S	W	S	S	W	W	S	W	W	S	S
Interior	S	W	W	W		W		S	W			W	S

*S means strong, probable, or direct design impact.
W means weak, possible, or indirect design impact.

2.1.1 Mass

The mass M_{JS} of the Jupiter system, i.e., planet plus satellites, may be most accurately determined from observations of the angular positions on the sky of certain minor planets and of the outer satellites of Jupiter. In both cases, the Sun and Jupiter furnish the major gravitational forces acting on the smaller bodies. The quantity which is directly derived from the analysis of the varying orbital elements is the "reciprocal mass" $M_\odot/M_{JS}$, the ratio of the mass of the Sun to that of the Jupiter system. Although JPL uses the value $M_\odot/M_{JS} = 1047.3908 \pm 0.0074$ (ref. 4), the associated uncertainty estimate is not broad enough to include other recent values cited by Klepczynski (ref. 5) and Bec (ref. 6). To include these results, the value and uncertainty $M_\odot/M_{JS} = 1047.39 \pm 0.04$ are adopted herein as the basis for the planetary mass values.

To obtain the mass of the planet M_J, two additional parameters are needed: the mass of the Sun, $M_\odot = (1.989 \pm 0.002) \times 10^{33}$ g (ref. 7), and the ratio of the mass of the four largest (Galilean) satellites to that of the planet, $(M_{JS} - M_J)/M_J = (1.955 \pm 0.085) \times 10^{-4}$ (ref. 8). The mass of Jupiter is then $M_J = (1.899 \pm 0.002) \times 10^{30}$ grams in which the uncertainty is traced to that in the value of $M_\odot$. Related discussion appears in section 2.2.

2.1.2 Dimensions

The angular diameters of Jupiter have been measured by various direct, visual techniques. In one widely quoted comparative analysis thereof, Rabe (ref. 10) derives 38.09 and 35.76 seconds of arc for the equatorial and polar diameters, respectively, for a mean Jupiter-Earth separation of 5.2028 AU. The uncertainties are large, somewhat less than one second of arc for each value. Dollfus* reports a diameter of 70850± 100 km for Jupiter from synthesis of double image micrometer observations, but the relationship of this value to the uppermost cloud layer has not been established. A value with reasonable uncertainty results from the thorough analysis of the duration of the eclipses of the Galilean satellites by Sampson (ref. 11) who derived an unweighted average of eight independent determinations (each from several observations) for the equatorial semi-diameter of 18.9275±0.05 seconds of arc at 5.2028 AU. This value requires knowledge only of satellite orbit dimensions, period, and eclipse timing. Orbit dimensions whose base is hundreds of seconds of arc come from many visual observations. Consequently, such observations give more precise results than direct diameter measurements. Precision of eclipse timing measurements is excellent. If the modern value for the astronomical unit of 1.49597893×10^8 km is employed (ref. 4), Sampson's work yields an equatorial radius R_J of 71422±200 km for Jupiter.

The value 0.06117 for the optical flattening obtained from the above angular diameters is probably reliable to only one significant figure. However, the shape of the planetary equipotential surfaces (approximately ellipsoids of revolution) may be derived from the

*Dollfus, A., "Surface and Interiors of Planets and Satellites", Academic Press, New York, 1970 and "New Optical Measurements of the Diameters of Jupiter, Saturn, Uranus, and Neptune", Icarus, vol. 12, 1970, p. 101.

parameters J_2 and J_4 of Jupiter's gravitational field (sec. 2.2) and the period of rotation T_0 (sec. 2.11.1). Calculation of the polar diameter of that surface which corresponds to the foregoing value of the equatorial radius derived from Sampson (ref. 11) and the values of J_2, J_4, and T_0 (adopted in the sections cited) leads to the value 0.0645 ±0.0008 for the flattening ϵ. It narrows the range of the optical values cited in the literature (ref. 9).

The conventional expression for the planetary radius R_s as a function of jovicentric latitude ϕ is

$$R_s = R_J[1 - \epsilon(\sin \phi)^2]. \quad (1)$$

Equation (1) is correct to first order in ϵ, and the retention of higher order terms is not justified because of the large uncertainty in R_J. Therefore, equation (1) is adopted here for the specification of the shape of the planet in visible light with the foregoing values of R_J and ϵ. R_s refers to a level near the clouds in Jupiter's atmosphere and not to a specific solid or liquid planetary surface (secs. 2.9 and 2.13).

2.1.3 Mean Density

The mean density $\bar{\rho}$ is given by the following relationship (ref. 9); it is correct only to first order in ϵ

$$\bar{\rho} = \frac{3 M_J(1 + \epsilon)}{4\pi R_J^3}. \quad (2)$$

Equation (2) and the foregoing values for M_J, R_J, and ϵ lead to the value 1.32 ± 0.01 g/cm^3 for $\bar{\rho}$, a specific gravity for the planetary material only slightly greater than that of water.

2.1.4 Rotational Quantities

The periods (near 10 hours) and angular velocities associated with the rotation of Jupiter are discussed in section 2.11.1. The specific values, $T_0 = 9^h\ 55^m\ 29^s.73 \pm 0^s.04$ and $\omega_0 = (1.758531 \pm 0.000002) \times 10^{-4}$ radian/sec, are adopted there.

The directions of Jupiter's rotational axis and equatorial plane (determined from measurements of the position angle on the sky of the oval disk's major axis or the banded surface features) suggest that the equatorial plane is identical with the invariable plane of the Galilean satellites. The determination of the equatorial plane by Souillart (ref. 12) has been adopted for this monograph. Accordingly, the celestial coördinates of the north pole of Jupiter's rotation (also the direction of its angular momentum vector with the usual right-hand convention) have been taken as $\alpha_R = 17^h\ 52^m\ 00^s.84 + 0^s.247$ (t - 1910.0) for right ascension and as $\delta_R = +64°\ 33'34''.6 - 0.60''$ (t - 1910.0) for declination. Here, t is in tropical years, 1910.0 implies noon Greenwich Mean Time, 1 January 1910, and

α_R and δ_R refer to the equator and equinox at time t. The North Pole points into the constellation Draco with the following approximate inclinations: 3°.07 to the north pole of Jupiter's orbit, 2°.00 to the north pole of the ecliptic, and 25°.45 to the north pole of the Earth's rotation.

The moment of inertia C of Jupiter about its rotational axis may be derived from numerical models of the planet's interior. Various sources (refs. 7, 13, and 14) give C in the range

$$C = (0.25 \pm 0.01)\, M_J\, R_J^2 = (2.4 \pm 0.1) \times 10^{49}\ \text{g cm}^2. \tag{3}$$

According to DeMarcus (ref. 13), the moment of inertia A about any equatorial axis may be derived simply in the approximate form

$$A = C - J_2 M_J R_J^2 = (2.25 \pm 0.1) \times 10^{49}\ \text{g cm}^2. \tag{4}$$

The angular momentum $C\omega_0$ of the planet is $(4.3 \pm 0.2) \times 10^{45}$ g cm^2/sec when the foregoing values are employed.

The dimensionless parameter, $\sigma_R = \omega_0^2\, R_J^3/GM_J$, is a useful measure of the atmospheric ratio of the centrifugal and gravitational forces and will be required in section 2.2. The value of 0.0889 ± 0.0008 may be derived for σ_R from the foregoing adopted values.

2.2 Gravity Field

The gravitational field of a planet is conventionally described in terms of a potential function Ψ, approximated by the first few terms of an infinite series,

$$\Psi = -\frac{GM_J}{R_J}\left[\frac{R_J}{R} + \frac{\sigma}{2}\left(\frac{R}{R_J}\cos\phi\right)^2 - J_2\left(\frac{R_J}{R}\right)^3 P_2(\sin\phi) + J_4\left(\frac{R_J}{R}\right)^5 P_4(\sin\phi)\right]. \tag{5}$$

The forces on a test body include those proportional to the gradient of Ψ to which other relevant forces, e.g., perturbations by the sun and planetary satellites, may be added. The coefficient σ of the term in Ψ proportional to R^2 must be set equal to zero if the forces are to be evaluated in an inertial coördinate system. The coefficient σ must be equal to σ_R (sec. 2.1.4) if they are to be evaluated in a coördinate system rotating with the planet, e.g., in the atmosphere.

2.2.1 Inertial Coordinates

An inertial coördinate frame is appropriate for bodies not constrained to move with the planet, e.g., spacecraft beyond Jupiter's atmosphere, and requires that the value $\sigma = 0$ be

substituted in expressions for Ψ and its derivatives. In the evaluation of the other constants in equation (5), the mass and radius values adopted in section 2.1 lead to $R_J = 71422 \pm 200$ km and $GM_J/R_J = 1774 \pm 5$ km^2/sec^2. Values for the harmonic coefficient J_2 (which measures the contribution of the planet's flattening to the gravity field) are derived from analyses of the observed positions of the Galilean satellites. The best determination (ref. 15) is $\frac{3}{2}J_2 = 0.02206 \pm 0.00022$. A less accurate value for J_4 has been obtained from analysis of the observed positions of J V, the innermost satellite, as $-\frac{15}{4}J_4 = 0.00253 \pm 0.00141$ (ref. 8). Thus, the maximum contribution of the J_2 and J_4 terms in Ψ is approximately 1.5 percent, and an appropriate approximate form for the gravitational potential is

$$\Psi = -(1774 \pm 30 \text{ km}^2/\text{sec}^2)(R_J/R). \tag{6}$$

The gravitational forces on a spacecraft additional to those proportional to the gradient of Ψ, caused by the gravity of the Sun and the four Galilean satellites, may be calculated from the data given in section 2.6 and the positions tabulated annually in the *American Ephemeris and Nautical Almanac* (ref. 16).

2.2.2 Corotating Coordinates

A corotating coördinate frame is appropriate in situations in which the body of interest is constrained to rotate with the planet, and in these cases $\sigma = \sigma_R$ (sec. 2.1.4). Although this frame can be applied to magnetospheric charged particles whose motions may be constrained by rotating magnetic field lines, it is used in this monograph only for regions in which the quantity $\sigma(R/R_J)^2$ is small compared to unity, applicable, for example, to an atmospheric entry vehicle. For convenience, the altitude z (here $z \ll R_J$) above the planetary surface (eq. 1) is defined by the relationship

$$R = R_J[1 - \epsilon(\sin\phi)^2 + z/R_J]. \tag{7}$$

The acceleration of gravity (directed at an angle η_1 equatorward of the inward radial direction and of magnitude g) then can be specified simply by expressions of first order in z, J_2, σ_R, and ϵ, namely

$$g = \frac{GM_J}{R_J^2}[1 - \sigma_R + \frac{3}{2}J_2 - \frac{2z}{R_J}][1 + (2\epsilon + \sigma_R - \frac{9}{2}J_2)(\sin\phi)^2] \tag{8}$$

and

$$\eta_1 = (\frac{3}{2}J_2 + \sigma_R/2)\sin 2\phi. \tag{9}$$

In the evaluation of these expressions, the approximate relationship, $\epsilon = \frac{3}{2}J_2 + \sigma_R/2$

(which is closely satisfied in Jupiter's case), may be used. With the foregoing values the range of magnitudes of the acceleration of gravity is 2500 ±200 cm/sec^2, and η_1 has maximum deflection of 3°.7 ±0°.3 at jovicentric latitude ϕ of 45°.

2.3 Magnetic Field and Magnetosphere

Properties of Jupiter's magnetic field and magnetosphere are inferred from the radio emissions (sec. 2.5.3) received at Earth from Jupiter. Carr and Gulkis (ref. 17) and Warwick (ref. 18) review the considerations involved. Section 2.7 treats charged particles within the magnetosphere.

2.3.1 Magnetic Field Strength and Configuration

The characteristics of Jupiter's UHF and HF radiation (sections 2.5.3.1 and 2.5.3.2) permit quantitative descriptions of the magnetic field strength and configuration to be formulated although the uncertainties are considerable. Appendix B includes formulas for calculation of the magnetic field strength and lines of force at any location in Jupiter's magnetosphere on the basis of the dipole moment, inclination, and displacement adopted in the following sections.

2.3.1.1 Dipole Moment

UHF data permit an order-of-magnitude determination of the magnetic field in the radiation belts (sec. 2.7.4); the values cited in the literature are near 1 gauss about 2 radii from the dipole (refs. 17, 18, and 19) which correspond to field strengths near 10 gauss about 1 radius from the dipole and dipole moment M_1 near 3×10^{30} gauss-cm^3. The UHF values at 1 radius are compatible with the narrower range commonly derived from the HF bursts if the burst frequency is taken to equal the local electron gyrofrequency at the source location. The local magnetic field strengths corresponding to observed HF frequencies near 30 MHz are near 12 gauss (refs. 18, 20, and 21). The dipole moment obtained from this field strength value depends sensitively on the relative locations of the dipole and the HF burst generation region. If the dipole is centered on the planet and the emission near 30 MHz is generated just above Jupiter's atmosphere in the magnetic equatorial plane, the moment corresponding to the 12 gauss field strength is approximately 4×10^{30} gauss-cm^3. This value is close to the value of 4.2×10^{30} gauss-cm^3 derived by Warwick (refs. 18 and 22), who completed a detailed analysis of the HF burst structure based on a severely offset dipole (sec. 2.3.1.3). To take into account published field strength and dipole moment values based on analyses of HF and UHF data (refs. 17, 19, 20, 21, and 23), an uncertainty factor of two and a nominal value of $M_1 = 4 \times 10^{30}$ gauss-cm^3 are adopted for this monograph. The consequent range of field strengths in the atmosphere is from 6 gauss at the equator to 48 gauss at the poles if the dipole is centered on Jupiter. The dipole and field have the opposite orientation from the Earth's as Jupiter's northern hemisphere contains its north-seeking magnetic pole (refs. 18 and 24).

2.3.1.2 Dipole Inclination

The UHF emission has a linearly polarized component whose position angle is roughly parallel to Jupiter's equator, but the position angle varies regularly by nearly 10^{o} with the period of Jupiter's rotation (sec. 2.11.1 and refs. 25 and 26). This slightly asymmetric variation results from the inclination of Jupiter's magnetic axis to its rotation axis by an angle nearly equal to the above amplitude and the rotation of the field and its sources. This small inclination has a far smaller effect on the field strengths than the large uncertainty in the dipole moment (sec. 2.3.1.1) and should therefore be ignored for design purposes.

2.3.1.3 Dipole Displacement

The asymmetric properties of the UHF polarization and intensity variations and of the HF burst probability and dynamic spectra cannot be explained in terms of an inclined, planet-centered dipole field (ref. 18). Although various authors have contended that significant magnetic field anomalies and quadrupole moment could be responsible for the asymmetries, Warwick (refs. 18 and 22) has claimed that displacement of the magnetic dipole approximately 0.7 radius south of Jupiter's center is responsible. In contrast, many investigators find such a large displacement unreasonable in view of postulated field maintenance processes in Jupiter's interior and of the measurements of the position of Jupiter's UHF emission centroid within 0.4 radius of the geometric center according to reference 27. Berge (ref. 28) has refined the measurement by reference 27 to find a small southward displacement of less than 0.2 radius for the emission centroid. If this displacement corresponds to that of the magnetic dipole, the influence on derived field strengths in the atmosphere or above is everywhere less than a factor two with respect to the centered situation. Thus, it is concluded that for design purposes any possible dipole displacement can be ignored in view of the large uncertainties associated with the dipole moment itself (sec. 2.3.1.1) and with the energetic charged particle fluxes (sec. 2.7.4).

2.3.2 Magnetosphere

Jupiter's magnetosphere is the region within which Jupiter's own magnetic field and charged particles (sec. 2.7) dominate. In the solar direction the magnetosphere boundary is conventionally fixed by equating the solar wind and planetary magnetic field pressures and consists of both a shock front (at which the solar wind velocity decreases abruptly) and a magnetopause (limiting Jupiter's regular magnetic field). The result is $50 \pm 20\ R_J$ which includes most estimates of the distance of the sunward boundary from Jupiter (refs. 17, 29, and 30). This distance is adopted here as the minimum radius of the magnetosphere. In other directions additional complex features, including distortion by Jupiter's rotation (sec. 2.11.1) and a more distant magnetosphere boundary, are expected by analogy with the Earth. In the anti-solar direction the length of Jupiter's magnetospheric tail is greater than $100\ R_J$ (refs. 17 and 31).

2.4 Electric Fields

There is very little evidence for static electric fields, either large scale or local, in any observations of Jupiter or in their interpretations.

The local value of the field strength suggested in the HF burst theory of Goldreich and Lynden-Bell (ref. 21) ranges up to approximately 10 volts/meter. The field which would be required to accelerate electrons (charge -e) electrostatically to the energy ($E \approx 6$ MeV, sec. 2.7.4.2) inferred from the UHF observations has the order of magnitude of $\mathcal{E} = E/eR_J = 0.1$ volt/meter. The electric field induced in an inertial coordinate system by the rotation of Jupiter's magnetic dipole field is perpendicular to the magnetic field lines and of the order of magnitude of $\mathcal{E} = vB = (\omega_0 R)(M_1/R^3) = (14 \text{ volts/meter})(R_J/R)^2$.

For this monograph, a range between zero and the largest of the foregoing estimates is adopted for the general field within the magnetosphere:

$$0 \leq \mathcal{E} \leq (14 \text{ volts/meter})(R_J/R)^2. \tag{10}$$

Local, time-varying electric fields could be associated with plasma waves of the disturbances implied by the HF bursts, but their field strengths are unknown.

Within the ionosphere the electrical conductivity of the plasma is probably large enough for the static field strengths already quoted to be ample upper limits. Below the region of maximum ionospheric electron density, the low atmospheric electric conductivity (sec. 2.12.1) is conducive to the build-up of static charge accumulations, particularly in regions of convection and cloud formation. By analogy with the Earth's atmosphere, randomly oriented electric fields of strength up to the order of 3×10^4 volts/meter might be expected in scales of hours and kilometers. Other fields up to the order of 10^6 volts/meter may occur in scales of seconds and centimeters just before lightning strikes sharp, projecting objects (ref. 32).

2.5 Electromagnetic Radiation

The electromagnetic radiation environment in the vicinity of Jupiter is divided into light, heat, and the radio spectrum for presentation in the following sections.

2.5.1 Light

This section treats X-rays, the ultraviolet, visible, and near infrared portions of the electromagnetic spectrum, i.e., wavelengths between about 1 Å and 5 μm.

2.5.1.1 Solar Radiation

Near Jupiter the Sun is the dominant source of light which may be direct, reflected, or scattered. NASA SP-8005 (ref. 1) summarizes the direct solar spectrum at 1 AU and specifies P_λ, the power per unit area and per unit wavelength interval for wavelengths between 50 Å and 100 cm. The values from reference 1 and standard relationships for intensity and flux (app. E) lead to the formulas given for the Sun in table VII (sec. 3.5).

2.5.1.2 Jupiter Reflected Radiation

The solar radiation reflected from Jupiter (or its clouds) has been observed only at phase angles less than 12° and is conventionally described in terms of astronomical magnitudes, colors, and albedos. The definition of geometric albedo p (app. E) leads to formulae for the intensity and flux of Jupiter-reflected radiation observed at zero phase angle and jovicentric distance R

$$I_\lambda = \frac{pP_\lambda}{\pi r^2} \tag{11}$$

and

$$F_\lambda = \frac{pP_\lambda}{r^2(R/R_J)^2} \tag{12}$$

where r^2 evaluated for Jupiter in $(AU)^2$ has the value 27 ±3. For other observable phase angles (< 12°), these quantities are smaller than the results of equations (11) and (12). Therefore, it can be inferred that the zero phase angle formulae constitute correct upper limits at all phase angles.

Photoelectric measurements of the geometric albedo p for Jupiter at wavelengths between 2000 Å and 1.5 μm are summarized in table II. Limiting values from table II are shown in figure 1, and although the data are restricted to one decade in wavelength, the albedo is apparently decreasing as both ends of the observed range are approached. Thus, a range of values for p between 0 and 0.3 at unobserved wavelengths in addition to the range from table II is adopted herein. Table II also lists the result of a photoelectric determination of the bolometric albedo p_b. That value and its substitution in the following expression for the integrated reflected flux

$$F = \frac{p_b S}{r^2 (R/R_J)^2}, \tag{13}$$

are adopted here.

2.5.1.3 Satellites and Planets

The brightnesses of Jupiter's satellites and other planets are specified by their magnitudes and colors (defined in appendix E) which are summarized in references 7, 9, and 38. Their variations with satellite rotation and phase angle a are limited respectively by ±0.3 magnitude (ref. 38) and probably by $(0.03 \pm 0.02)a$ for a in degrees; the phase angle uncertainty includes all Jupiter satellite observations ($a \leq 12°$) and the complete phase variations for Venus (deep atmosphere) and the Moon (no atmosphere) to within 0.1 magnitude. When

the geometry of satellite illumination and observation is specified in terms of α, r, and Δ (r and Δ in AU only and α in degrees), the relationship

$$m_v = (m_0 \pm 0.3) + 5\,log(r\Delta) + (0.03 \pm 0.02)\alpha \qquad (14)$$

applies. Equation 14 is adopted for use with the magnitudes and colors given in table IX (sec. 3.5) for both Jupiter's satellites and other planets.

TABLE II

OBSERVED GEOMETRIC ALBEDOS FOR JUPITER*

Wavelength** (Å)	Geometric Albedo p	Source
1730	0.2 ± 0.15	Moos et al. (ref. 33)
2100	0.2 ± 0.15	Stecher (ref. 34), Jenkins et al. (ref. 35), and Anderson et al. (ref. 36)
2800	0.23 ± 0.1	
3530 (U)	0.31 ± 0.05	Irvine et al. (ref. 37) and Harris (ref. 38)
4480 (B)	0.42 ± 0.05	
5540 (V)	0.50 ± 0.05	
6900 (R)	0.47 ± 0.05	Harris (ref. 38)
8200 (I)	0.35 ± 0.05	
10635	0.31 ± 0.1	Irvine et al. (ref. 37)
15000	0.15 ± 0.1	Danielson estimate (ref. 39)
Bolometric Albedo	$p_b = 0.28 \pm 0.03$	Taylor (ref. 40)

*Uncertainties are estimated from comparison with additional published data.

**Letters specify pass bands in the conventional magnitude system.

2.5.1.4 Atmospheric Illumination

Within Jupiter's atmosphere the foregoing intensities, fluxes, and magnitudes most likely represent appropriate upper limits on radiation from the Sun, Jupiter's clouds, its satellites, and other planets if $r^2 = 27 \pm 3\ (AU)^2$ and $R/R_J = 1$. Additional sources of light radiation which might be expected are scattering, airglow, aurorae, and lightning. No simple description of any of these phenomena of Jupiter's atmosphere is possible, but the light reflected from Jupiter's clouds is adopted as an upper limit for the intensities and fluxes of the first three. Lightning could presumably be as intense as that in the Earth's atmosphere and thus could require that light-sensitive devices be covered during storms.

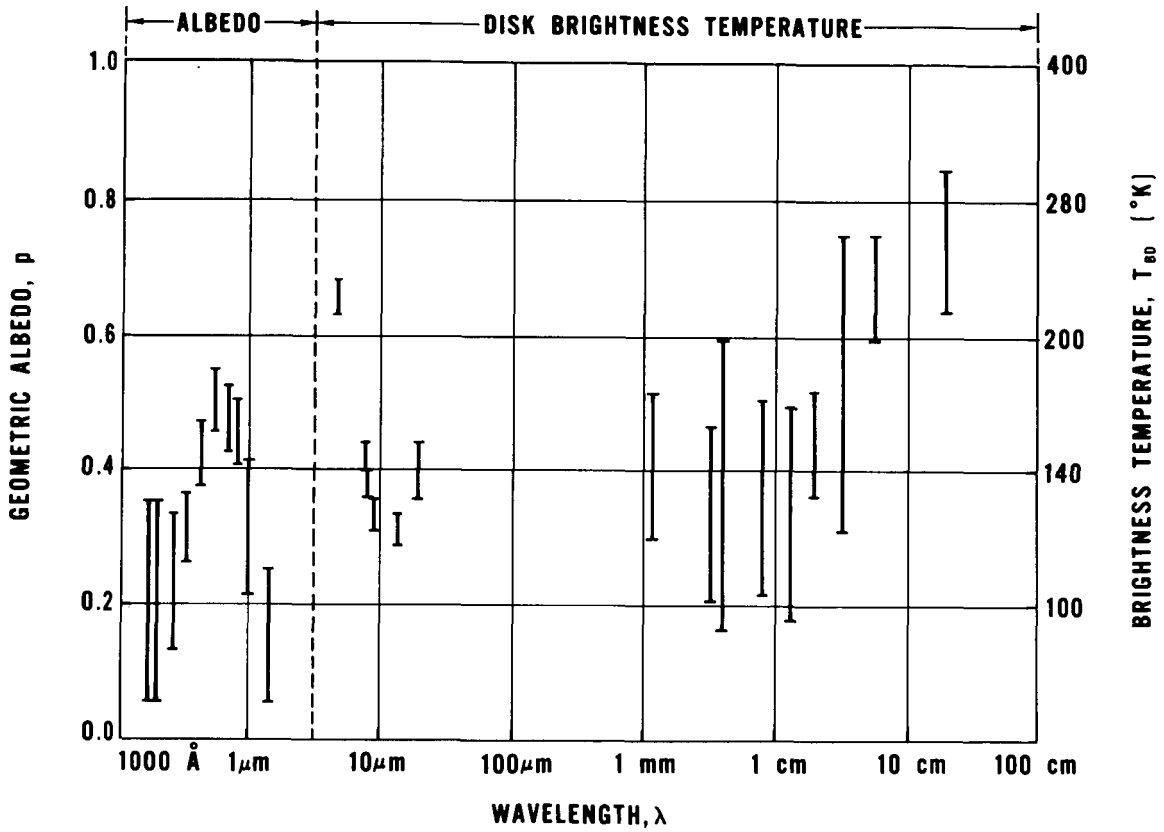

Figure 1.– Typical values of geometric albedo p and disk brightness temperature T_{BD}, taken from table II and references cited in section 2.5.2. (The temperature scale is logarithmic.)

2.5.2 Heat

Direct solar radiation and intrinsic, thermal Jupiter radiation are important in the wavelength range between μm and 1 cm. The solar contribution is covered in section 2.5.1.

The determination of Jupiter's infrared spectrum is difficult because terrestrial atmospheric absorption distorts data observed even at great altitudes. The difficulty is especially severe at wavelengths near 20 μm where Jupiter's thermal radiation is greatest. Even the thorough discussion of data at wavelengths shorter than 14 μm by Gillett et al. (ref. 41) may not have completely eliminated the absorption problem from ground-based observations. At longer wavelengths, extending into the microwave radio region (sec. 2.5.3.1), Kellermann (ref. 42) summarizes the data of many observers in terms of the brightness temperature T_{BD} of Jupiter's thermal disk radiation (fig. 1, sec. 2.5.1). For wavelengths between 1 μm and 100 cm, the band labelled T_{BD} in figure 7 indicates (with ample uncertainty limits, and reasonable extrapolations into unobserved regions) the range of values reported by these authors. The increase of T_{BD} with wavelength in the centimeter range implies that the radiation emerges from lower, warmer atmospheric levels at longer wavelengths. Ammonia absorption is responsible for the dip in T_{BD} near 1 cm wavelength. The intensity and flux of the thermal disk radiation may be computed readily from the brightness temperature through the Planck function $B_\lambda(T)$ or $B_\nu(T)$, tabulated, for example, by Allen (ref. 7) and the formulas given in table VII (sec. 3.5).

The effective temperature of Jupiter resulting from data obtained with an aircraft-borne Germanium bolometer is given as $T_e = 134 \pm 4°K$ (ref. 43). However, the uncertainty may be too small because Jupiter was observed on only one date and the 8 to 14 μm results commonly fall below 130°K (ref. 44). Thus, it is concluded that for this monograph the uncertainty be increased slightly to $T_e = 134 \pm 6°K$, corresponding to a 20 percent uncertainty in the flux of energy from Jupiter. This energy, given in table VII (sec. 3.5), almost certainly is radiated nearly uniformly over the planet's surface.

2.5.3 Radio

The range considered here includes all wavelengths greater than approximately 1 cm (or, equivalently, frequencies less than 30 000 MHz). Radio observations of Jupiter conventionally are made in two distinct spectral regions and indicate that three distinct source mechanisms are involved.

2.5.3.1 Decimetric (UHF) Radiation

Thermal radiation from Jupiter's disk (sec. 2.5.2) contributes significantly to the UHF radiation environment near Jupiter. It is randomly polarized and continuous in frequency. Its brightness temperature is constant in time and uniform over the surface to the accuracy shown in figure 7. Its radio intensity and flux may be calculated from figure 7 and the relationships given in appendix C.

Non-thermal UHF radiation is observed from a region several Jupiter radii in extent, elongated parallel to Jupiter's magnetic equator. As Jupiter rotates, this radiation varies by

about 15 percent in intensity because of the changing magnetic latitude of the observer, and the position angle of its linearly polarized component (maximum about 30 percent near λ = 30 cm) moves roughly parallel to the magnetic equator. An observer at a distance of 4.04 AU receives 7±3 flux units (1 FU = 10^{-26} watt/m^2 Hz) at all wavelengths between 1 and 300 cm with perhaps 50 percent greater uncertainty outside the wavelength range 3 to 100 cm. Dickel et al. (ref. 45) summarize the UHF spectrum and cite some of the many references from which the foregoing brief description was compiled. The non-thermal component synchrotron radiation from relativistic electrons trapped in Jupiter's magnetic field (secs. 2.3.1 and 2.7.4).

Close to Jupiter the specification of the spatial distribution of the synchrotron radiation requires the utilization of data reported by Berge (ref. 24) and Branson (ref. 46) at 10.4 and 21 cm wavelengths. Figures 2 and 3 show their reconstructed emission distributions as seen from the Earth in terms of brightness temperatures at resolutions of the order of Jupiter's radius R_J. Although some data suggest that the source may extend to significantly greater distances from Jupiter at longer wavelengths (refs. 47 and 48), this concept does not have general concurrence (ref. 18). To provide a model which yields approximately correct brightness temperatures for the synchrotron source, the following approach is suggested. Figure 8 illustrates the volume enclosed by a sphere of radius 3 R_J, centered on the magnetic dipole and truncated by two planes parallel to and 1 R_J away from the magnetic equator. Then if D is the path length within the described volume in the direction of observation (extending either to the planetary surface or to infinity), the brightness temperature is given by

$$T_{BS} = \frac{D\lambda^2}{R_J} (0.30 \pm 0.15)^\circ K \tag{15}$$

for λ in cm. The uncertainty in this expression is large enough so that D can be obtained from a reasonable estimate instead of from a geometric calculation. Thus over the center of the disk, by taking D = 2 R_J, the T_{BS} values 66 ±33°K and 260 ±130°K are obtained at λ 10.4 and 21 cm; just beyond the limb, by taking D = 5 R_J, the values 165 ±82°K and 650 ±325°K are obtained at the same two wavelengths. The results of Berge (ref. 24 and Branson (ref. 46) are included within the uncertainties quoted.

The intensity of the UHF synchrotron radiation is then given in terms of the brightness temperature T_{BS} by the Rayleigh-Jeans law (app. C). The maximum flux is 7 ± 3 flux units, independent of λ, at 4.04 AU, proportional to R^{-2} for $R >> R_J$ and nearly independent of R within the source, i.e., for $R \lesssim 2 R_J$. An expression satisfying these requirements is

$$F_\nu = \frac{(5 \pm 2) \times 10^8}{4 + (R/R_J)^2} FU \tag{16}$$

and its maximum value is consistent with the intensity and brightness temperature formulation at the maximum D $\approx$ 5 R_J. The multiplication of equation (16) by the appropriate bandwidth (approximately 3000 MHz) yields the corresponding integrated flux. Table VII (sec. 3.5) summarizes the foregoing conclusions.

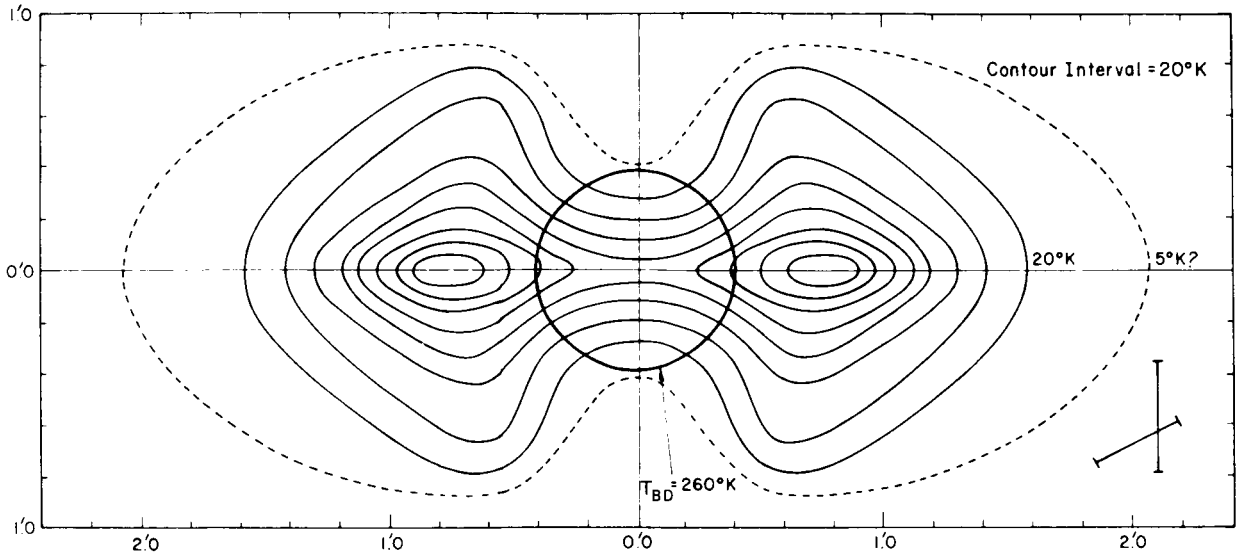

Figure 2.—Aperture synthesis map of Jupiter's 10.4 cm radiation. The central circle represents Jupiter's optical disk, the curved lines represent contours of constant brightness temperature, and the bars at lower right indicate the instrumental resolution (from ref. 24).

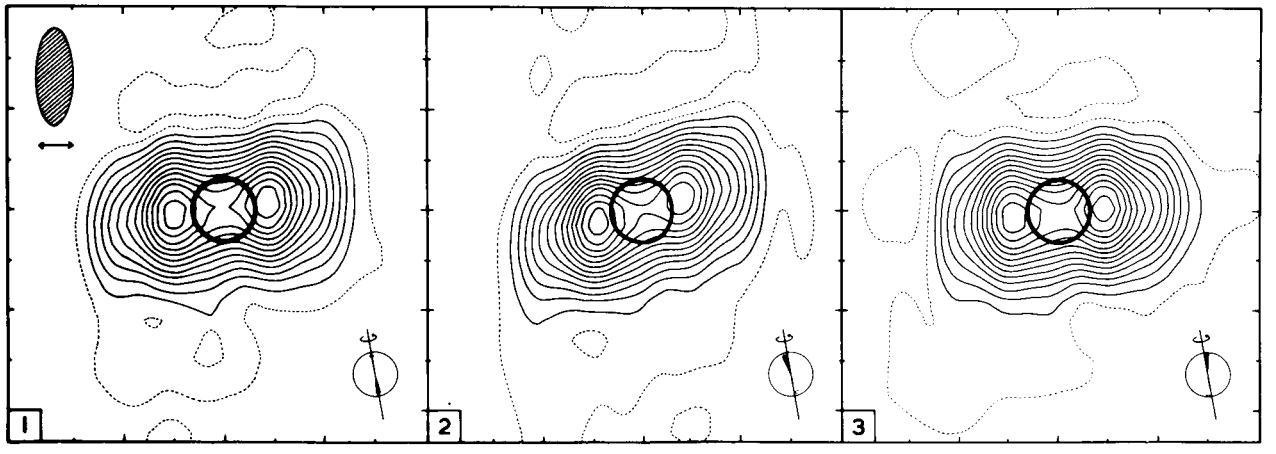

Figure 3.—Three aperture synthesis maps of Jupiter's 21 cm radiation. The central circles represent Jupiter's optical disk, the curved lines represent contours of constant brightness temperature (interval 47°K), the oval at upper left represents the instrumental resolution, and the figures at lower right represent the orientations of the rotational and magnetic axes (from ref. 46).

2.5.3.2 Decametric (HF) Radiation

HF bursts are observed in the frequency range 5 to 39.5 MHz (wavelengths between 7.6 and 60 meters). Many features of their polarization, directionality, and time and frequency structure display great variety although some properties (notably burst detectability and dynamic spectra) are correlated with the relative orientations of the Earth, Jupiter, and the Galilean satellite, Io. Their characteristics are reviewed by Warwick (ref. 49) and Carr and Gulkis (ref. 17) who give numerous references to original observations and analysis. Because sizes of HF burst sources are small in comparison to planetary dimensions (refs. 50 and others), because bursts are sporadic, and because there is no consensus for any of the proposed generation mechanisms (refs. 18, 20, 21, and 51), it is not appropriate to propose particular characteristics for HF radiation near Jupiter. Because the intensities could be very high (ref. 18), however, the use of spacecraft equipment sensitive to external radiation at wavelengths longer than 100 cm is not recommended near Jupiter.

2.6 Satellites and Meteoroids

The distribution and properties of the solid particles in the Jupiter environment beyond the planet's atmosphere may be inferred from optical, telescopic observations of the natural satellites of Jupiter. The bodies divide naturally into three categories.

2.6.1 Galilean Satellites

The four largest satellites are visible with even very small telescopes. Analysis of their observed angular positions with respect to Jupiter implies orbits of negligible eccentricity and inclinations to Jupiter's equatorial plane, separations from Jupiter's center between 5.9 and 27 R_J, and periods between 42 and 400 hours, i.e., between 4.2 and 40 Jupiter days. Analysis of their mutual perturbations leads to masses between 0.00002 and 0.0001 times that of Jupiter (ref. 9). Visual observations and measurements (ref. 52) indicate that their rotation is synchronous with their orbits and that values for their diameters are of the order of one second of arc as seen from the Earth.

Photometric and spectroscopic observations (refs. 38 and 53) do not furnish much information on the satellite properties. Surface temperatures may be variable within the range from 3°K to 170°K (refs. 54 and 55). With these thermal and appropriate gravitational conditions, the presence of satellite atmospheres is not excluded, but attempted observations thereof have been inconclusive.

Some of the most certain information available for these satellites is presented in table X (sec. 3.6) and references 4, 7, 9, and 56. Photometric information is discussed in section 2.5.1.3, and detailed orbital information is presented in the *American Ephemeris and Nautical Almanac* (ref. 16).

2.6.2 Smaller Satellites

Eight smaller satellites (identified as J V through XII), each much smaller than the Galilean satellites, have been observed photographically. The orbital elements of J V vary because of

strong perturbations by Jupiter's oblateness, whereas the orbital elements of the others vary because of perturbations by the Sun. The latter divide naturally into the categories J VI, VII, and X with prograde orbits of periods near 260 days and J VIII, IX, XI, and XII with retrograde orbits of periods near 700 days. Because the eight smaller satellites are so faint (magnitudes + 13 to + 19 as seen from the Earth), their masses (probably less than 10^{+23} grams), radii, and physical properties are not known. There is speculation that their physical properties resemble those of the asteroids. Other undiscovered, even smaller satellites of Jupiter also may exist.

Some of the most certain information available for these objects is presented in table X. Additional information and references may be found in table 14 of reference 4.

2.6.3 Meteoroids

There is no direct evidence of meteoroidal debris in the environment of Jupiter. Traditionally, the meteoroid environment near a planet has been inferred from the presumed gravitational enhancement of the nearby interplanetary cometary debris (ref. 3). Although such an enhancement is definitely to be expected, the uncertainties involved in the evaluation of the interplanetary debris distribution and the enhancement characteristics in the case of Jupiter amount to several orders of magnitude.

Another reasonable approach is to consider Jupiter's irregular satellites (J VI through XII) as the observable, large body end of a meteoroid distribution analogous to that expected in the asteroid belt. Such an approach assumes that the smaller satellites of Jupiter have individual properties and a mass distribution comparable to those of the asteroids, an assumption which is neither confirmed nor denied by the meager satellite data available.

The masses M_n in grams and radii R_n in cm for J V through XII presented in table X are derived from the relationships

$$\log M_n = 26 \pm 1 - 0.6\, m_0 \tag{17}$$

and

$$\log R_n = 8.3 \pm 0.3 - 0.2\, m_0 \tag{18}$$

which are reasonable for asteroids of absolute magnitude m_0, mass density 3.5 g/cm^3, and visual albedo 0.2. If the positions of the outer seven satellites are distributed uniformly within a volume centered on Jupiter of radius $500\,R_J$* and at latitudes within ±30°, the number per unit volume N_M of particles of mass $M \geq 10^{18.5}$ grams is $10^{-31 \pm 1}$ m^{-3}. This is almost identical to the peak spatial density at this mass in the asteroid belt (ref. 3). Application of a crude mass distribution similar to that in reference 3 gives

$$\log N_M = -31 \pm 1 - (0.8 \pm 0.1)(\log M - 18.5). \tag{19}$$

Equation (19) requires N_M in particles/m^3 and applies for $10^{-9} \leq M \leq 10^{20}$ grams within the foregoing given volume near Jupiter.

*The inner boundary for meteoroids could be $100R_J$ because of sweeping action by the satellites and gravitational forces. However, an inner boundary of $1R_J$ is assumed herein.

Omnidirectional fluxes of particles may be computed by multiplying N_M by v/4 where the speed v of the particles relative to a spacecraft (with speed v_s) is approximately $v = [v_s^2 + (R_J/R)(40\ km/sec)^2]^{1/2}$*. The particle density is $3.5 \times 2^{\pm 1}$ g/cm^3. Lack of relevant data makes it impossible to decide whether such a distribution dominates anticipated cometary debris of lower density, but it is recommended that cometary debris be neglected on the basis of the small fluxes suggested in reference 3.

2.7 Charged Particles

Figure 4 schematically shows various charged particle environments near Jupiter. The following sections describe the number density, energy, and flux for each; transfer properties are discussed in section 2.8.

2.7.1 Galactic Cosmic Rays

Near the Earth, galactic cosmic ray intensities are modulated by the interplanetary magnetic field. In general, it is expected that this modulation reduces the intensities more severely at lower energies, closer to the Sun, and during intervals of greater solar activity. Quantitative predictions of the intensities near Jupiter have not been made, however. Jupiter's own magnetic field may reduce the intensities further, particularly at low energies and latitudes. Thus the approach adopted is to specify the fluxes in the energy range observed (0.1 to 10^{10} GeV) as between zero and a spectrum extrapolated from the highest energies observed for the most abundant particle kinds at times near minimum solar activity. This spectrum can be approximated by the following expression for the flux of particles with kinetic energy greater than E

$$\Phi_E = A(E + m_0 c^2)^{-1.5} \qquad (20)$$

where $m_0 c^2$ is the rest energy of the particle and E is the particle kinetic energy in GeV (per nucleon for alpha-particles). The summary given by Haffner (ref. 57, fig. 2-3) specifies $A \approx 10\ cm^{-2}\ sec^{-1}$ for protons and $A \approx 1\ cm^{-2}\ sec^{-1}$ for alpha-particles; Fanselow (ref. 58) specifies $A \simeq 0.2\ cm^{-2}\ sec^{-1}$ for electrons.

2.7.2 Solar Particle Events

Protons and alpha-particles of energy greater than 1 MeV are emitted sporadically by the Sun and have been detected by ground-based and spacecraft-borne instrumentation. Their fluxes near the Earth vary over several orders of magnitude in time, have both directional and isotropic components, and frequently can be identified with specific solar flares. Properties of sample events observed near the Earth are described in NASA TR R-169 (ref. 59). The recent theoretical model by Englade (ref. 60) cites the important references which treat the complex processes involved. This literature shows that neither the probability of occurrence of an event nor the variation of the particle fluxes with solar distance can be reliably estimated at this time.

*The average particle velocity relative to Jupiter is taken here as the orbital velocity (40km/sec at $R/R_J=1$) which is distinct from the escape velocity given in reference 3.

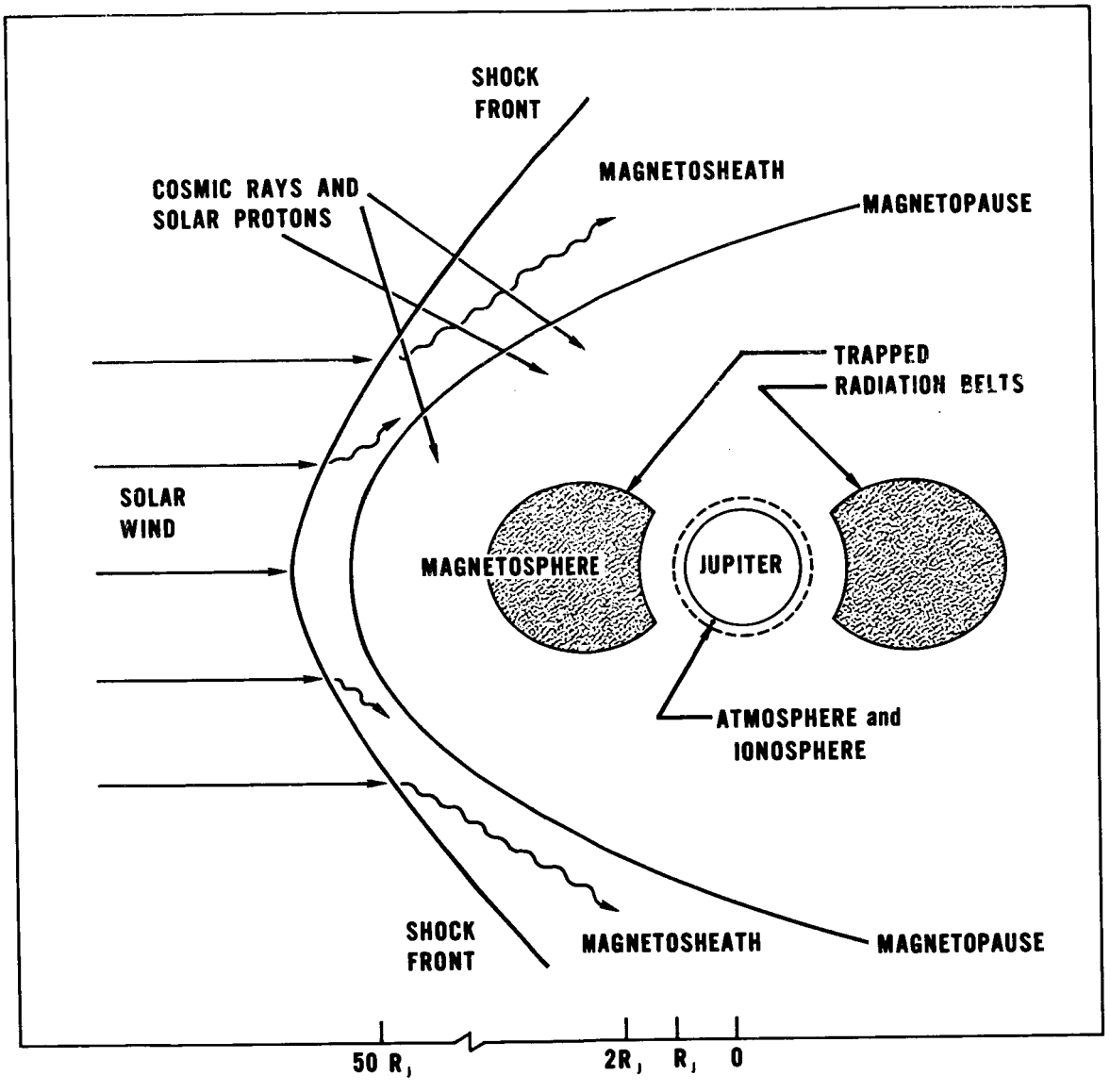

Figure 4.–Schematic of charged particle regions near Jupiter.

2.7.3 Solar Wind

Properties of the solar wind are summarized by Hundhausen (ref. 61). On the basis of observations from Mariner spacecraft at 0.8 to 1.5 AU from the Sun, protons and electrons during quiet solar conditions have concentrations of approximately $5r^{-2}\,cm^{-3}$ (for r in AU) and are streaming radially away from the Sun at speeds near 320 km/sec. Increases in solar activity are accompanied by temporary increases up to factors of 10 in the concentration and 3 in the speed. The applicable theory suggests that the extrapolation of these conditions on the basis of heliocentric distance r to the orbit of Jupiter is justified. The interaction of the solar wind with Jupiter's magnetic field is responsible for the formation of the outer boundary of Jupiter's magnetosphere (sec. 2.3.2).

2.7.4 Trapped Radiation Belts

The high energy (several MeV) electron component of Jupiter's charged particle environment is the only one about which inferences can be made directly from phenomena observed from the Earth. Part of Jupiter's UHF radiation (sec. 2.5.3.1) is interpreted as synchrotron radiation from electrons trapped in Jupiter's dipole magnetic field (sec. 2.3.1).

The theoretical relationships which may be used to predict the features of such synchrotron radiation are sufficiently complex that a unique solution for the electron distributions in energy, position, and pitch angle is not possible from observations so far made of the UHF radiation from Jupiter. The complexity increases if the magnetic field is treated as an unknown to be determined from the UHF data analysis. Thus, many electron density estimates are simply order-of-magnitude such as made by Carr and Gulkis (ref. 17) who suggest that a region roughly enclosed by two right circular cylinders centered on Jupiter of radii 1 and 3 R_J and height 2 R_J is characterized by a magnetic field of 1 gauss and contains 14-MeV electrons at a density near 10^{-3} cm^{-3} and a flux near 3×10^7 cm^{-2} sec^{-1}.

2.7.4.1 Relativistic Electron Flux

a. Peak Flux

Figure 5 shows the dependence of the total relativistic (kinetic energy $E > 0.5$ MeV, the electron rest energy) electron flux Φ (in cm^{-2} sec^{-1}) on distance L (in Jupiter radii) in the plane of the magnetic equator. Here L is the magnetic shell parameter as in app. B. Near $L = 2$ the existence of a flux peak is a common interpretation of the 10 and 21 cm UHF emission patterns derived by Berge (ref. 24) and Branson (ref. 46) from aperture synthesis and reproduced in figures 2 and 3 (sec. 2.5.3.1). The models of Haffner (ref. 63) and Koepp-Baker (ref. 64) place their values of the flux in this peak (fig. 5) on the assumption that the synchrotron power is radiated isotropically from Jupiter. This approach neglects the strong beaming of the UHF radiation into the magnetic equatorial plane which is required by observations (ref. 65) and theory (ref. 18) and thus overestimates the total power and the electron flux required to produce it.

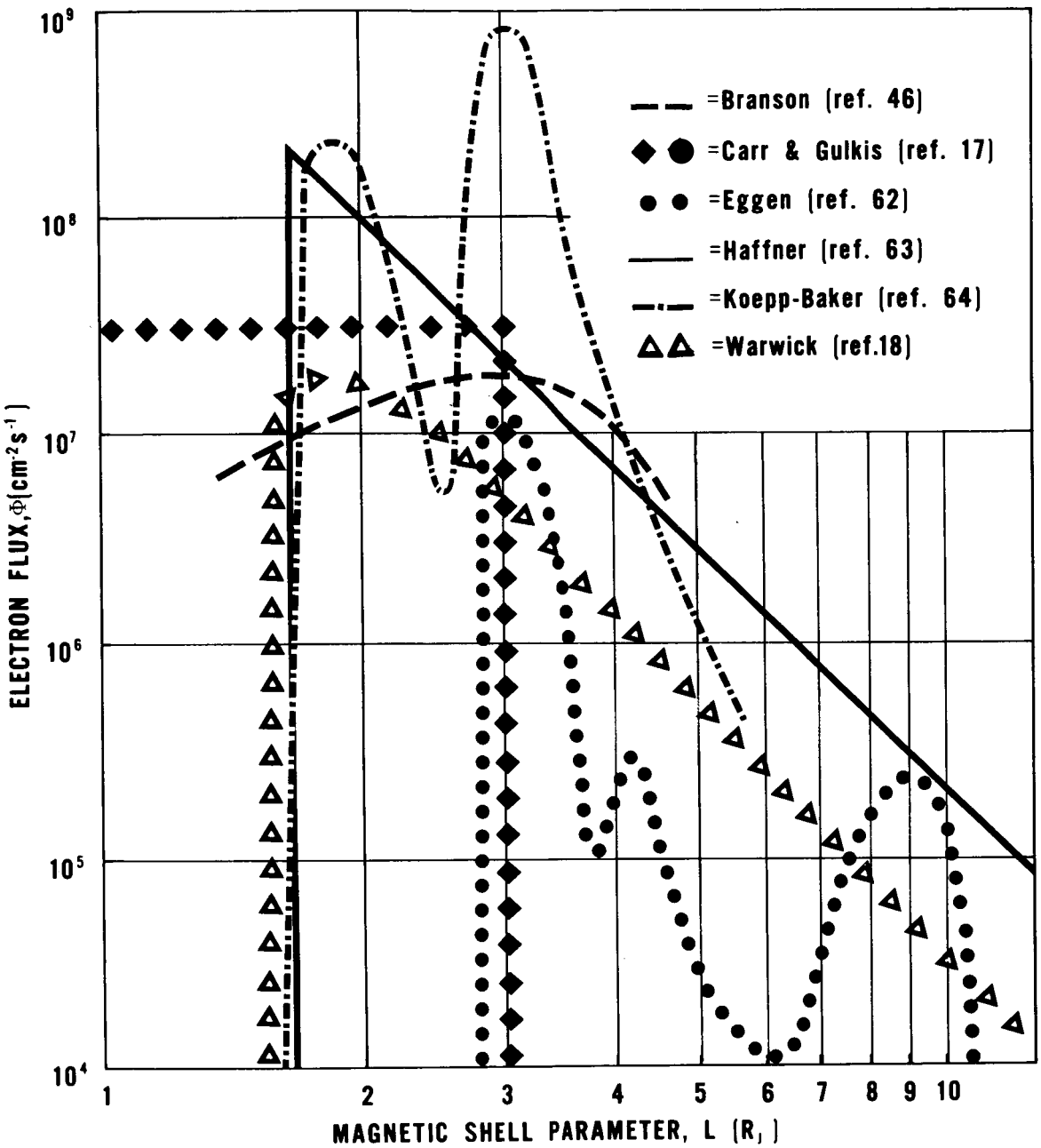

Figure 5.– Flux of relativistic electrons as a function of the distance from the dipole in the plane of the magnetic equator, for proposed models of Jupiter's trapped radiation belt.

Warwick (ref. 18) derives a flux 1.9 $\times$ 10^7 cm^{-2} sec^{-1} for the peak near L = 2 by using the value of the magnetic field strength (2.0 gauss at L = 1.8 and ϕ = 0) derived from the dipole moment quoted in section 2.3.1, an electron energy of 6.2 MeV (sec. 2.7.4.2), and an estimate for the UHF brightness temperature (183°K) above the center of the disk from Branson's map 1 at 21 cm (ref. 46). The order-of-magnitude estimates of Eggen (ref. 62), Branson (ref. 46), and Carr and Gulkis (ref. 17) support the Warwick flux level. As an estimate of the correct flux at the major electron peak in Jupiter's belts, this monograph adopts $2 \times 10^7 cm^{-2} sec^{-1}$ with an uncertainty factor of three.

b Distribution with Distance

The distributions of radiating electrons as functions of distance from the dipole within Jupiter's belts shown in figure 5 are derived from Earth analogy, analysis of the distribution of the UHF radiation, and theory. Eggen's model (ref. 62) shows several peaks derived entirely from Earth analogy, and although there may be various peaks in Jupiter's electron distribution, it is unlikely that this simply-scaled model locates them correctly. Also, the observations (fig. 2, sec. 2.5.3.1) indicate that significant flux levels occur with L < 3.

Koepp-Baker's model (ref. 64) derives its double peak distribution from an interpretation of the Stokes parameters associated with a UHF emission map derived by Berge from 10.4 cm observations and reported by Roberts (ref. 65). Emission maps have since been improved, and Branson's smooth, single peak model, derived directly from his own 21 cm observations (ref. 46), is more reasonable.

McAdam (ref. 47) and Gulkis (ref. 48) report 75 cm wavelength observations which support the existence of a distribution extending to a greater distance from Jupiter than L = 3 or possibly additional flux peaks there. McAdam's results, obtained with a Mills cross, are of too low a resolution (more than 2 radii) to warrant acceptance of his conclusion that a significant fraction of the radiation is generated near L = 6 (refs. 18 and 48). Gulkis' results (ref. 48), obtained from the observation of a lunar occultation of Jupiter with a single 140-foot radio telescope, suggest a more modest breadth, i.e., L = 4 or 5. On this basis it is reasonable to conclude that the uncertainties in the flux levels at L = 3 or beyond should be taken as sufficiently larger than those near L = 2 to permit the possibility of broad trapped radiation belts.

Warwick (ref. 18) has noted that if conservation of the magnetic moment of the electrons at the peak of the radiation belt is applied in an extrapolation to the magnetic field strengths expected in the solar wind near Jupiter, energies are predicted that are reasonable for electrons which share some of the proton energy as they are trapped by Jupiter's magnetic field from the solar wind. Thus, he suggested L-shell diffusion with magnetic moment conservation as a possible mechanism for the population of Jupiter's magnetosphere with electrons from the solar wind. The non-relativistic treatment of Davis and Chang (ref. 66) for the diffusion has been modified by Davis* to include correct relativistic relations among speed, momentum and energy. The resulting equation for the flux dependence on position in the diffusion region is

$$\Phi = \Phi_1 \left(\frac{L_1}{L}\right)^6 \left(\frac{E_1}{m_o c^2} + 1\right) \Bigg/ \left\{\left[\left(\frac{E_1}{m_o c^2} + 1\right)^2 - 1\right] \frac{L_1^3}{L^3} + 1\right\}^{1/2} \qquad (21)$$

*Private Communication, L. Davis Jr. (California Institute of Technology), Aug. 16, 1971.

where the flux and energy are Φ_1 and E_1 respectively at $L = L_1$. Additionally, for small L values the synchrotron radiation may be responsible for particle loss of energy. Thus, as a schematic representation of the L-dependence of the electron flux in Jupiter's belts, this monograph adopts the values quoted at the end of the section 2.7.4.1a for $L \leqslant 2$ and the dependence specified by equation (21) for $2 \leqslant L < 50$ where E_1 and Φ_1 are evaluated at $L_1 = 2$. An uncertainty factor of 3 is applied to the flux Φ everywhere. These results are consistent with the conclusions reached at the Jupiter Radiation Belt Workshop.** At any given time and location, zero flux is an appropriate lower limit because local particle loss mechanisms could be strong.

c. Distribution with Latitude

Because the radio observations display poorer angular resolutions parallel to Jupiter's magnetic dipole than perpendicular to it, they provide few details of the electron distribution with latitude. The 10-cm map (fig. 2, sec. 2.5.3.1) of Berge (ref. 24) suggests that the UHF source extends perhaps 1 R_J above and below the magnetic equator (compared to 2 R_J on either side of the dipole along the equatorial plane). This suggests that the characteristic latitude extent of the belts may be of the order of 26° ($\tan^{-1} 0.5$) with higher values to 45° not excluded. This monograph adopts for the latitude distribution a form proportional to $exp[-(\phi/\phi_0)^2]$ where $\phi_0 \simeq 30°$.

d. Directionality

The particle fluxes are probably greatest in directions perpendicular to the magnetic field lines, corresponding to large pitch angles near 90°, but this is likely to affect vehicle design in the same way as an isotropic flux distribution which accordingly is adopted here. Fluxes are calculated by multiplying the concentration and the corresponding speed; for electrons the speed of light c is appropriate, whereas the protons are subrelativistic and their speed depends on their energy. Electron concentrations and fluxes are summarized by the formulas in table XII (sec. 3.7) in which the specified uncertainty factors are large enough to bound likely unknown variations in position and time.

2.7.4.2 Relativistic Electron Energy

According to the synchrotron theory, a single relativistic electron of kinetic energy E_1 and pitch angle θ in the presence of a magnetic field of strength B emits UHF radiation within the wide frequency bandwidth, $W = (40\ MHz/MeV^2 Gauss) E_1^2 B sin\theta$, at frequencies near and below W itself (ref. 18). However Barber and Gower (ref. 67) quote a constant 2.5 times smaller. To estimate E_1, it is appropriate to select the values $\theta = 90°$, B = 2.0 gauss at L = 1.8 from the dipole moment (sec. 2.3.1), and W = 3000 MHz from the UHF observations which extend to wavelengths shorter than 10 cm; the resulting value is $E_1 = 6.2$ MeV (ref. 18). The reasonable uncertainties of factors 2 in B, 2.5 in the constant, and 2 in W lead to an uncertainty of a factor 3 in E_1. The value and uncertainty thus derived are adopted for the characteristic energy for the relativistic electrons in the flux peak near L = 1.8. The uncertainty includes many of the energy values suggested by several authors on the basis of the UHF data, 14 or 15 MeV (refs. 17 and 68), 10 MeV (refs. 48 and 67), and 1 to 30 MeV (ref. 46).

**Held 13-15 July 1971 at Jet Propulsion Laboratory, Pasadena, California.

Because the frequency distribution of the radiation emitted by a single electron is so broad, it would be possible to reproduce many of the characteristics of the observed UHF data from monoenergetic electrons (say 6.2 MeV) trapped on a single set of field lines (say at L = 1.8). Such sharp distributions seldom, of course, occur in nature, and the L-shell distribution has already been discussed (sec. 2.7.4.1). In order to compare the energy distributions suggested in the literature, figure 6 shows the ratio of N_E (the number of electrons with energies greater than E) to N_5 (the number with energies greater than 5 MeV, i.e., near the characteristic energy) at the location of the peak flux in each of several models, as a function of electron kinetic energy E. The order-of-magnitude energy distributions of Warwick (ref. 18) and Carr and Gulkis (ref. 17) are monoenergetic and are not intended to be fully realistic descriptions. Because it has been demonstrated on the basis of the theory (refs. 69 and 70) that a distribution in which dN is proportional to $E^{-1}\,dE$ over a wide but limited energy range leads to a flat, i.e., constant flux density, emission spectrum, many authors have adopted such a distribution. Some of these results (refs. 62, 64, and 46) are shown in figure 6. Haffner (ref. 63) has adopted an exponential energy distribution in which dN is proportional to $e^{-E/E_o}\,dE$ on the basis of his understanding of the energy distributions in the Earth's belts, extending to zero energy. Gulkis (ref. 48) discusses the energy spectra carefully and concludes that the failure of the observed intensity to increase at long wavelengths requires that the low-energy cutoff in the E^{-1} distribution occur at an energy smaller than, but comparable to, the characteristic energy. The conclusion, supported by reference 18, to be drawn from this survey is that the number of relativistic electrons at energies below perhaps 5 MeV must be small compared to the total, at least in those regions of greatest field strength where the observed UHF emission is generated. Such a requirement is not in agreement with the low-energy portions of the Haffner (ref. 63) and Koepp-Baker (ref. 64) distributions shown in figure 6. It is also an apparent consensus from references 46 and 48 that the distribution does not contain a significant fraction of electrons at energies greater than about 30 MeV.

The concept of a nearly monoenergetic distribution is supported by the theoretical possibility of an energy-selective acceleration mechanism, whereas that of a broad distribution, extending particularly to low energies, is supported by the likelihood of energy loss mechanisms which could smear out energy peaks. Although these theoretical arguments are inconclusive, the data (ref. 48) favor the adoption of a distribution which does not permit a significant fraction of the electrons to have energies more than a factor two or three different from the characteristic energy for the distribution.

To satisfy the foregoing suggestions, a new electron energy distribution is proposed here as an artificial but reasonable compromise between monoenergetic and exponential energy distributions. The flux Φ_E of electrons with energy greater than E and the differential flux $d\Phi$ are given for all relativistic values of E by

$$\Phi_E = \Phi_0 \left(1 + \frac{E}{E_0}\right) \exp\left(-\frac{E}{E_0}\right)$$

$$d\Phi = -\Phi \frac{E}{E_0^2} \exp\left(-\frac{E}{E_0}\right) dE \qquad (22)$$

Here Φ_0 is the flux parameter*, and E_0 is the local characteristic energy. The integrated number ratios corresponding to the distribution adopted (equation 22) have also been plotted in figure 6 for E_0=6.2 MeV. The adopted distribution has only 19 percent of its electrons at energies E<5MeV and only 5 percent at energies E>30MeV. The uncertainty in the flux at a given energy can be specified as part of the uncertainty in Φ_0 or E_0 without the additional specification of an uncertainty in the foregoing relative energy distribution functions.

The UHF data do not contain sufficient information from which the variation with position in the belts of the characteristic energy E_0 might be derived. Gulkis (ref. 48) claims that the reality of a broad emission source at long wavelengths perhaps extending to L = 3 at 75 cm, compared to L = 2 at 21 cm (sec. 2.7.4.1), would require greater fluxes of higher energy particles at greater distances from the dipole. He views this as unlikely on intuitive grounds, and Warwick (ref. 18) claims as well that the reality of such outer belts is not required because the supporting data have been obtained at marginal resolution. The theoretical treatment which has been applied (sec. 2.7.4.1) to the variation of the flux

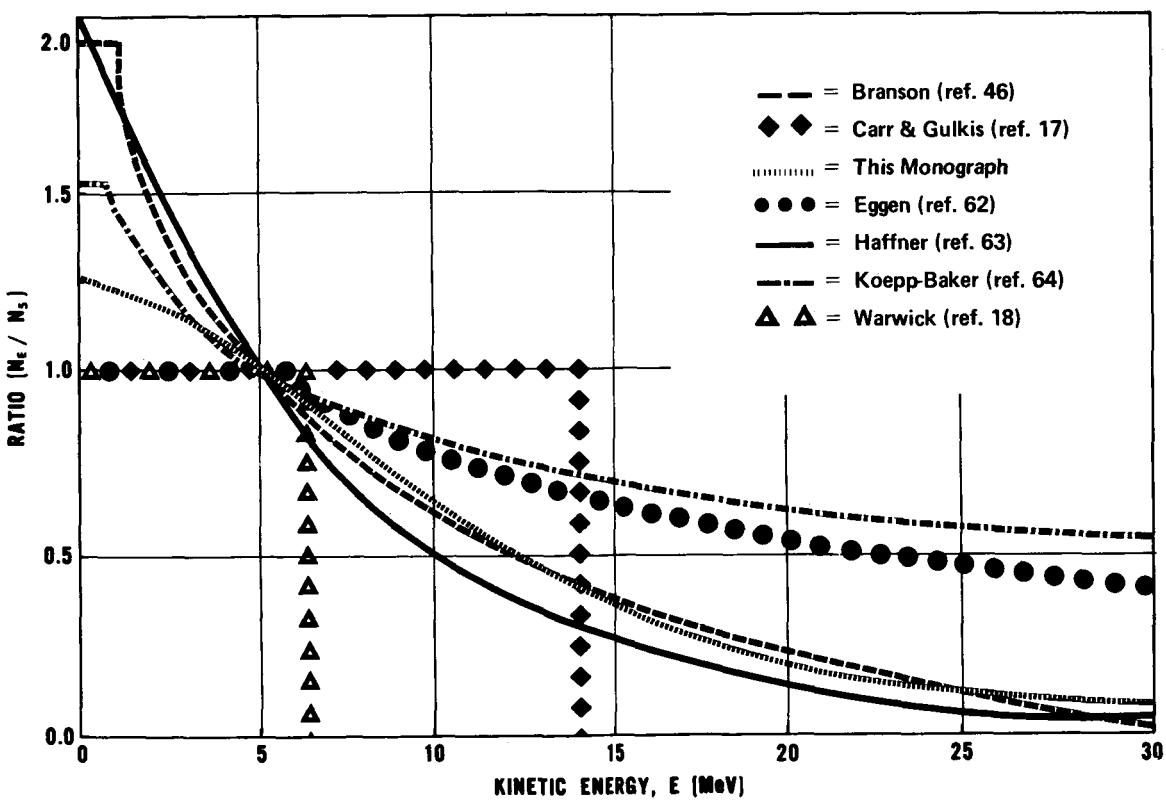

Figure 6.– Ratio of the number of relativistic electrons with kinetic energy ≥ E to the number with energy ≥ 5 MeV for proposed trapped radiation belt models, evaluated at their innermost flux peaks.

*See Symbols (app. A).

with position requires that the energy dependence reflect the conservation of the magnetic moment. Simple, relativistic considerations* lead to the relationship

$$E_o = m_o c^2 \left[\left\{ \left[\left(\frac{E_1}{m_o c^2} + 1 \right)^2 - 1 \right] \frac{L_1^3}{L^3} + 1 \right\}^{1/2} - 1 \right] \qquad (23)$$

where E_1 may be interpreted as the local characteristic energy at $L = L_1$ and E_o is the local characteristic energy elsewhere. For $E_o << m_o c^2$ equation (23) implies that $E_o L^3$ is approximately constant (independent of L). In the Earth's belts, the variation of energy is not so steep, with L exponents of 2 and 1.36 being reported as compatible with the data (refs. 18 and 63). For Jupiter, the synchroton radiation reduces the energy at small L values. Thus, this monograph adopts a nominal E_o = 6.2 MeV for $L \leqslant 2$ and the nominal energy elsewhere is joined to this value at $L_1 = 2$ by equation (23) for $2 \leqslant L < 50$. An uncertainty factor of 3 yields an appropriate upper limit for E_o at $L \leqslant 2$, and the upper limit energy elsewhere is joined to the value E_o = 19 MeV at $L_1 = 2$ by equation (23).

2.7.4.3 Energetic Protons

There are no positive Jupiter data from which proton fluxes in Jupiter's radiation belts can be inferred. Energy-dependent upper limits can be set on the basis of trapping by the magnetic field, but it is not considered likely that the proton population approaches these comparatively extreme upper limits. The three published studies which derive peak proton fluxes on the basis of Earth analogy do so in very different ways. The resulting characteristic energies diverge widely for the innermost belt, 0.1 to 4 MeV (ref. 62), 9.4 GeV (ref. 63), and 10^3 MeV (ref. 64). Various unpublished studies** apply cosmic ray albedo neutron decay theory to Jupiter and also derive widely divergent parameters for the protons.

This monograph adopts the conclusions** of several knowledgeable scientists that an L-shell diffusion model is appropriate for a nominal description of the protons, such that equations (21) and (23) describe the flux and energy for the entire range $1 < L < 50$. This assumes that at $L_1 = 2$ the flux is $\Phi_1 = 7 \times 10^6 \, cm^{-2} sec^{-1}$ (corresponding to a number density equal to that of the electrons) and the characteristic energy is E_1=60 MeV (equal to ten times that of the electrons). Because the uncertainties are so large, a considerably more severe upper limit model is adopted in which the fluxes are limited at intermediate L values by ion cyclotron instabilities.** The characteristic energy is given by equation(23) where E_1 = 100 MeV at $L_1 = 2$, but the dependence of the flux on L is the complicated function shown in figure 9 and table XII (sec. 3.7.3). Because local proton loss mechanisms such as satellite sweeping could be strong, an appropriate lower limit is zero flux.

2.7.4.4 Low Energy Particles

The arguments suggested in the foregoing sections do not apply at energies below about 1 MeV, and few observations have been so interpreted. This situation contrasts with the Earth's radiation belts in which particle energies in the range 1 keV to 1 MeV are common.

*Private Communication, L. Davis Jr. (California Institute of Technology), Aug. 16, 1971.
**Jupiter Radiation Belt Workshop, held 13-15 July 1971 at the Jet Propulsion Laboratory, Pasadena, Calif.

Warwick (ref. 18) and Goldreich and Lynden-Bell (ref. 21) require electrons of several keV energy in their HF burst generation mechanisms, but such particles would exist just above Jupiter's atmosphere and their fluxes are not intended to apply to the trapped radiation belts. Thus all that can be said about low energy particles is that their concentrations should not exceed the total magnetospheric plasma density (sec. 2.7.5) or the maximum which could be trapped in, and share the rotation of, Jupiter's magnetic field. The latter energy- and L-dependent limit can be simply derived for protons, and, assuming equal concentrations, the following limit also applies to electrons

$$N_E < \frac{(M_1/R_J^3)^2}{8\pi L^6 \left[E + (m_p/2)(LR_J\omega_0)^2\right]} . \tag{24}$$

If the nominal values for M_1 and R_J (secs. 2.3.1 and 2.1.2) are substituted in this expression, the numerical limit

$$N_E < \frac{3.6 \times 10^{12}}{L^6(E + 3.3L^2)} \tag{25}$$

is obtained for N_E in cm^{-3} and E in eV.

2.7.5 Magnetospheric Plasma

Theoretical discussions of the distribution of thermal ions and electrons in Jupiter's magnetosphere are complicated by the strong influences of magnetic, gravitational, and centrifugal forces as well as by uncertainties in the plasma temperature and source mechanism. Melrose (ref. 30) and Carr and Gulkis (ref. 17) present thorough mathematical and qualitative discussions of many of the foregoing considerations, and the importance of possible instability, fragmentation, and ring current formation is stressed. The present, inconclusive state of the art permits a range in electron number density of several orders of magnitude and leaves open whether the plasmasphere is cool and close to the planet or is warm and populates the magnetosphere. Consequently, very broad limits, representing extremes of values suggested by the literature are adopted herein. The plasma temperature ranges from 150°K (typical of ionospheric temperatures, section 2.7.6) to 10^5°K (refs. 17 and 71). The plasma electron density ranges from 0.1 cm^{-3} (credited to Brice by reference 17) to 10^7 cm^{-3} (a high ionosphere electron density estimate). For $L > 4.2$, the upper limit electron density which can be contained by the magnetic field is given by $10^{12}/L^8$ cm^{-3} (eq. 25 and ref. 17). The plasma corotates with Jupiter's magnetic field at least as far out as $L = 7$ or 8 (ref. 30).

There are few discussions based on observations. Warwick (ref. 18) argues that the total Faraday rotation experienced by an HF wave propagating from its source near $R = R_J$ to

the observer on Earth is less than one rotation. This reasoning requires that, if the electron (or proton) density N is either uniform or decreases with increasing distance R from Jupiter, the upper limit

$$N < \frac{(40\ \text{cm}^{-3})}{(1 - R_J^2/R^2)} \tag{26}$$

must be satisfied everywhere. The reality of the mode coupling which is basic in deriving this result has been challenged (ref. 17); and until this difference is settled, the foregoing cannot be adopted as a firm upper limit.

2.7.6 Ionosphere

There are two approaches to the description of Jupiter's ionosphere. The first is theoretical in which considerations such as photoionization and solar UV flux values (useful in understanding the Earth's ionosphere) are applied to Jupiter. The other approach is based on inferences from the HF bursts to which various generation mechanisms and requirements are applied. Within the rather large uncertainties inherent in the two approaches, agreement is quite satisfactory.

The theoretical approach is exemplified by the work of Gross and Rasool (ref. 72). Their results are supported by those derived by Shimizu (ref. 73), Hunten (ref. 74), Henry and McElroy (ref. 75), and Capone and Barrow (ref. 76) which consider similar processes in less detail. In reference 72, solar ultraviolet radiation at wavelengths of the order of 1000 Å is responsible for the photoionization of molecular and atomic hydrogen down to those altitudes at which it is fully absorbed. Secondary reactions, e.g., recombination, occur such that the equilibrium abundances of the species H_2, He, H, H^+, and e^- (listed roughly in order of decreasing concentration) are significant near the maximum of charged particle density, approximately 10^6 electrons/cm^3 and 10^6 protons/cm^3. The local gas pressure at that maximum is approximately 3 dyn/cm^2; atmospheric models suggest that this level occurs within the altitude range $z_0 = 250 \pm 150$ km (sec. 2.9.4). Below this altitude the electron density becomes negligible within several kilometers, whereas upward the electron density decreases roughly exponentially with a scale height approximately 100 km. According to the same authors, the ionospheric temperature ranges from 100 to 200°K.

Numerous arguments from mechanisms of HF burst generation have yielded electron density values independent of the foregoing considerations. Warwick (ref. 18) suggests that a maximum electron number density of the order of 10^7 cm^{-3} may be required to cause reflection of the HF bursts at the ionosphere. Investigations by Ellis (ref. 20) and Papadopoulos and Lerche (ref. 71) use various HF burst mechanisms to derive values within one or two orders of magnitude of the preceding density.

The presence in the Earth's ionosphere of several distinct layers of electron and ion concentration suggests that a one-layer model is probably too simplistic for Jupiter. For this reason and on the basis of the foregoing derived values, it is appropriate to adopt a peak

number density of 10^6 cm^{-3} for electrons and protons and to estimate the uncertainty as an order of magnitude in either direction.

2.8 Transfer Properties in the Magnetosphere and Ionosphere

The presence of magnetic fields and charged particles in the magnetosphere and ionosphere may lead to values for the electrical and thermal conductivity, opacity, and index of refraction different than those for a vacuum or a neutral gas. In most cases, these parameters must be evaluated by applying appropriate theory to the charged particle environment given in section 2.7 because there are scant data for determining them directly.

2.8.1 Electrical and Thermal Conductivity

The discussion by Hess and Mead (ref. 77) of the electrical conductivity of an ionized gas in a magnetic field can be applied to Jupiter's magnetosphere and ionosphere. The fact that the electron gyro-frequency is comparable to or greater than the collision frequency leads to strongly anisotropic electrical conductivity. In directions parallel to the magnetic field lines, current flow is not affected, and direct conductivity is appropriate. However, if the current is perpendicular to the field lines, it is inhibited by the inability of the electrons to move far from their original field lines and so the Pederson and Hall conductivities apply which are much smaller than the direct conductivity.

In the magnetosphere, the medium (secs. 2.3.2 and 2.7.5) is a highly ionized, low density hydrogen plasma in which Coulomb collisions among the ions and electrons determine the collision frequency. For this case Alfvén and Fälthammar (ref. 78) have graphed the value of the direct conductivity. It is nearly independent of the electron density but depends strongly on the temperature, approximately as $(1.35 \times 10^{-3}$ mho/meter$)T^{3/2}$ with T in °K. Thus, the temperature uncertainty in section 2.7.5 leads to the range of values 2.5 to 4.3×10^4 mho/meter for the direct conductivity. The formulae given by Hess and Mead (ref. 77) lead to Pederson and Hall conductivities which are less than 10^{-6} times the direct.

In the ionosphere, the medium (sec. 2.7.6) is a weakly ionized, low density plasma in which collisions with neutral particles determine the collision frequency. In this case the direct conductivity depends weakly on temperature but strongly on electron and neutral particle densities. The formulae of Hess and Mead (ref. 77) lead to the range of values $10^{-2\pm2}$ mho/meter for the direct conductivity at the peak of Jupiter's ionosphere. Their formulae also indicate that the Pederson and Hall conductivities are less than 10^{-2} times the direct. Because the concentration of neutral particles falls off rapidly with increasing altitude, the conductivities increase above the electron density peak.

For design purposes, it does not seem worthwhile to consider the foregoing complexities because it may not be possible to ascertain electron densities and temperatures and spacecraft component orientations in advance. Thus, for this monograph the range for electrical conductivity of 0 to 4.3×10^4 mho/meter for altitudes $z > 400$ km is adopted for the magnetosphere; for the ionosphere the range of 0 to 1 mho/meter is adopted for altitudes $100 < z < 400$ km.

The corresponding thermal conductivities are so small that conduction is negligible by comparison with radiative heat transport processes.

2.8.2 Opacity and Index of Refraction

The formulas and discussions provided by Ratcliffe (ref. 79) apply to the evaluation of the opacity and index of refraction. These quantities are related to the local electron gyro-frequency, the local plasma frequency, and the local electron-neutral particle collision frequency. For all electromagnetic radiation at wavelengths shorter than one meter, the wave frequency ($\nu > 300$ Hz) is much greater than the frequencies given in section 2.8.1 for the ionosphere and magnetosphere. Therefore, the expressions given by Ratcliffe (1959) for the index of refraction n reduce to

$$n^2 = 1 - \nu_P^2/\nu(\nu \pm \nu_B \cos\theta). \tag{27}$$

In equation (27), θ is the angle between the direction of propogation and the magnetic field B, ν_B is the electron gyro-frequency (given by $\nu_B = (2.8\ \text{MHz})B$ for B in gauss), and ν_P is the plasma frequency (given by $\nu_P = (9\ \text{kHz})N_e^{1/2}$ where N_e is the electron concentration in cm^{-3}).

For $N_e \leq 10^7\ \text{cm}^{-3}$, as given in section 2.7, the range of values for n is

$$1 \geq n \geq 1 - (4.5 \times 10^{-7})\lambda^2 \tag{28}$$

for wavelengths λ in cm. The corresponding opacity and optical thickness are negligible; this conclusion is supported by the observation that the thermal radiation from the atmosphere passes through these regions apparently without attenuation. For lower frequency radio waves (wavelengths longer than one meter), the foregoing frequencies, ν_B and ν_P, can be comparable to the wave frequency. Under such circumstances, there is some expectation that complex refraction, reflection, absorption, and Faraday rotation processes will occur in the ionosphere and magnetosphere. There are insufficient data to predict these processes with confidence, however.

2.9 Atmospheric Structure

The variable image of the disk of Jupiter, as observed telescopically in visible light, strongly indicates an active atmosphere of sufficient thickness to obscure any features of a solid planetary surface. Current understanding of the composition, temperature, pressure, density, and other significant physical quantities within this atmosphere and a set of numerical models are given in the following sections.

2.9.1 Composition

Recent papers by Owen (ref. 80) and McElroy (ref. 81) summarize the latest abundance results from visible and infrared spectra in which absorption lines of H_2, CH_4 and NH_3 can be identified as originating in the atmosphere of Jupiter. They conclude that the abundance

ratios are consistent with those of a solar mixture of elements which has evolved into simple hydrogen-bearing molecules with modification by saturation and condensation of some species, particularly NH_3 and H_2O. This conclusion is adopted herein although it must be stressed that absorption lines of He, a presumably important constituent, and minor constituents such as H_2O and Ne have not been observed in the spectra. In view of the uncertainty thereby introduced and the uncertain solar ratios of elements (particularly He), it is appropriate to consider the fractions by mass of all molecules other than H_2 uncertain by a factor of two in either direction. Table III shows the nominal and limiting compositions adopted for the atmosphere which is assumed homogeneous below the clouds. The nominal values of the H and He abundances are consistent with the results of Torres-Peimbert et al. (ref. 82), whereas the ratios of H to C, N, O, and Ne are based on Lambert (ref. 83).

2.9.2 Lower Atmosphere

The lower atmosphere is thought to be in hydrostatic equilibrium and convective to a very great depth. The variable appearance of the planet in visible light, analogous to weather patterns on the Earth (ref. 84), is attributed to large-scale cloud features which are condensates formed in upward convecting gas. Among the numerous references treating the clouds, the most complete in describing physical processes is that of Lewis (ref. 85) who concludes that the three most significant condensates in upper regions of the lower atmosphere are ammonia ice, NH_4SH, and water. The water may be ice or liquid with NH_3 in solution. Even in the presence of such condensates, the lapse rate is nearly equal to the "dry", i.e., condensation free, adiabatic value appropriate to the gas composition adopted.

In addition, a pressure-temperature correspondence at some point is required for a model. Attempts to establish such a correspondence from measurements of spectral line widths, equivalent widths, and their ratios are available but open to serious questions. In particular, "cloud top reflection layer" and ammonia saturation concepts (ref. 84) are not considered satisfactory; and on-going discussions of rotational temperatures and the associated abundance (refs. 86, 87, and 88) are incomplete. An alternate approach by Gillett et al. (ref. 41) combines the 125°K temperature measured near 12 μm with the calculated opacity of the dominant absorber H_2 at that wavelength to give an abundance of 12 km-atm H_2 * and a partial pressure of 1/4 atm H_2. This correspondence and the foregoing composition and lapse rate lead to a reasonable lower atmosphere model, similar to that of Owen (ref. 89), which explains many of the observed features of the reflection and emission spectra.

Observation of infrared (thermal) radiation emitted in the lower atmosphere at wavelengths longer than about five μm leads to two important conclusions: (1) that the disk is uniform within about 20 percent in brightness between 8 and 14 μm (ref. 44), and (2) that the planet radiates considerably more energy than it receives from the Sun (ref. 43). These conclusions suggest that lower atmospheric parameters need not be specifically associated

*This means that the H_2 on Jupiter above the level at which the radiation is emitted would form a layer 12 km thick if it were of uniform density at standard temperature and pressure (0° C and 1 atm) and no other gases were present.

with planetary latitudes and time of day but that these variations should be included within the uncertainty specified by a single set of models.

The most comprehensive survey (ref. 43) of Jupiter's infrared emission suggests an effective temperature near 134°K. Following Owen (ref. 89), it is reasonable to take the upper boundary of the lower atmosphere as the level at which the temperature reaches $(0.5)^{1/4}$ (134°K) = 113°K and to overlay that level with an isothermal stratosphere extending upward at least one scale height.

2.9.3 Upper Atmosphere

For upper atmosphere strata (above the regions of significant radiation reflection, absorption, and emission), observational data are meager. Wrixon (ref. 90) attributes narrow emission lines in the NH_3 absorption feature near 1.25 cm wavelength to an atmospheric inversion layer near 145°K temperature and 6.5 mb pressure. The most thorough theoretical analyses (refs. 72, 74, 75, and 91) rely heavily on calculations of equilibrium among absorption, photodissociation, photoionization, diffusion, and recombination of H_2, He, CH_4, H, H^+, and e^-. The results have some quantitative uncertainty because the rates are poorly known and qualitative aspects have been emphasized. The major conclusions are (1) that the temperatures are probably near 150°K (ref. 92) but because of possible effects of the solar cycle may range as high as 500°K (ref. 49) and (2) that molecular hydrogen predominates up to heights of the order of 500 km where pressures are less than 10^{-6} atm.

2.9.4 Model Atmospheres

Several numerical models of Jupiter's atmosphere have been presented in the literature; those of Kuiper (ref. 84), Gross and Rasool (ref. 72), Trafton (ref. 93), and Lewis (ref. 85) emphasize distinct, important aspects of the physical processes involved. Except for that of Smith and Weidner (ref. 94), based on the work of Gross and Rasool (ref. 72), none of the available models completely tabulates the basic parameters of height, temperature, pressure, and density. Besides, the models do not incorporate some of the recent observational information cited in the foregoing sections. Therefore, it has seemed appropriate to derive a new set of models. These models assume hydrostatic equilibrium and the perfect gas law and follow smoothly varying adiabatic lapse rates in the troposphere (app. D). Local adjustments of the troposphere lapse rate for the partial replacement of convective transport by radiative equilibrium and for the inclusion of "wet" saturation and cloud condensation effects have not been made because these additional complications were considered unwarranted in view of other large uncertainties.

The nominal model has been constructed with the constant values of T_e = 134°K, g = 2500 cm/sec^2, and u = 2.30 which correspond to the "nominal" composition and other quantities shown in table III. The convective troposphere has an adiabatic lapse rate near -2°K/km, extends indefinitely downward from the tropopause boundary temperature of 113°K, and includes the correspondence level established at P = 0.30 atm and T = 125°K. Above the tropopause an isothermal stratosphere extends upward one scale height (16.3 km). Above the stratosphere an inversion layer of constant (P/T)(dT/dP) is

limited by an uppermost level at which P = 6.5 mb and T = 145°K. An isothermal region extends indefinitely upward from the latter level.

The limiting models are "cool" and "warm" in the sense that for a given pressure of the nominal model they provide extremes of temperature and density which are thought to bracket the range of possible Jupiter values. The values for model construction were selected as reasonable limits to the nominal values and are given in table III. The numerical values calculated for these models are based on the atmospheric relationships described in appendix D, and are given in tables XIV, XV, and XVI for the pressure range between 2×10^{-7} and 10^3 atmospheres beyond which various assumptions become insupportable. By analogy with the Earth, zero altitude is set at the level at which the pressure P equals one atmosphere in all three models. This level is near the ammonia clouds (sec. 2.10) and corresponds to the optical surface or limb of the planet. The profiles of pressure, temperature, density, and altitude are shown in figures 10 through 14 (sec. 3.9).

2.10 Cloud Properties

2.10.1 Observations

Monitoring of the planet Jupiter visually and photographically has resulted in the accumulation of a great deal of detailed information about the visible markings. Representative extended and brief summaries of such information appear in Peek (ref. 95) and Michaux (ref. 9), respectively. The changeable positions, sizes, shapes, and colors of both the short-lived and permanent markings have led to the conclusion that the visible atmospheric layers are affected by both winds and clouds.

Beyond approximately ±50° latitude are the two polar regions which are dark and featureless at the resolution and wavelengths observed from the Earth. At lower latitudes the planet has stripes parallel to the equator, classified as zones and belts. As usually observed from the Earth in visible light, the zones are bright and the belts dark. Their latitudes and relative and absolute brightnesses vary with longitude, time, and wavelength of observation, i.e., color effects are important. The semi-permanent, well documented, generally uniform belts and zones occasionally are divided by thin bands also parallel to the equator and sometimes are blemished by light or dark spots whose motions in latitude and longitude have provided information on planetary rotation and atmospheric currents (sec. 2.11). These spots have characteristic horizontal dimensions ranging from 1000 to 10 000 km and lifetimes ranging from a few hours to weeks. Their resolution is marginal from Earth observations so that very little is known about their actual properties. The spots are comparable in size and possibly in nature to major weather systems in the Earth's atmosphere.

One much larger feature has existed for at least three centuries, namely the Great Red Spot. In a presentation of recent observational results, Solberg (refs. 96 and 97) reports that the Red Spot usually contrasts sharply with its surroundings in light of wavelengths $\lambda < 5000$ Å (very dark). Its oval shape extends horizontally about 13 000 km in latitude and 40 000 km in longitude, and its area varies by about 50 percent. The latitude of its center is usually within 3° of 22° South. Its longitude oscillates with an amplitude near 0°.8

TABLE III

COMPOSITIONS AND OTHER PARAMETERS
FOR MODEL ATMOSPHERES OF JUPITER*

PARAMETER		COOL MODEL	NOMINAL MODEL	WARM MODEL
Fractions by mass (or weight)	H_2	0.50696	0.75348	0.87674
	He	0.46000	0.23000	0.11500
	CH_4	0.00857	0.00429	0.00214
	NH_3	0.00219	0.00109	0.00055
	H_2O	0.01601	0.00800	0.00400
	Ne	0.00229	0.00115	0.00057
	others	0.00398	0.00199	0.00100
Fractions by number (or volume)	H_2	0.68454	0.86578	0.93754
	He	0.31057	0.13214	0.06149
	CH_4	0.00145	0.00062	0.00028
	NH_3	0.00035	0.00015	0.00007
	H_2O	0.00240	0.00102	0.00048
	Ne	0.00031	0.00013	0.00006
	others	0.00038	0.00016	0.00008
Mean molecular weight, u (grams/mole)		2.70	2.30	2.14
Acceleration of gravity, g (cm/sec^2)		2700	2500	2300
Effective temperature, T_e (°K)		128	134	140
Troposphere lapse rate parameters	β_o	0.222	0.236	0.259
	K_1 (°K)	500	500	500
	K_2 (°K)	500	295	324
Correspondence level temperature (°K)		125	125	125
Correspondence level pressure (atm)		0.50	0.30	0.20
Stratosphere temperature (°K)		108	113	118
Stratosphere vertical extent (scale heights)		∞	1.0	1.0
Inversion level temperature (°K)		(none)	145	500
Inversion level pressure (atm)		(none)	0.0065	2×10^{-7}

*The zero of altitude, at the distance R_s from the center (eq. 1), is taken as having a pressure of 1 atm in all three models.

and a period near 90 days, and drifts with respect to longitude System II* at a rate of several degrees/year. The Red Spot's nature and how it retains its integrity are enigmatic although Hide (ref. 98) has developed the Taylor column hypothesis in which relatively uniform, stagnant fluid overlies some topographical feature in the rotating fluid which forms Jupiter's deep atmosphere.

2.10.2 Theories

Theories of cloud formation and structure have been applied to the vertical distribution of condensates in Jupiter's lower atmosphere (sec. 2.9.2). Techniques based on the analysis of Lewis (ref. 85) have been applied to the models given in section 2.9.4 with numerical data for the condensates of ammonia and water from the International Critical Tables (ref. 99) and Lange (ref. 100). Some of the cloud properties (calculated in accordance with app. D) are given in tables XIV, XV, and XVI and figures 10, 11, 13 and 14. Cloud altitudes, masses, and compositions, primarily H_2O and NH_3 ices with a dilute NH_3-H_2O solution replacing H_2O in the cool model, show broad ranges which may be exceeded in the real atmosphere for any of the following reasons: (1) additional condensates, particularly NH_4SH and NH_4Cl, may form clouds of their own or contaminate the ones considered, leading to non-uniform cloud structure and color (ref. 85); (2) convection may carry the condensates to other altitudes; and (3) in downward convecting regions (cooler than upward-moving ones at a given pressure), condensates are less likely to be present so there is a reasonable basis for equating downward convecting regions with Jupiter's dark belts. Lastly, by Earth analogy, it would not be surprising if storms were occasionally present in regions of high cloud activity, leading to rain, hail, snow, thunder and lightning within the lower atmosphere.

2.11 Atmospheric Motions

The properties of horizontal motions in the troposphere of Jupiter may be derived directly from the variable apparent positions of well-observed spots at latitudes up to 50°. Vertical motions, motions at polar latitudes, motions above the tropopause, and motions on distance scales smaller than about 1000 km can only be inferred from assumptions and theories consistent with the data. Roughly the motions may be classified as rotation and winds.

2.11.1 Rotation

The rotation rate derived from the radio observations is probably the most physically significant of the rates which have so far been deduced. Recent determinations of the rotation rate have been made from the periodicities in the temporal variations of both the UHF data (ref. 26) and the HF burst data (ref. 101). The resulting rotation periods agree within the associated uncertainties given in the foregoing two references; that from reference 101, $T_0 = 9^h\ 55^m\ 29\overset{s}{.}73 \pm 0\overset{s}{.}04$, is adopted here. Because the rotation rate is that of the planetary dipole magnetic field, it is probably also that of Jupiter's deep interior

*Rotational coordinate system, defined in Glossary (app. E).

where the field presumably is generated. This was recognized early in the history of the radio observations, and the then current value of the radio period $T_3 = 9^h\ 55^m\ 29^s.37$ was adopted in the definition of longitude in System III (1957.0)* to which Jupiter's radio events are often referred (ref. 9).

Rotation periods derived from the observed positions of spots and other visible features on the planetary disk have a range of several minutes although the uncertainty of the period of any given spot observed for several rotations may be near ±1 second. Averages over such periods resulted in the adoption of two distinct periods, $T_1 = 9^h\,50^m\,30^s.003$ for latitudes within approximately ±10° of the equator and $T_2 = 9^h\,55^m\,40^s.632$ for all other latitudes. The longitude specifications for features observable on the planetary disk employ Systems I and II* which correspond to the foregoing periods. Reference 9 provides details and further references. The foregoing derivations of several values for the rotation period constitute substantial evidence for actual variation in rotation rates.

2.11.2 Winds

In accord with Chapman's concept of the horizontal surface motions on Jupiter (ref. 102), it is appropriate to define winds as any motions differing from solid body planetary rotation (assumed to have a period equal to that for Jupiter's radio sources). At latitudes within 50° of the equator, visual and photographic observations of the positions of spots and features on the Jupiter disk imply horizontal winds on scales larger than 1000 km that are zonal, i.e., parallel to the equator, and apparently unceasing. According to Chapman (ref. 102), the major winds can be described by (1) a westerly equatorial current between latitudes ±10° of average speed near 100 m/sec, corresponding to the fast System I* rotation period T_1, with local winds up to 10 m/sec in any direction with respect to the prevailing wind, (2) local winds between latitudes 10° and 50°N up to 10 m/sec in any direction with a frequent westerly current (the north temperature current) of speeds up to 100 m/sec within 10° of latitude 25°N, (3) local winds between latitudes 10° and 50°S up to 20 m/sec of which the most prominent and persistent (the circulating current) has an easterly component near 20°S and a westerly component near 25°S, and (4) a wind having counter-clockwise vorticity near the edges of the Great Red Spot of speeds near 10 m/sec. Additional details of the winds may be inferred from the observational analysis of Peek (ref. 95) and the theoretical analyses of Hide (ref. 103) and Ingersoll and Cuzzi (ref. 104). Winds have not been observed on a smaller scale, at latitudes beyond ±50°, or moving in vertical directions; but a reasonable assumption is that for such winds the characteristic speed of 10 m/sec holds. The limits in height and depth to which these winds might extend are unknown, but a reasonable assumption is that the horizontal winds may occur everywhere in the atmosphere, whereas the vertical ones are confined to the troposphere (sec. 2.10). The literature contains no estimate of the magnitude of wind shear.

2.12 Transfer Properties in the Atmosphere

Consideration of the atmospheric models in section 2.9.4 in conjunction with theoretical and empirical gas properties leads to values of transfer properties for which there are no

*Rotational coordinate system, defined in Glossary (app. E).

supporting observations. The following sections separately treat the various transfer properties.

2.12.1 Electromagnetic

At optical wavelengths, ($\lambda < 1$ μm), the major sources of opacity are (1) Rayleigh scattering by molecular hydrogen (ref. 7), (2) absorption and scattering by cloud particles (ref. 105), and (3) molecular absorption bands of CH_4 and NH_3 (ref. 106). These references lead to an opacity of $\kappa_R = (1.8 \pm 0.6) \times 10^{-5}/\lambda^4$ cm^2/g (for λ in μm) for Rayleigh scattering throughout the atmosphere. Within the clouds the opacity is expected to be considerably larger but cannot be predicted because the cloud masses and particle sizes are uncertain and probably variable. Absorption by the molecules CH_4 and NH_3 can be inferred from laboratory data but depends strongly on wavelength and weakly on pressure. Because of these complications, the opacity is taken herein as the Rayleigh scattering value above the clouds and zero visibility is adopted near and below the clouds, This simple approximation should be considered only as an interim model until a more rigorous solution becomes available.

The index of refraction n may be calculated from the information provided in the Smithsonian Physical Tables (ref. 107) and is roughly independent of wavelength. It is given by $n = 1 + (n_s - 1)\, PT_s/P_sT$ where n_s,P_s, and T_s represent values for the gas mixture at standard temperature and pressure. The quantity $(n_s - 1)$ has values in the range 0.00012 ± 0.00002 for the compositions listed in section 2.9.1 and $n = 1.00019 \pm 0.00003$ at the level at which P = 1 atm in the model atmospheres of section 2.9.4.

In the infrared, the opacity is that of collision-induced transitions in molecular hydrogen (refs. 93, 108, and 109) and of rotational bands of ammonia (ref. 110). Both opacities depend strongly on pressure, and simple formulae for the opacity cannot be obtained. A similarly complex situation exists in the microwave region where the opacity results not only from the molecular hydrogen absorption but also from the center and wings of the strong ammonia band near 1.3 cm wavelength (refs. 90 and 111). The brightness temperature data (sec. 2.5.2) for the Jupiter disk indicate that the opacity decreases as the wavelength increases beyond this band and that optical depth unity is reached at pressures of the order of magnitude of a few atmospheres near 10 cm wavelength. It is thus reasonable to expect that communications wavelengths greater than 10 cm would encounter less atmospheric absorption and would be able to penetrate deeper layers of the atmosphere. In addition, however, the possibly complex transmission properties of the ionosphere (sec. 2.8) must be considered at wavelengths much longer than 100 cm.

The electrical conductivity of gas mixtures involves complex, unpredictable phenomena, and the important effects of impurities are uncertain (ref. 112). However, Jupiter's atmosphere is expected to be an excellent insulator like the Earth's atmosphere.

2.12.2 Mechanical and Thermal

The calculation of viscosity and thermal conductivity is simplified by the graphical procedures in reference 113. The application of these techniques to the gas mixtures of

section 2.9 yields temperature-dependent values of the viscosity η and thermal conductivity λ_t which can be summarized for the range of the model atmospheres by

$$\log \eta = (0.4 \pm 0.1) + (0.65)\log T \tag{29}$$

and

$$\log \lambda_t = -(5.3 \pm 0.1) + (0.77)\log T \tag{30}$$

where T must be in °K, η in micropoise,* and λ_t in cal/cm-sec°K. The uncertainty arises primarily from the range of model compositions and the inaccuracy of the log-linear fit. Neither of the uncertainty factors depends on pressure or density.

The range of specific heat values for molecular hydrogen (ref. 114) is so broad for the range of atmospheric temperatures that the variations added by the inclusion of other constituents and condensates are not significant. That range is specified simply by $C_v = 21 \pm 7$ joule/mole°K and $C_p = 29 \pm 7$ joule/mole°K. The ratio of specific heats has the corresponding range of $\gamma = 1.45 \pm 0.15$. Inclusion of the range of molecular weights in the formula for the speed of sound, $c_s = (\gamma R_g T/u)^{1/2}$ where T is in °K, yields $c_s = (70 \pm 10$ m/sec)$T^{1/2}$.

2.13 Interior

The interior of Jupiter is that portion of the planet below the atmospheric altitudes at which radiation of various wavelengths escapes. The only compositions capable of retaining the low mean density of Jupiter (sec. 2.1.3) at the pressures required by its high gravity consist primarily of hydrogen and possibly include helium and other elements per table III. Theoretical models of the interior have been constructed by DeMarcus (ref. 115) and refined by Peebles (ref. 116); thermal effects are included in references 117, 118, and 119. The models suggest the following probable conclusions. (1) The planet is fluid either everywhere or throughout much of its bulk with the metallic phase of hydrogen being likely in the central regions; a small, heavy-element core is not excluded. (2) The pressure, density, and temperature increase in moving inward; the rate of increase is uncertain because the equation of state is poorly known. The temperature reaches values near the center of the order of magnitude of 10^4°K. (3) Energy is released to the exterior from cooling and gravitational contraction at the luminosity suggested in section 2.5.2. (4) The energy is transported by convection in most layers of the planet, and electron conduction is significant elsewhere. (5) Convection in the rotating, conducting fluid hydrogen interior is responsible for the maintenance of the planetary magnetic field. (The magneto-hydrodynamic processes involved are not well understood.) (6) Although phase transitions may occur even in the probably chemically homogeneous interior, they do not constitute a rigid, solid "surface" at any level but are characterized by density and viscosity graduation over a radial distance scale of kilometers or greater. Therefore, the atmosphere is considered to be an extension of the interior rather than a distinct entity.

*One micropoise equals 10^{-7}Ns/m^2.

3. CRITERIA

The following descriptions of the physical properties of the environment of Jupiter are recommended for application to the design of spacecraft intended to function within that environment. When uncertainty estimates or limiting values are given, they represent the extreme range of possible values to be used for design although the real environment probably will provide some surprises. For design purposes the probability that a particular environmental value is appropriate is nearly uniform within range but greatest at the nominal value.

3.1 Physical Properties

Values and uncertainties for Jupiter's mass, radius, figure, moments of inertia, rotation, and angular momentum are presented in table IV. In visible light the planet is axially symmetric about the rotation axis and has radius values R_s which depend on latitude ϕ through the relationship

$$R_s = R_J[1 - \epsilon(\sin \phi)^2]. \tag{31}$$

The planet is gaseous to at least 1000 km below the radius specified by equation 31. Jupiter does not have a readily identifiable solid or liquid surface.

3.2 Gravity Field

Table V gives parameters and their uncertainties for Jupiter's gravitational field.

3.3 Magnetic Field and Magnetosphere

The parameters of Jupiter's magnetic field are given in table VI. Appendix B specifies the magnetic field components and lines of force in terms of the parameters. Jupiter's northern hemisphere contains the north-seeking end of the magnetic dipole. The uncertainties in table VI include the field strength ranges expected on the basis of the small dipole inclination and displacement from Jupiter's rotational axis and geometric center. Jupiter's magnetic field dominates within the elongated, teardrop-shaped magnetosphere whose dimensions are given in table VI.

3.4 Electric Fields

Static electric fields of intensity $0 \leq \mathcal{E} \leq (14 \text{ volts/meter})(R_J/R)^2$ occur in the magnetosphere and ionosphere, in any direction, but usually perpendicular to the magnetic lines of force.

In the troposphere, field strengths up to 3×10^4 volts/meter on the scale of kilometers and hours may occur in the neighborhood of cloud formations. Field strengths up to 10^6 volts/meter on the scale of centimeters and seconds may occur prior to strokes of lightning.

TABLE IV

PHYSICAL PARAMETERS OF JUPITER

Distance from Sun	$r = 5.20 \pm 0.25$ AU
Period of revolution about Sun	$T = 11.862$ years
Mass of planet, excluding satellites	$M_J = (1.899 \pm 0.002) \times 10^{30}$ gram
Equatorial radius	$R_J = 71422 \pm 200$ km
Mean density	$\bar{\rho} = 1.32 \pm 0.01$ g/cm^3
Flattening (dynamical)	$\epsilon = 0.0645 \pm 0.0008$
Period of rotation	$T_0 = 9^h\ 55^m\ 29^s.73 \pm 0^s.04$
Rotational angular velocity	$\omega_0 = (1.758531 \pm 0.000002) \times 10^{-4}$ rad/sec
Angular momentum	$C\omega_0 = (4.3 \pm 0.2) \times 10^{45}$ g cm^2/sec
Celestial coordinates of North Pole	$\alpha_R = 17^h\ 52^m\ 0^s.84 + 0^s.247(t - 1919.0)$ $\delta_R = +64^\circ\ 33'34''.6 - 0''.60(t - 1910.0)$
Moment of inertia about rotational axis	$C = (2.4 \pm 0.1) \times 10^{49}$ g cm^2
Moment of inertia about equatorial axes	$A = (2.25 \pm 0.1) \times 10^{49}$ g cm^2

TABLE V

GRAVITATIONAL PARAMETERS OF JUPITER

Gravitational potential in an inertial coördinate system at distance R from Jupiter	$\Psi = -(1774 \pm 30\ km^2/sec^2)(R_J/R)$
Escape velocity at distance R	$(-2\Psi)^{1/2} = (59.6 \pm 0.6\ km/sec)(R_J/R)^{1/2}$
Period of Keplerian orbit of semi-major axis a	$T_a = (2.95\ hour)(a/R_J)^{3/2}$
Atmospheric acceleration of gravity –	
Magnitude (includes rotation)	$g = 2500 \pm 200\ cm/sec^2$
Equatorward deflection from jovicentric direction at latitude ϕ	$\eta_1 = (3°.70 \pm 0°.03) \sin 2\phi$

TABLE VI

PARAMETERS OF JUPITER'S MAGNETIC FIELD AND MAGNETOSPHERE

Dipole Moment (centered with respect to planet)	$M_1 = (4 \times 2^{\pm 1}) \times 10^{30}$ gauss-cm^3
Atmospheric field strength –	
At equator	$M_1/R_J^3 = 12 \times 2^{\pm 1}$ gauss
At poles	$2M_1/R_J^3 = 24 \times 2^{\pm 1}$ gauss
Magnetosphere dimensions –	
Standoff in solar direction	$50 \pm 20\ R_J$
Length in anti-solar direction	$> 100\ R_J$

3.5 Electromagnetic Radiation

3.5.1 Above the Tropopause

Beyond Jupiter's atmosphere (here the tropopause at altitude $z = 35 \pm 15$ km is the appropriate limit), the formulae in table VII specify the ranges of intensities, fluxes, and temperatures associated with the electromagnetic radiation environment under conditions of maximum illumination. Under partial illumination, total shadowing, or eclipse the values for intensities and fluxes range down to zero from the maximum illumination conditions of table VII and temperatures range down to $3^{\circ}K$. The wavelength of interest determines which of the radiation sources listed in table VII should be considered. Figure 7 shows the geometric albedo p and brightness temperature T_{BD} as functions of the wavelength. In table VII the quantity D is the approximate path length of the line of sight through the schematic synchrotron emission volume shown in figure 8.

In addition, Jupiter's satellites and the other planets constitute light sources, but their fluxes near Jupiter are minor compared to the sources listed in table VII. Their positions are published annually in the *American Ephemeris and Nautical Almanac* (ref. 16), and their visual magnitudes and colors are specified by

$$m_v = (m_0 \pm 0.3) + 5 \log r \Delta + (0.03 \pm 0.02)\alpha \qquad (32)$$

and the parameters in table IX where α is in degrees, and r and Δ in AU. The radiation from stars and other non-solar-system objects is identical to that beyond the Earth's atmosphere.

3.5.2 Below the Tropopause

Below the tropopause, i.e., altitudes $z < 35 \pm 15$ km, the maximum contributions of the Sun and the synchrotron source are identical to those specified in table VII which uses the geometric albedo p and brightness temperature T_{BD} given in figure 7. The reflected sunlight intensity and flux in table VII are appropriate but must be considered omnidirectional to account for the maximum scattered light. The thermal radiation is specified by table VIII. In addition, sporadic lightning may require that light-sensitive surfaces be covered when local meteorological conditions are stormy.

Radiation and its effects at wavelengths shorter than 1 Å (γ-rays) should be ignored. The power emitted sporadically in the HF bursts near Jupiter ranges up to 4×10^{16} erg/sec at wavelengths longer than 7.5 meters; intensities at wavelengths longer than 1 meter are unknown but probably high compared to communications intensities.

3.6 Satellites and Meteoroids

Four categories of known satellites of Jupiter are listed in table X which specifies some of their properties. Additional photometric data for the Galilean satellites are given in section 3.5. Detailed ephemerides may be found in the *American Ephemeris and Nautical Almanac* (ref. 16) and the references specified there.

Within the volume centered on Jupiter of radius $500\ R_J$ and at latitudes within $\pm 30^{\circ}$, asteroidal meteoroids of mass density $3.5 \times 2^{\pm 1}$ g/cm^3 and relative velocity

TABLE VII

ELECTROMAGNETIC RADIATION PARAMETERS NEAR JUPITER WITH MAXIMUM ILLUMINATION

Parameters	Direct Sunlight*	Reflected Sunlight*	Thermal Radiation**	Synchrotron UHF Radiation***
Wavelength	$1\ \text{Å} < \lambda < 100$ cm	$1\ \text{Å} < \lambda < 10\ \mu$m	$1\ \mu\text{m} < \lambda < 100$ cm	$1\text{ cm} < \lambda < 100$ cm
Intensity — Power/Area-wavelength-solid angle	$I_\lambda = \dfrac{P_\lambda}{(0.000068\ \text{sterad})}$	$I_\lambda = \dfrac{pP_\lambda}{(90 \pm 10)}$	$I_\lambda = B_\lambda(T_{BD})$	
Power/Area-frequency-solid angle			$I_\nu = B_\nu(T_{BD})$	$I_\nu = 2kT_{BS}/\lambda^2$
Flux — Power/Area-wavelength	$F_\lambda = \dfrac{P_\lambda}{r^2}$	$F_\lambda = \dfrac{pP_\lambda}{(27 \pm 3)(R/R_J)^2}$	$F_\lambda = \dfrac{\pi B_\lambda(T_{BD})}{(R/R_J)^2}$	
Power/Area-frequency			$F_\nu = \dfrac{\pi B_\nu(T_{BD})}{(R/R_J)^2}$	$F_\nu = \dfrac{(5 \pm 2) \times 10^8}{4 + (R/R_J)^2}$ FU
Integrated Flux — Power/Area-	$F = \dfrac{(1.353 \pm 0.021) \times 10^6}{r^2}\left(\dfrac{\text{erg}}{\text{cm}^2\text{sec}}\right)$	$F = \dfrac{(1.4 \pm 0.2) \times 10^4}{(R/R_J)^2}\left(\dfrac{\text{erg}}{\text{cm}^2\text{sec}}\right)$	$F = \dfrac{(1.8 \pm 0.3) \times 10^4}{(R/R_J)^2}\left(\dfrac{\text{erg}}{\text{cm}^2\text{sec}}\right)$	$F = \dfrac{(15 \pm 7) \times 10^{-6}}{4 + (R/R_J)^2}\left(\dfrac{\text{erg}}{\text{cm}^2\text{sec}}\right)$
Brightness Temperature			T_{BD}	$T_{BS} = \dfrac{D\lambda^2}{R_J}(0.30 \pm 0.15)°\text{K}$
Effective Temperature	$5800 \pm 15°\text{K}$		$T_e = 134 \pm 6°\text{K}$	

*Solar irradiance from NASA SP-8005 (ref. 1), solar distance r in AU only, and geometric albedo p from figure 7.

**Brightness temperature T_{BD} from figure 7 and Planck functions $B_\lambda(T)$ and $B_\nu(T)$ from Allen (ref. 7) or elsewhere.

***Use λ in cm only and estimate D/R_J from figure 8 with D being the approximate path length of line of sight through the volume. Radiation is up to 30 percent linearly polarized.

TABLE VIII

THERMAL RADIATION PARAMETERS BELOW
THE TROPOPAUSE IN JUPITER'S ATMOSPHERE

Wavelength	$1\ \mu m < \lambda < 100$ cm
Intensities*	$I_\lambda = B_\lambda(t)$ $I_\nu = B_\nu(t)$
Fluxes*	$F_\lambda = \pi B_\lambda(t)$ $F_\nu = \pi B_\nu(t)$
Integrated Fluxes	$F = \begin{cases} (1.8 \pm 0.3) \times 10^4 \left(\frac{erg}{cm^2 sec}\right) & \text{for } T < 134°K \\ \left(\frac{T}{134}\right)^4 (1.8 \pm 0.3) \times 10^4 \left(\frac{erg}{cm^2 sec}\right) & \text{for } T > 134°K \end{cases}$
Brightness Temperature	t = larger of T and T_{BD}

*t is the larger of the brightness temperature T_{BD} shown in figure 7 and the local tropospheric temperature T (sec. 3.9); Planck functions $B_\lambda(T)$ and $B_\nu(T)$ from Allen (ref. 7) or elsewhere should be used.

$v = [v_s^2 + (R_J/R)(40\ km/sec)^2]^{1/2}$ have a concentration of particles of mass greater than M given by

$$log N_M = -31 \pm 1 - (0.8 \pm 0.1)(log M - 18.5) \quad (33)$$

where v_s is the spacecraft speed, N_M is in m^{-3}, and M is in grams ranging from 10^{-9} to 10^{20}. The corresponding isotropic meteoroid flux is $N_M v/4$. The observed, small satellites of Jupiter form the large-mass end of this distribution.

3.7 Charged Particles

3.7.1 Particle Types

Table XI presents formulas and parameters for galactic cosmic rays, solar protons, solar wind, low energy trapped radiation belts, magnetospheric plasma, and the ionosphere. Table XII

TABLE IX

MAGNITUDES AND COLORS FOR SATELLITES OF JUPITER AND PLANETS*

	m_0	U-B	B-V
Jupiter V (Amalthea)	6.3	–	–
I (Io)	- 1.90	1.30	1.17
II (Europa)	- 1.53	0.52	0.87
III (Ganymede)	- 2.16	0.50	0.83
IV (Callisto)	- 1.20	0.55	0.86
VI-XII	$\geq$ 7.0	–	–
Mercury	- 0.36	–	0.93
Venus	- 4.29	0.50	0.82
Earth	- 3.87	–	0.2
Mars	- 1.52	0.58	1.36
Jupiter	- 9.25	0.48	0.83
Saturn	- 8.88	0.58	1.04
Uranus	- 7.19	0.28	0.56
Neptune	- 6.87	0.21	0.41
Pluto	- 1.01	0.27	0.80

*Symbols defined in appendix A and parameters obtained from reference 38.

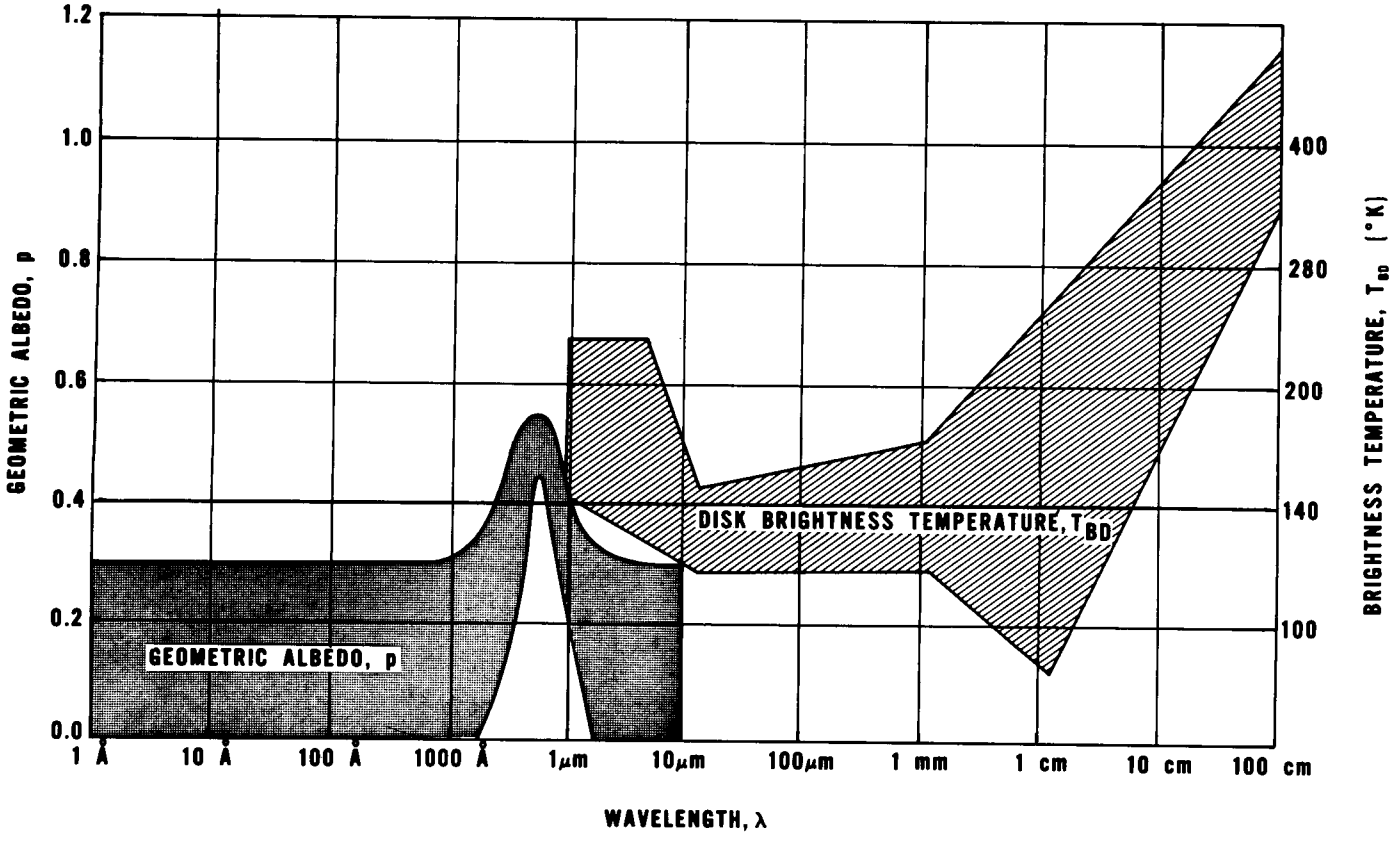

Figure 7.– Ranges of geometric albedo and disk brightness temperature as functions of wavelength.

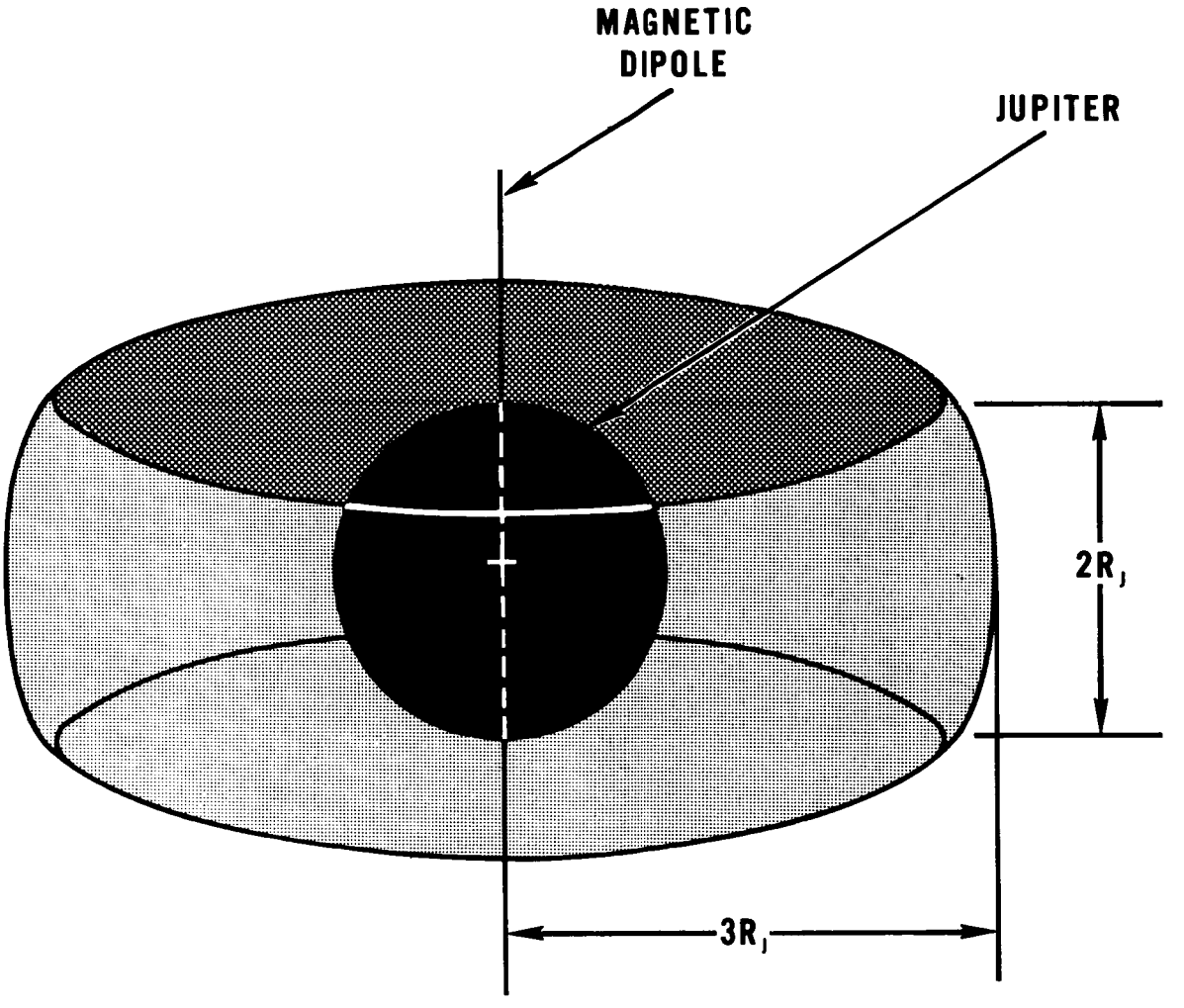

Figure 8.—Schematic volume for the calculation of the brightness temperature, T_{BS}, of Jupiter's synchrotron emission source.

TABLE X

PROPERTIES OF JUPITER'S SATELLITES

Satellite	Orbital Period (days)	Range of Distance from Jupiter (radii of Jupiter, R_J)	Maximum Jovicentric Latitude (degrees)	Orbital Speed (km/sec)	Radius R_n (km)	Mass M_n (g)
V (Amalthea)	0.498	2.539 ± 0.08	0.4	26	$100 \times 2^{\pm 1}$	$10^{22} \pm 1$
I (Io)	1.76914	5.905	0	17	1800 ± 160	$(7.2 \pm 0.6) \times 10^{25}$
II (Europa)	3.55118	9.396	0	14	1550 ± 100	$(4.7 \pm 0.1) \times 10^{25}$
III (Ganymede)	7.15455	14.99	0	11	2600 ± 400	$(15.5 \pm 0.2) \times 10^{25}$
IV (Callisto)	16.68902	26.36	0	8	2400 ± 400	$(9.6 \pm 0.8) \times 10^{25}$
VI	251	161 ± 25	29	3	$70 \times 2^{\pm 1}$	$10^{21.5 \pm 1}$
VII	260	164 ± 34	28	3	$10 \times 2^{\pm 1}$	$10^{19 \pm 1}$
X	253	164 ± 23	29	3	$7 \times 2^{\pm 1}$	$10^{18.5 \pm 1}$
VIII	737	300 ± 200	33	2	$8 \times 2^{\pm 1}$	$10^{19 \pm 1}$
IX	758	330 ± 120	23	2	$7 \times 2^{\pm 1}$	$10^{18.5 \pm 1}$
XI	692	313 ± 63	18	2	$7 \times 2^{\pm 1}$	$10^{18.5 \pm 1}$
XII	631	290 ± 50	34	2	$7 \times 2^{\pm 1}$	$10^{18.5 \pm 1}$

TABLE XI

PARAMETERS OF CHARGED PARTICLES NEAR JUPITER*

Particle	Location	Temperature, Energy or Velocity***	Number Density or Flux***
Galactic Cosmic Rays	Everywhere	$0.1 < E < 10^{10}$ GeV (GeV/nucleon for alphas)	$\Phi_E = A(E + m_0c^2)^{-1.5}$ for E in units of adjacent column Electrons: $0 \leqq A \leqq 0.02\ cm^{-2}sec^{-1}$ Protons: $0 \leqq A \leqq 10\ cm^{-2}sec^{-1}$ Alphas: $0 \leqq A \leqq 1\ cm^{-2}sec^{-1}$
Solar Cosmic Rays (Protons)	Everywhere	$10 < E < 10^4$ MeV	Sporadic, with fluxes between 0.0 and 1.0 times those specified in NASA TR R-169 (ref. 59)
Solar Wind (electrons and protons)	Beyond Magnetosphere (sec. 3.3)	$v = 320$ km/sec (up to 960 km/sec, at peak solar activity)	$N_0 = 0.2\ cm^{-3}$ (up to 2.0 cm^{-3}, at peak solar activity)
Trapped Radiation* (electrons and protons)	Within Magnetosphere (sec. 3.3)**	$10 < E < 10^6$ eV	$0 < N_E < \frac{3.6 \times 10^{12}}{(E+3.3L^2)L^6}\ cm^{-3}$ or $N_E < 10^7\ cm^{-3}$ whichever is smaller.
Magnetospheric Plasma (electrons and protons)	Within Magnetosphere (sec. 3.3)**	$150 < T < 10^5$°K $10^{-2} < E < 10$ eV	$0.1 < N_0 < 10^7\ cm^{-3}$ for $L \leqq 4.2$ $0 < N_0 < 10^{12}/L^8$ for $L \geqq 4.2$
Ionosphere (electrons and protons)	For $z > z_0$ where $z_0 = 250 \pm 150$ km	$T = 150 \pm 50$°K	$N_0 = (10^{6\pm1}\ cm^{-3})exp\left(-\frac{z - z_0}{100\ km}\right)$

*Except trapped radiation at energies > 1 MeV to which tables XII and XIII apply.

**Shares the rotation of Jupiter's magnetic field (sec. 3.3).

***As defined in appendix A.

TABLE XII

FORMULAS FOR ENERGETIC CHARGED PARTICLES IN JUPITER'S TRAPPED RADIATION BELTS

MODEL	LOCATION	FLUX PARAMETER, Φ_0 ($cm^{-2}\ sec^{-1}$)	CHARACTERISTIC ENERGY, E_0 (MeV)
NOMINAL ELECTRONS	$1 < L \leq 2$	2.0×10^7	6.2
	$2 \leq L < 50$	$\frac{1.7 \times 10^{10}}{L^6}\left(\frac{1377}{L^3} + 1\right)^{-1/2}$	$(0.51)\left[\left(\frac{1377}{L^3} + 1\right)^{1/2} - 1\right]$
UPPER LIMIT ELECTRONS	$1 < L \leq 2$	6.0×10^7	20.0
	$2 \leq L < 50$	$\frac{1.5 \times 10^{11}}{L^6}\left(\frac{12930}{L^3} + 1\right)^{-1/2}$	$(0.51)\left[\left(\frac{12930}{L^3} + 1\right)^{1/2} - 1\right]$
NOMINAL PROTONS	$1 < L < 50$	$\frac{4.7 \times 10^8}{L^6}\left(\frac{1.06}{L^3} + 1\right)^{-1/2}$	$(938)\left[\left(\frac{1.06}{L^3} + 1\right)^{1/2} - 1\right]$
UPPER LIMIT PROTONS	$1 < L \leq 6$	$\frac{1.0 \times 10^{12}}{L^6}\left(\frac{1.8}{L^3} + 1\right)^{-1/2}$	$(938)\left[\left(\frac{1.8}{L^3} + 1\right)^{1/2} - 1\right]$
	$6 \leq L \leq 12$	$(2.8 \times 10^{10})\, L^{-4} + (5.2 \times 10^7) \exp\left[-(12 - L)^2\right]$	
	$12 \leq L < 50$	$\frac{1.6 \times 10^{14}}{L^6}$	
DISTRIBUTIONS WITH ENERGY AND LATITUDE*	$\Phi_E = \Phi_0\left(1 + \frac{E}{E_0}\right) \exp\left(-\frac{E}{E_0} - \frac{\phi^2}{1000}\right)$		

* Latitude ϕ in degrees only.

TABLE XIII

ENERGETIC CHARGED PARTICLE FLUXES FOR INDIVIDUAL ENERGY INTERVALS AT THE LOCATION OF THE PEAK ELECTRON FLUXES IN JUPITER'S TRAPPED RADIATION BELTS (L = 2 and $\phi = 0$)

Particle Type	Energy Interval (MeV)	Flux, $(\Delta\Phi)_E$ in cm^{-2} sec^{-1}	
		Nominal	Upper Limit
Electrons	1-3	1.5×10^6	5.4×10^5
	3-10	7.9×10^6	4.8×10^6
	10-30	9.5×10^6	2.1×10^7
	30-100	9.3×10^5	3.1×10^7
	100-300	34	2.4×10^6
	300-1000	0.0	300
Protons	1-3	7.4×10^3	5.5×10^6
	3-10	7.8×10^4	6.0×10^7
	10-30	5.4×10^5	4.6×10^8
	30-100	2.8×10^6	3.2×10^9
	100-300	3.2×10^6	7.6×10^9
	300-1000	2.8×10^5	2.8×10^9
	1000-3000	7.0	7.0×10^6
	3000-10000	0.0	0.041

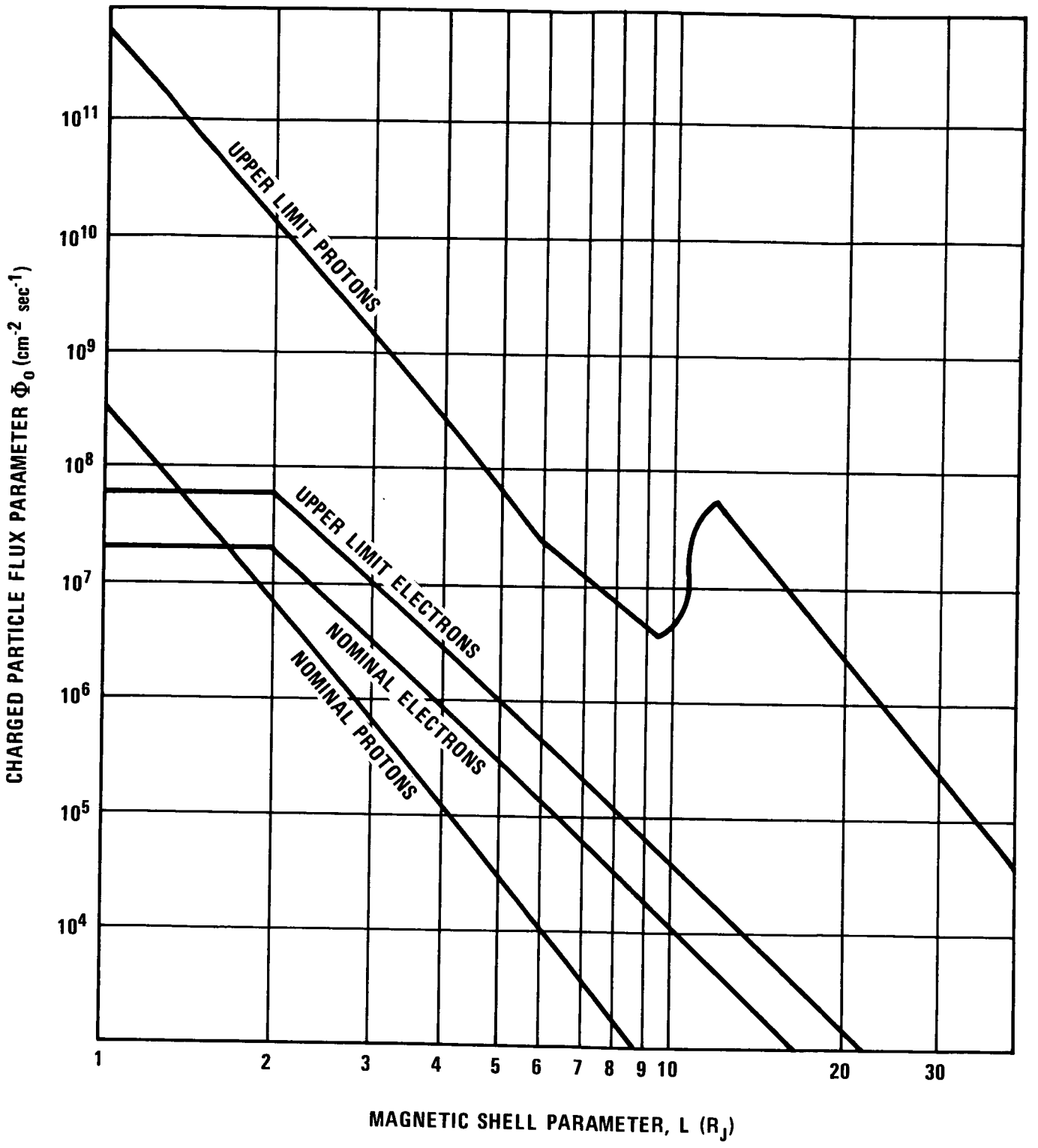

Figure 9. - Fluxes of charged particles in Jupiter's trapped radiation belts as functions of distance from the magnetic dipole in the magnetic equatorial plane.

presents formulas and parameters for relativistic electrons and energetic protons in the trapped radiation belts, and table XIII evaluates their nominal and upper limit fluxes in several energy intervals at the location of the peak electron fluxes in the belts (L=2 and ϕ=0).

3.7.2 Calculation of Low Energy Radiation Belt Number Densities

Upper limits to the number densities for trapped electrons and protons having energies less than 1 MeV are specified by the formulas given in table XI. The pertinent entry in table XI specifies the upper limit to the concentration N_E (in cm^{-3}) of particles of energy greater than or equal to E (in MeV) as a function of magnetic shell parameter L, subject to the condition that N_E does not exceed 10^7 cm^{-3}. In case a higher value for N_E is obtained, the upper limit is taken as 10^7 cm^{-3}. Although the upper limit specifies the maximum concentration at any energy, the concentration may not equal this upper limit at more than one energy at any given time and location.

3.7.3 Calculation of Radiation Belt Fluxes

To calculate particle fluxes from the formulas in table XII for a specific position (specified by distance R and latitude ϕ with respect to Jupiter) and energy interval (between E and E+ΔE), the following procedures should be employed. *1.* Calculate the magnetic shell parameter L from $L=R/R_J(\cos\phi)^2$. *2.* Evaluate the flux parameter Φ_0 (shown in figure 9) and the characteristic energy E_0 from the first several rows in the table, chosen according to the value of L, the particle type, and the model required. *3.* With the last formula in table XII, calculate Φ_E, the particle flux for energy greater than E, for both end-points of the energy interval and take the difference to obtain $(\Delta\Phi)_E$, the flux in the interval of interest.

At any given time and location, the minimum, or lower limit flux is zero.

3.8 Transfer Properties in the Magnetosphere and Ionosphere

The range of values for the anisotropic electrical conductivity in the magnetosphere (the altitude range between 400 km and 50 $\pm$20R_J) is 0 to 4.3 $\times$ 10^4 mho/meter. In the ionosphere, between 100 and 400 km altitude, the anisotropic conductivity range is 0 to 1 mho/meter. In both regions, thermal conduction is negligible compared to heat transport by radiative processes.

For electromagnetic radiation at wavelengths shorter than one meter (frequency $\nu > 300$ MHz), the index of refraction n is bounded by

$$1 \geq n \geq 1 - (4.5 \times 10^{-7})\lambda^2 \qquad (34)$$

where λ is the wavelength in cm. At these wavelengths the opacity and optical thickness of the ionosphere and magnetosphere are neglected. At wavelengths greater than one meter, unpredictable refraction, reflection, absorption, and Faraday rotation effects occur.

3.9 Atmospheric Structure

The nominal model atmosphere of Jupiter given in table XIV contains values for the temperature T, density ρ, altitude z, pressure and density scale heights H_p and H_ρ, and cloud mass w as functions of pressure P (for 0.2 mb $\leq$ P $\leq$ 1000 atm). Tables XV and XVI give the "cool" and "warm" model atmospheres which encompass observational uncertainty and variations expected with planetary latitude, time of day, and local features. The models represent cool and warm extremes at given pressures not altitudes. The compositions for the three models are given in table XVII which does not take into account condensation effects. For all models, the zero of altitude is arbitrarily set at a pressure of one Earth atmosphere (1.01325×10^6 dyn/cm^2) and corresponds to the distance from Jupiter's center of R_s, given by

$$R_s = R_J [1 - \epsilon(\sin \phi)^2] \tag{35}$$

where $R_J = 71\,422 \pm 200$ km, $\epsilon = 0.0645 \pm 0.0008$, ϕ is the latitude, and R_s specifies the level of the optical disk of the planet but not a real liquid or solid surface. Interpolation and extrapolation beyond the tabulated pressure range should be carried out linearly in *log* P, *log* T, *log* ρ, and z. Figures 10 through 14 present the three models graphically.

3.10 Cloud Properties

The ranges of altitude and mass of the clouds and their composition (primarily water and ammonia ices and solution with additional unknown coloring agents and minor compounds) are specified in tables XIV, XV, and XVI and figures 10, 11, 13 and 14. Condensates are expected to be common in the bright zones (rising gas) and infrequent in the dark belts (descending gas), but Jupiter's clouds like Earth's are associated with complex and hard-to-predict weather phenomena. Hazards to spacecraft from corrosive properties of the clouds and from occasional water and ammonia rain, hail, snow, thunder, and lightning are anticipated. Among the highly variable cloud features, the most distinctive and permanent is the Great Red Spot which is dark at wavelengths less than 5000 Å and drifts slowly in longitude but remains near 22° South latitude.

3.11 Atmospheric Motions

The planetary rotation underlying the atmosphere is prograde at an angular velocity $\omega_0 = (1.758531 \pm 0.000002) \times 10^{-4}$ radian/sec, corresponding to the radio period $T_0 = 9^h\,55^m\,29^s.73 \pm 0^s.04$. Within the convective troposphere (altitudes below 35 ±15 km), there exist subsonic prevailing zonal winds, westerly at approximately 100 m/sec within 10° of the equator and variable at 10 ±10 m/sec easterly or westerly elsewhere. In the same region turbulence (local horizontal and vertical winds) of order of magnitude 10 m/sec occurs in random directions with respect to the prevailing winds. Within the stratosphere and beyond (altitudes above 35 ±15 km), turbulence of the same magnitude occurs horizontally but not vertically. The strength of possible wind shear has not been estimated.

TABLE XIV

NOMINAL MODEL ATMOSPHERE OF JUPITER

P (atm)	T (°K)	ρ (g/cm^3)	z* (km)	H_p (km)	H_ρ (km)	w (mg/liter)	Remarks
2.00×10^{-7}	145.0	3.86×10^{-11}	313.4	21.0	21.0		
3.00×10^{-7}	145.0	5.80×10^{-11}	304.9	21.0	21.0		
1.00×10^{-6}	145.0	1.93×10^{-10}	279.7	21.0	21.0		
3.00×10^{-6}	145.0	5.80×10^{-10}	256.6	21.0	21.0		
1.00×10^{-5}	145.0	1.93×10^{-9}	231.4	21.0	21.0		
3.00×10^{-5}	145.0	5.80×10^{-9}	208.3	21.0	21.0		
1.00×10^{-4}	145.0	1.93×10^{-8}	183.1	21.0	21.0		
3.00×10^{-4}	145.0	5.80×10^{-8}	160.0	21.0	21.0		
0.00100	145.0	1.93×10^{-7}	134.8	21.0	21.0		
0.00300	145.0	5.80×10^{-7}	111.7	21.0	21.0		
0.00650	145.0	1.26×10^{-6}	95.5	21.0	21.0		Top of inversion layer
0.0100	139.0	2.02×10^{-6}	86.7	20.1	18.3		
0.0300	124.8	6.73×10^{-6}	65.7	18.1	16.4		
0.0829	113.0	2.06×10^{-5}	48.3	16.3	16.3		Stratopause
0.100	113.0	2.48×10^{-5}	45.2	16.3	16.3		
0.225	113.0	5.59×10^{-5}	31.9	16.3	16.3		Tropopause
0.267	120.0	6.24×10^{-5}	29.1	17.4	26.8		
0.300	125.0	6.72×10^{-5}	27.0	18.0	27.9	0.00119	Correspondence level
0.350	132.0	7.44×10^{-5}	24.1	19.1	29.3	0.00583	
0.406	139.0	8.20×10^{-5}	21.2	20.1	30.8	0.0243	
0.469	146.0	9.00×10^{-5}	18.3	21.1	32.3	0.0888	NH_3 ice cloud base
1.00	189.1	1.48×10^{-4}	0.0	27.3	41.2		Zero of altitude*
1.27	205.0	1.74×10^{-4}	-6.9	29.7	44.4		
1.80	230.0	2.20×10^{-4}	-17.8	33.3	49.5	0.0743	
2.13	243.0	2.46×10^{-4}	-23.6	35.1	52.1	0.292	
2.41	253.0	2.68×10^{-4}	-28.0	36.6	54.2	0.758	
2.76	264.2	2.93×10^{-4}	-33.0	38.2	56.4	2.02	H_2O ice cloud base
3.00	271.3	3.10×10^{-4}	-36.2	39.2	57.8		
10.0	395.8	7.08×10^{-4}	-96.7	57.2	82.5		
30.0	550.0	1.53×10^{-3}	-168.3	79.6	112.6		
100.0	777.0	3.61×10^{-3}	-282.8	112.4	156.3		
300.0	1052.6	7.99×10^{-3}	-427.2	152.3	209.1		
1000.0	1452.9	1.93×10^{-2}	-643.7	210.1	285.4		

*The zero of altitude is specified by equation 35 (sec. 3.9).

TABLE XV

COOL MODEL ATMOSPHERE OF JUPITER

P (atm)	T (°K)	ρ (g/cm^3)	z* (km)	H_p (km)	H_ρ (km)	w (mg/liter)	Remarks
2.00×10^{-7}	108.0	6.09×10^{-11}	192.8	12.3	12.3		
3.00×10^{-7}	108.0	9.14×10^{-11}	187.8	12.3	12.3		
1.00×10^{-6}	108.0	3.05×10^{-10}	173.0	12.3	12.3		
3.00×10^{-6}	108.0	9.14×10^{-10}	159.5	12.3	12.3		
1.00×10^{-5}	108.0	3.05×10^{-9}	144.6	12.3	12.3		
3.00×10^{-5}	108.0	9.14×10^{-9}	131.1	12.3	12.3		
1.00×10^{-4}	108.0	3.05×10^{-8}	116.3	12.3	12.3		
3.00×10^{-4}	108.0	9.14×10^{-8}	102.7	12.3	12.3		
0.00100	108.0	3.05×10^{-7}	87.9	12.3	12.3		
0.00300	108.0	9.14×10^{-7}	74.3	12.3	12.3		
0.0100	108.0	3.05×10^{-6}	59.5	12.3	12.3		
0.0300	108.0	9.14×10^{-6}	46.0	12.3	12.3		
0.100	108.0	3.05×10^{-5}	31.1	12.3	12.3		
0.259	108.0	7.88×10^{-5}	19.4	12.3	12.3		Tropopause
0.300	111.6	8.84×10^{-5}	17.6	12.7	16.4		
0.500	125.0	1.32×10^{-4}	10.7	14.3	18.3		Correspondence Level
0.833	140.0	1.96×10^{-4}	3.0	16.0	20.5	0.0276	
1.00	145.8	2.26×10^{-4}	0.0	16.6	21.4	0.0793	Zero of altitude*
1.14	150.0	2.49×10^{-4}	-2.2	17.1	22.0	0.162	
1.42	157.6	2.96×10^{-4}	-6.1	18.0	23.1	0.534	NH_3 ice cloud base
3.00	186.1	5.30×10^{-4}	-20.7	21.2	27.3		
10.0	243.1	1.35×10^{-3}	-50.0	27.7	35.6	0.406	
16.1	270.0	1.96×10^{-3}	-63.8	30.8	39.6	3.00	
22.1	290.0	2.51×10^{-3}	-74.1	33.1	42.5	10.3	
30.0	310.2	3.18×10^{-3}	-84.5	35.4	45.5	30.4	
32.3	315.4	3.37×10^{-3}	-87.2	36.0	46.3	39.2	Solution cloud base (NH_3-H_2O)
100.0	405.3	8.12×10^{-3}	-133.3	46.2	59.4		
300.0	517.2	0.0191	-190.9	59.0	75.8		
1000.0	675.7	0.0487	-272.3	77.1	99.1		

*The zero of altitude is specified by equation 35 (sec. 3.9).

TABLE XVI

WARM MODEL ATMOSPHERE OF JUPITER

P (atm)	T (°K)	ρ (g/cm^3)	z* (km)	H_p (km)	H_ρ (km)	w (mg/liter)	Remarks
2.00×10^{-7}	500.0	1.04×10^{-11}	634.8	84.5	75.8		
3.00×10^{-7}	477.4	1.64×10^{-11}	601.3	80.7	72.4		
1.00×10^{-6}	416.1	6.27×10^{-11}	510.6	70.3	63.1		
3.00×10^{-6}	367.1	2.13×10^{-10}	438.0	62.0	55.7		
1.00×10^{-5}	320.0	8.15×10^{-10}	368.2	54.1	48.5		
3.00×10^{-5}	282.3	2.77×10^{-9}	312.4	47.7	42.8		
1.00×10^{-4}	246.1	1.06×10^{-8}	258.7	41.6	37.3		
3.00×10^{-4}	217.1	3.60×10^{-8}	215.8	36.7	32.9		
0.00100	189.2	1.38×10^{-7}	174.5	32.0	28.7		
0.00300	166.9	4.69×10^{-7}	141.5	28.2	25.3		
0.0100	145.5	1.79×10^{-6}	109.8	24.6	22.1		
0.0300	128.4	6.09×10^{-6}	84.4	21.7	19.5		
0.0627	118.0	1.39×10^{-5}	69.0	19.9	19.9		Stratopause
0.100	118.0	2.21×10^{-5}	59.7	19.9	19.9		
0.171	118.0	3.77×10^{-5}	49.1	19.9	19.9		Tropopause
0.179	120.0	3.88×10^{-5}	48.2	20.3	31.8	0.000340	
0.200	125.0	4.17×10^{-5}	45.8	21.1	33.0	0.00119	Correspondence level
0.223	130.0	4.47×10^{-5}	43.5	22.0	34.3	0.00378	
0.248	135.0	4.78×10^{-5}	41.1	22.8	35.5	0.0110	
0.270	139.2	5.05×10^{-5}	39.2	23.5	36.6	0.0253	NH_3 ice cloud base
0.300	144.6	5.41×10^{-5}	36.6	24.4	37.9		
0.756	200.0	9.85×10^{-5}	9.9	33.8	51.7	0.00550	
0.871	210.0	1.08×10^{-4}	5.0	35.5	54.7	0.0180	
1.00	220.2	1.18×10^{-4}	0.0	37.2	56.6	0.0537	Zero of altitude*
1.06	225.0	1.23×10^{-4}	-2.4	38.0	57.8	0.0867	
1.21	235.0	1.34×10^{-4}	-7.3	39.7	60.2	0.221	
1.36	244.7	1.45×10^{-4}	-12.1	41.3	62.6	0.505	H_2O ice cloud base
3.00	318.6	2.45×10^{-4}	-49.5	53.8	80.4		
10.0	470.2	5.55×10^{-4}	-128.9	79.4	116.2		
30.0	661.4	1.18×10^{-3}	-233.0	111.8	160.9		
100.0	949.0	2.72×10^{-3}	-395.2	160.4	227.4		
300.0	1306.2	5.98×10^{-2}	-602.9	220.7	309.5		
1000.0	1837.3	1.42×10^{-2}	-919.9	310.5	413.3		

*The zero of altitude is specified by equation 35 (sec. 3.9).

TABLE XVII

COMPOSITIONS OF MODELS OF JUPITER'S ATMOSPHERE

Parameter		Cool Model	Nominal Model	Warm Model
Fractions by mass (or weight)	H_2	0.50696	0.75348	0.87674
	He	0.46000	0.23000	0.11500
	CH_4	0.00857	0.00429	0.00214
	NH_3	0.00219	0.00109	0.00055
	H_2O	0.01601	0.00800	0.00400
	Ne	0.00229	0.00115	0.00057
	others	0.00398	0.00199	0.00100
Fractions by number (or volume)	H_2	0.68454	0.86578	0.93754
	He	0.31057	0.13214	0.06149
	CH_4	0.00145	0.00062	0.00028
	NH_3	0.00035	0.00015	0.00007
	H_2O	0.00240	0.00102	0.00048
	Ne	0.00031	0.00013	0.00006
	others	0.00038	0.00016	0.00008
Mean molecular weight u (grams/mole)		2.70	2.30	2.14

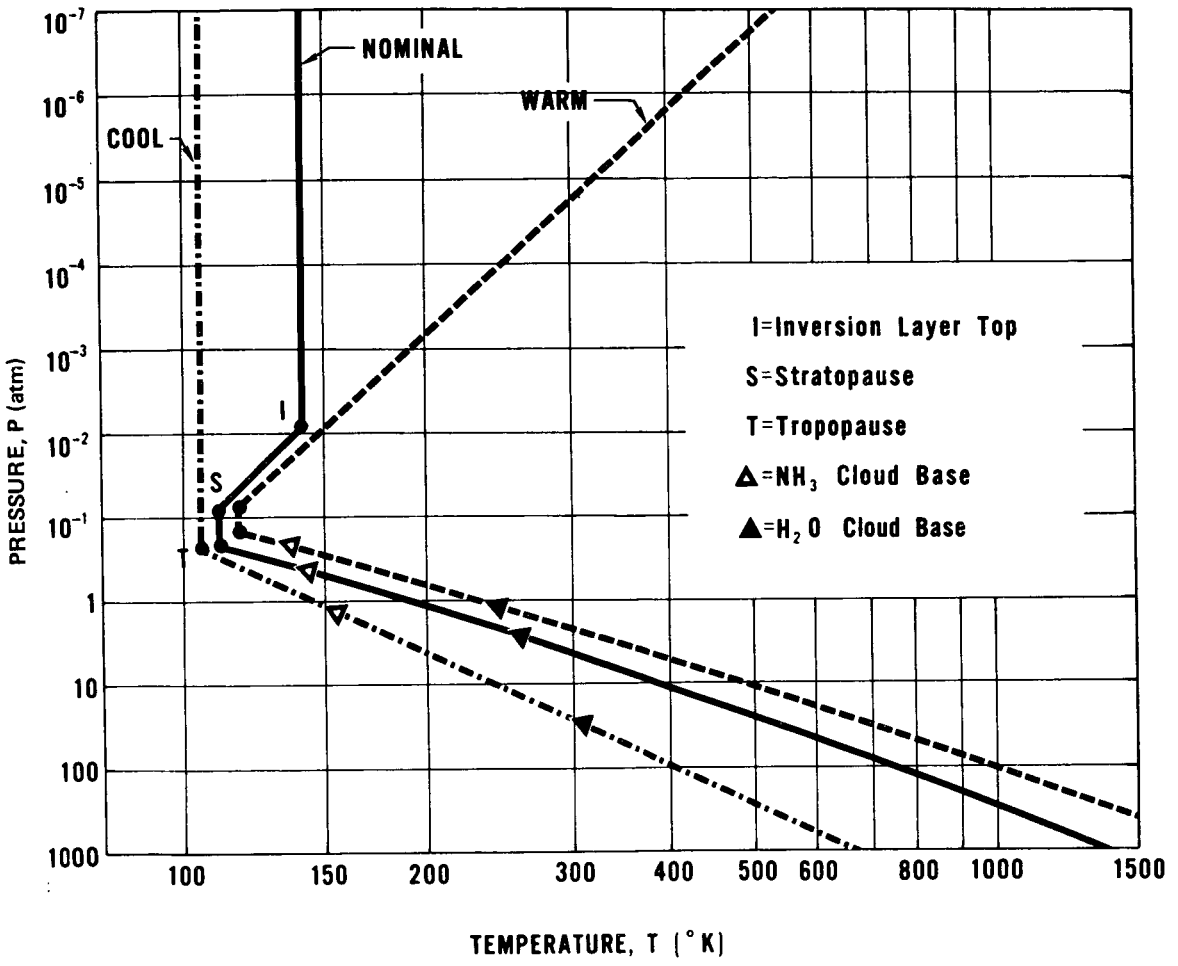

Figure 10.–Pressure vs temperature for the Jupiter model atmospheres.

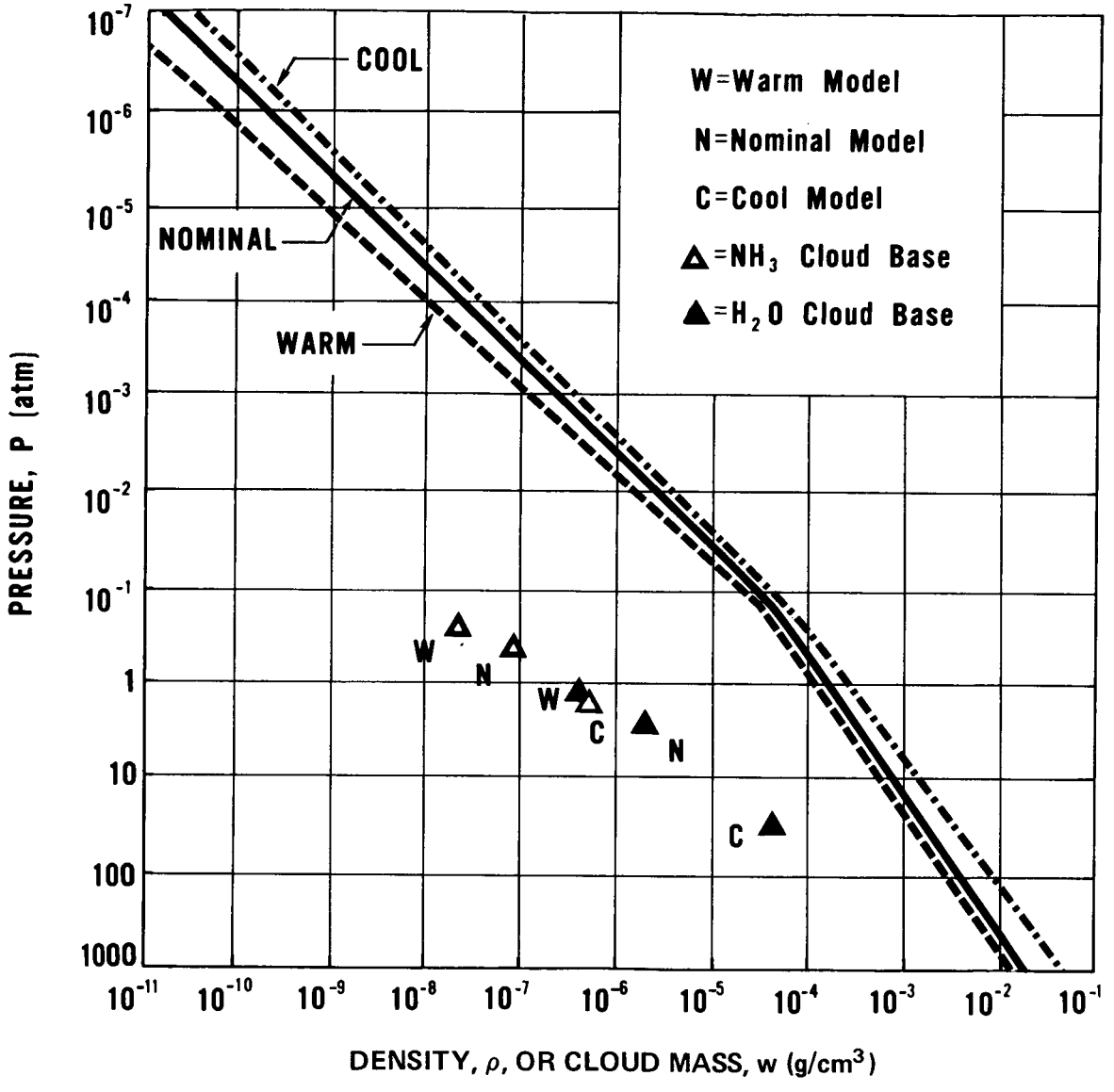

Figure 11.—Pressure vs density and cloud masses at cloud bases for the Jupiter model atmospheres.

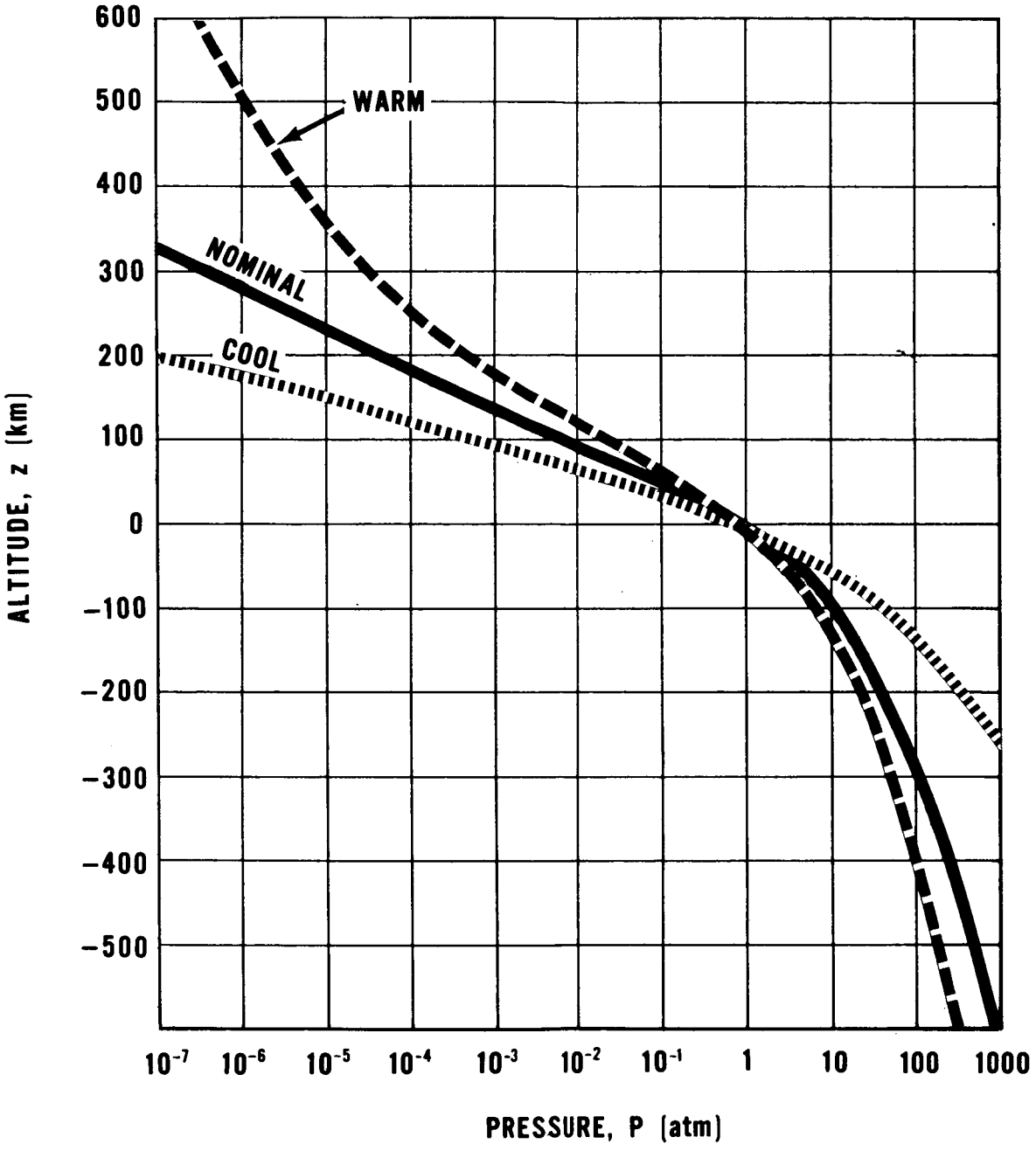

Figure 12.—Pressure vs altitude for the Jupiter model atmospheres. The zero of altitude is specified by equation 35 (sec. 3.9).

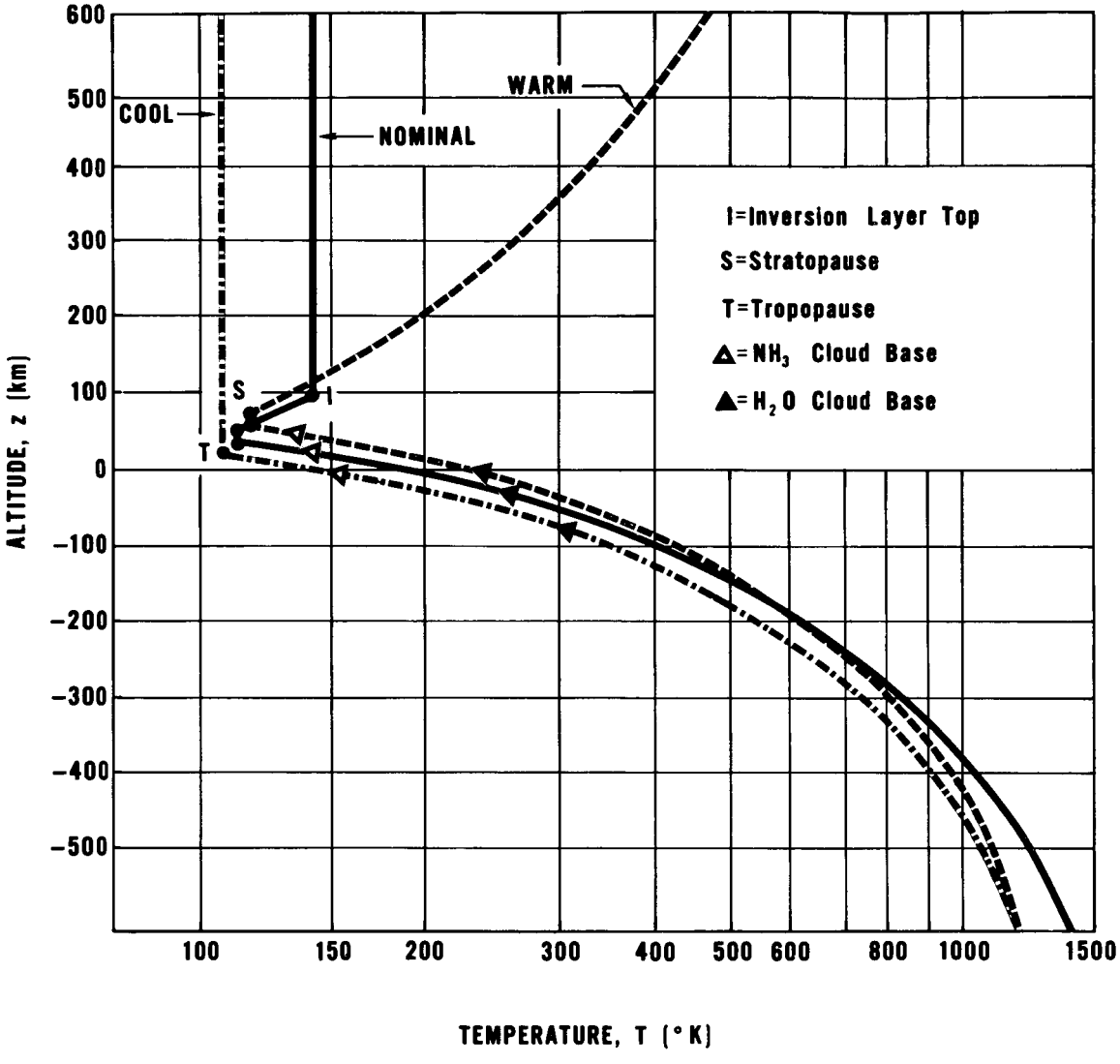

Figure 13.–Temperature vs altitude for the Jupiter model atmospheres. The zero of altitude is specified by equation 35 (sec. 3.9).

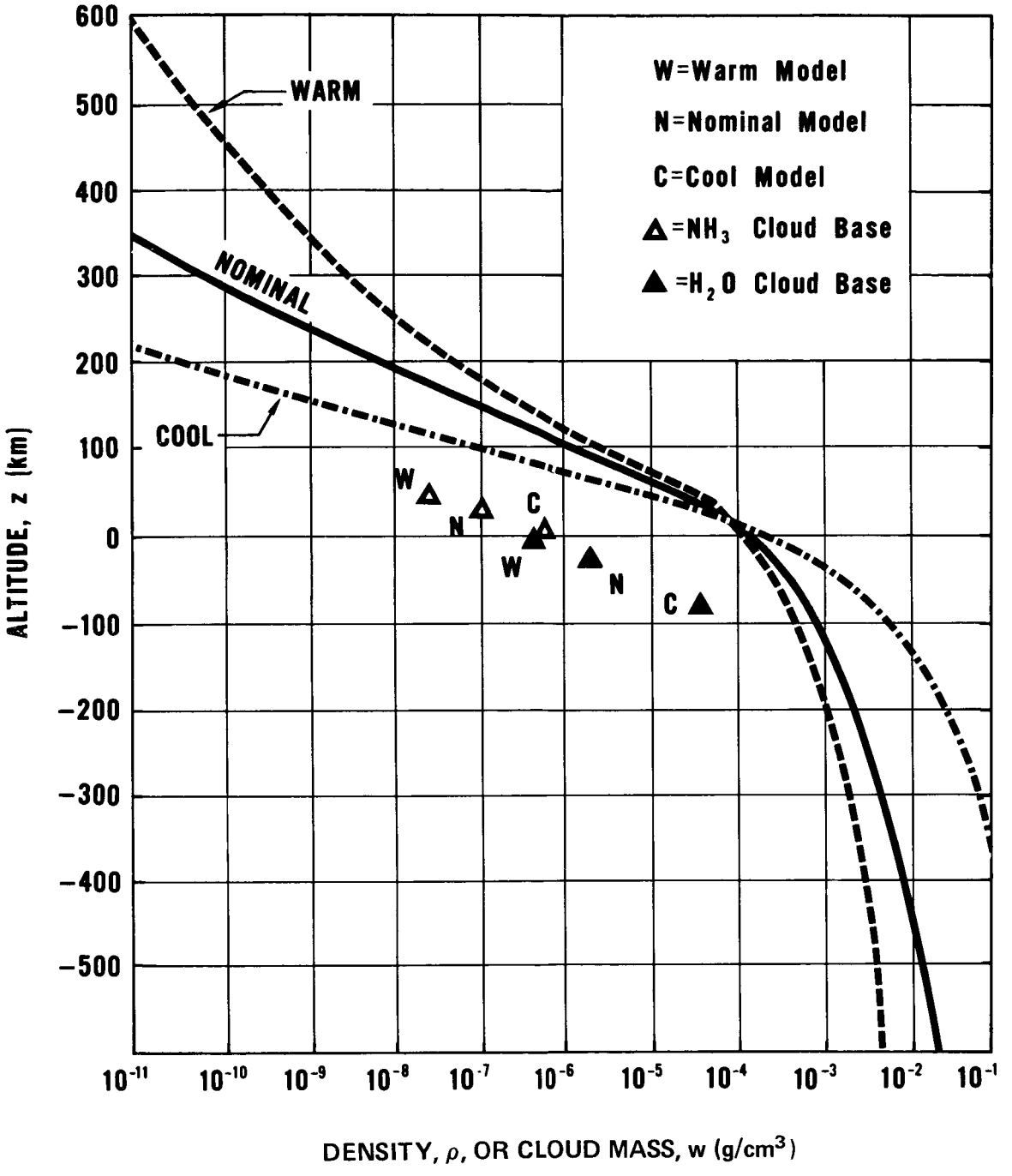

Figure 14.–Density vs altitude and cloud masses at cloud bases for the Jupiter model atmospheres. The zero of altitude is specified by equation 35 (sec. 3.9).

3.12 Transfer Properties in the Atmosphere

Table XVIII provides expressions for electromagnetic, thermal, and mechanical transfer properties in the atmosphere.

TABLE XVIII

TRANSFER PROPERTIES IN JUPITER'S ATMOSPHERE

Opacity κ (cm^2/gram)*	$\kappa = (1.8 \pm 0.6) \times 10^{-5}/\lambda^4$
Index of refraction n**	$n = 1.0 + (0.033 \pm 0.005)P/T$
Viscosity η (micropoise)***	$log\ \eta = (0.4 \pm 0.1) + (0.65) log\ T$
Thermal conductivity λ_t*** (cal/cm sec °K)	$log\ \lambda_t = (-5.3 \pm 0.1) + (0.77) log\ T$
Specific heats C_v, C_p (joule/mole °K)	$C_v = 21 \pm 7$ $C_p = 29 \pm 7$
Ratio of specific heats γ	$\gamma = C_p/C_v = 1.45 \pm 0.15$
Speed of sound c_s(m/sec)***	$c_s = (70 \pm 10)\ T^{1/2}$

*For $\lambda < 1\ \mu$m and altitude $z > 35 \pm 15$ km; elsewhere opacity cannot be specified.
**For P in atm and T in °K only.
***For T in °K only. One micropoise equals 10^{-7} Ns/m^2.

3.13 Interior

Below the deepest levels specified in section 3.9, the interior pressure, density, and temperature of the convective, hydrogen-rich interior increase inward toward the center of the planet, but their relationships (the equation of state) cannot be anticipated with reliability. No solid or liquid surface is expected to exist at any depth within the atmosphere or interior.

REFERENCES

1. Anon.: Solar Electromagnetic Radiation. NASA SP-8005, Revised May 1971.

2. Anon.: Magnetic Fields – Earth and Extraterrestrial. NASA SP-8017, Mar. 1969.

3. Anon.: Meteoroid Environment Model-1970 (Interplanetary and Planetary). NASA SP-8038, June 1970.

4. Melbourne, W. G.; Mulholland, J. D.; Sjogren, W. L.; and Sturns, F. M., Jr.: Constants and Related Information for Astrodynamic Calculations, 1968. TR 32-1306, Jet Propulsion Laboratory, Pasadena, California, 1968.

5. Klepczynski, W. J.: The Mass of Jupiter and the Motion of Four Minor Planets. Astronom. J., vol. 74, no. 6, 1969, p. 774.

6. Bec, A.: Détermination de la masse de Jupiter par l'étude du mouvement de son neuvième satellite. Astronomy & Astrophysics, vol. 2, no. 3, 1969, p. 381.

7. Allen, C. W.: Astrophysical Quantities (Second Edition). Athlone Press, Univ. of London, 1963.

8. Brouwer, D.; and Clemence, G. M.: "Orbits and Masses of Planets and Satellites", Solar System. Kuiper, G. P., and Middlehurst, B. M., eds., Univ. of Chicago Press, vol. 3, chapter 3, 1961, p. 31.

9. Michaux, C. M.: Handbook of the Physical Properties of the Planet Jupiter. NASA SP-3031, 1967.

10. Rabe, W.: Untersuchungen uber die Durchmesser der grossen Planeten, Astronomische Nachrichten, vol. 234, no. 5600-01, 1926, p. 153.

11. Sampson, R. A.: Tables of the Four Great Satellites of Jupiter, Univ. of Durham, London, 1910.

12. Souillart, M.: Théorie Analytique des Mouvements des Satellites de Jupiter. Mem. Acad. Sci., Savants Etrangers, vol. 30, no. 1, 1899, p. 1.

13. DeMarcus, W. C.: "Planetary Interiors", Handbuch der Physik, S. Flügge, ed., Springer-Verlag, Berlin, vol. 52, 1959, p. 419.

14. Wildt, R.; and Neubauer, F. M.: Vortragsreihe von Professor Wildt. Bundesministerium f. Wissenschaftliche Forschung, Forschungsbericht W67-40, 1967, p. 10.

15. DeSitter, W., Jupiter's Galilean Satellites, Royal Astronomical Soc. Monthly Notices, vol. 91, no. 7, 1931, p. 706.

16. The American Ephemeris and Nautical Almanac. U.S. Government Printing Office.

17. Carr, T. D.; and Gulkis, S.: The Magnetosphere of Jupiter. Annual Review of Astronomy and Astrophysics, vol. 7, 1969, p. 577.

18. Warwick, J. W.: Particles and Fields near Jupiter. NASA Contractor Report CR-1685, 1970.

19. Dickel, J. R.: Microwave Observations of Jupiter. Magnetism and the Cosmos, Hindmarsh, W. R.; Lowes, F. J.; Roberts, P. H.; and Runcorn, S. K.; editors, American Elsevier Publ. Co., 1967, p. 296.

20. Ellis, G. R. A.: The Decametric Radio Emissions of Jupiter. J. Research Radio Science, vol. 69D, no. 12, 1965, p. 1513.

21. Goldreich, P.; and Lynden-Bell, D.: Io, A Jovian Unipolar Inductor. Astrophys. J., vol. 156, no. 1, 1969, p. 59.

22. Warwick, J. W.: Dynamic Spectra of Jupiter's Decametric Emission, 1961. Astrophys. J., vol. 137, no. 1, 1963, p. 41.

23. Luthey, J. L.; and Beard, D. B.: The Electron Energy and Density Distribution in the Jovian Magnetosphere. University of Kansas, 1970.

24. Berge, G. L.: An Interferometric Study of Jupiter's Decimeter Radio Emission. Astrophys. J., vol. 146, no. 3, 1966, p. 767.

25. Roberts, J. A.; and Komesaroff, M. M.: Observations of Jupiter's Radio Spectrum and Polarization in the Range from 6 cm to 100 cm. Icarus, vol. 4, no. 2, 1965, p. 127.

26. Whiteoak, J. B.; Gardner, F. F.; and Morris, D.: Jovian Linear Polarization at 6-cm Wavelength. Astrophys. Letters, vol. 3, no. 3, 1969, p. 81.

27. Roberts, J. A.; and Ekers, R. D.: The Position of Jupiter's Van Allen Belt. Icarus, vol. 5, no. 2, 1966, p. 149.

28. Berge, G. L.: The Position of Jupiter's Radio Emission Centroid at 21 cm Wavelength. Presented to Commissions 16 and 40, Fourteenth General Assembly, International Astronomical Union, Brighton, England, Aug. 24, 1970.

29. Ellis, G. R. A.: The Radio Emissions from Jupiter and the Density of Jovian Exosphere. Australian J. of Physics, vol. 16, 1963, p. 74.

30. Melrose, D. B.: Rotational Effects on the Distribution of Thermal Plasma in the Magnetosphere of Jupiter. Planetary & Space Sci., vol. 15, no. 2, 1967, p. 381.

31. Haffner, J. W.: The Magnetospheres of Jupiter and Saturn. AIAA Paper No. 71-30, 1971.

32. Johnson, J. C.: Physical Meteorology. M.I.T. Press, Cambridge, Mass., 1954.

33. Moos, H. W.; Fastie, W. G.; and Bottema, M.: Rocket Measurement of Ultraviolet Spectra of Venus and Jupiter Between 1200 and 1800 Å. Astrophys. J., vol. 155, no. 3, 1969, p. 887.

34. Stecher, T. P., The Reflectivity of Jupiter in the Ultraviolet. Astrophys. J., vol. 142, no. 3, 1965, p. 1186.

35. Jenkins, E. B.; Morton, D. C.; and Sweigart, A. V.: Rocket Spectra of Venus and Jupiter from 2000 to 3000 Å. Astrophys. J., vol. 157, no. 2, 1969, p. 913.

36. Anderson, R. C.; Pipes, J. G.; Broadfoot, A. L.; and Wallace, L.: Spectra of Venus and Jupiter from 1800 to 3200 Å. J. of the Atmospheric Sciences, vol. 26, no. 5, 1969, p. 874.

37. Irvine, W. M.; et al.: Multicolor Photoelectric Photometry of the Brighter Planets II. Observations from le Houga Observatory. Astronom. J., vol. 73, no. 4, 1968, p. 251.

38. Harris, D. L.: "Photometry and Colorimetry of Planets and Satellites". Solar System, Kuiper, G. P., and Middlehurst, B. M., eds., Univ. of Chicago Press, vol. 3, chapter 8, 1961, p. 272.

39. Danielson, R. E.: The Infrared Spectrum of Jupiter, Astrophys. J., vol. 143, no. 3, 1966, p. 949.

40. Taylor, D. J.: Spectrophotometry of Jupiter's 3400-10,000 A° Spectrum and a Bolometric Albedo for Jupiter. Icarus, vol. 4, no. 4, 1965, p. 362.

41. Gillett, F. C.; Low, F. J.; and Stein, W. A.: The 2.8-14-Micron Spectrum of Jupiter. Astrophys. J., vol. 157, no. 2, 1969, p. 925.

42. Kellermann, K. I.: Thermal Radio Emission from the Major Planets. Radio Science, vol. 5, no. 2, 1970, p. 487.

43. Aumann, H. H.; Gillespie, C. M., Jr.; and Low, F. J.: The Internal Powers and Effective Temperatures of Jupiter and Saturn. Astrophys. J., vol. 157, no. 1, 1969, p. L 69.

44. Wildey, R. L.: Structure of the Jovian Disk in the ν_2-band of Ammonia at 100,000 Å. Astrophys. J., vol. 154, no. 2, 1968, p. 761.

45. Dickel, J. R.; Degioanni, J. J.; and Goodman, G. C.: The Microwave Spectrum of Jupiter. Radio Science, vol. 5, no. 2, 1970, p. 517.

46. Branson, N. J. B. A.: High Resolution Radio Observations of the Planet Jupiter. Royal Astronomical Soc. Monthly Notices, vol. 139, 1968, p. 155.

47. McAdam, W. B.: The Extent of the Emission Region on Jupiter at 408 Mc/s. Planetary & Space Sci., vol. 14, no. 11, 1966, p. 1041.

48. Gulkis, S.: Lunar Occultation Observations of Jupiter at 74 cm and 128 cm. Radio Science, vol. 5, no. 2, 1970, p. 505.

49. Warwick, J. W.: Radiophysics of Jupiter. Space Sci. Reviews, vol. 6, no. 6, 1967, p. 841.

50. Slee, O. B.; and Higgins, C. S.: The Solar Wind and Jovian Decametric Radio Emission. Australian J. Physics, vol. 21, no. 3, 1968, p. 341.

51. Duncan, R. A.: Theory of Jovian Dekametric Emission. Planetary and Space Science, vol. 18, 1970, p. 217.

52. Dollfus, A.; "Visual and Photographic Studies of Planets at the Pic du Midi". Solar System, Kuiper, G. P., and Middlehurst, B. M., eds., Univ. of Chicago Press, vol. 3, chapter 15, 1961, p. 534.

53. Owen, T.: Saturn's Ring and the Satellites of Jupiter: Interpretations of Infrared Spectra. Science, vol. 149, no. 3687, 1965, p. 974.

54. Murray, B. C.; Wildey, R. L.; and Westphal, J. A.: Observations of Jupiter and the Galilean Satellites at 10 Microns. Astrophys. J., vol. 139, no. 3, 1964, p. 986.

55. Low, F. J.: Planetary Radiation at Infrared and Millimeter Wavelengths. Lowell Observatory Bulletin No. 128, vol. 6, no. 9, 1965, p. 184.

56. Price, M. J.; and Spadoni, D. J.: Preliminary Feasibility Study of Soft-Lander Missions to the Galilean Satellites of Jupiter. IIT Research Institute Report No. M-19, 1970.

57. Haffner, J. W.: Radiation and Shielding in Space. Academic Press, 1967.

58. Fanselow, J. L.: The Primary Cosmic-Ray Electron Spectrum between 0.09 and 8.4 BeV in 1965. Astrophys. J., vol. 152, 1968, p. 783.

59. McDonald, F. B.; editor: Solar Proton Manual. NASA TR R-169, 1963.

60. Englade, R. C.: A Computational Model for Solar Flare Particle Propagation. University of Chicago, July 1970.

61. Hundhausen, A.J.: Direct Observations of Solar-Wind Particles. Space Science Reviews, vol. 8, No. 5/6, 1968, p. 690.

62. Eggen, J. B.: The Trapped Radiation Zones of Jupiter. Report FZM-4789, Fort Worth Div., General Dynamics Corp., 1967, 44 pp.

63. Haffner, J. W.: Calculated Dose Rates in Jupiter's Van Allen Belts. Am. Inst. of Aeronautics and Astronautics Journal, vol. 7, no. 12, 1969, p. 2305.

64. Koepp-Baker, N. B.: A Model of Jupiter's Trapped Radiation Belts. Report 68 SD 263, Missile and Space Division, General Electric Corp., 1968.

65. Roberts, J. A.: Jupiter, as Observed at Short Radio Wavelengths. J. Research Radio Science, vol. 69D, no. 12, 1965, p. 1543.

66. Davis, L., Jr.; and Chang, D. B.: On the Effect of Geomagnetic Fluctuations on Trapped Particles. J. Geophysical Research, vol. 67, no. 6, 1962, p. 2169.

67. Barber, D.; and Gower, J. F. R.: The Spectral Index of the Radiation from Jupiter between 178 and 610 Megacycles/second. Planetary and Space Sci., vol. 13, no. 9, 1965, p. 889.

68. Berge, G. L.: Interferometric Study of Jupiter at 10 and 21 cm. J. Research Radio Science, vol. 69D, no. 12, 1965, p. 1552.

69. Thorne, K. S.: The Theory of Synchrotron Radiation from Stars with Dipole Magnetic Fields. Astrophys. J., vol. 137, 1963, p. 1.

70. Thorne, K. S.: Dependence of Jupiter's Decimeter Radiation on the Electron Distribution in its Van Allen Belts. J. Research Radio Science, vol. 69D, no. 12, 1965, p. 1557.

71. Papadopoulos, K.; and Lerche, I.: Collective Bremsstrahlung from Relativistic Electrons as a Possible Mechanism in Radio Sources. Astrophys. J., vol. 158, no. 3, 1969, p. 981.

72. Gross, S. H.; and Rasool, S. I.: The Upper Atmosphere of Jupiter. Icarus, vol. 3, no. 4, 1964, p. 311.

73. Shimizu, M.: The Atomic and Molecular Processes in the Upper Atmospheres of Planets. Report of Ionosphere and Space Research in Japan, vol. 20, no. 3, 1966, p. 271.

74. Hunten, D. M.: The Upper Atmosphere of Jupiter. J. of the Atmospheric Sciences, vol. 26, no. 5, 1969, p. 826.

75. Henry, R. J. W.; and McElroy, M. B.: The Absorption of Extreme Ultraviolet Solar Radiation by Jupiter's Upper Atmosphere. J. of the Atmospheric Sciences, vol. 26, no. 5, 1969, p. 912.

76. Capone, L. A.; and Barrow, C. H.: The Upper Atmosphere of Jupiter. Am. Astronomical Society Bulletin, vol. 1, no. 2, 1969, p. 214.

77. Hess, W. N.; and Mead, G. D.: Introduction to Space Science. Second Edition, Gordon and Breach, New York, 1968, 1056 pp.

78. Alfvén, H.; and Fälthammar, C.-G.: Cosmical Electrodynamics: Fundamental Principles (Second Edition). Clarendon Press (Oxford, U. K.), 1963.

79. Ratcliffe, J. A.: The Magneto-Ionic Theory and its Applications to the Ionsophere. University Press, Cambridge, U. K., 1959.

80. Owen, T.: The Atmosphere of Jupiter. Science, vol. 167, no. 3926, 1970, p. 1675.

81. McElroy, M. B.: Atmospheric Composition of the Jovian Planets. J. of the Atmospheric Sciences, vol. 26, no. 5, 1969, p. 798.

82. Torres-Peimbert, S.; Simpson, E.; and Ulrich, R. K.: Studies in Stellar Evolution. VII. Solar Models. Astrophys. J., vol. 155, no. 3, 1969, p. 957.

83. Lambert, D. L.: The Abundances of the Elements in the Solar Photosphere. I. Carbon, Nitrogen and Oxygen. Royal Astronomical Soc. Monthly Notices, vol. 138, no. 2, 1968, p. 143.

84. Kuiper, G. P.: "Planetary Atmospheres and Their Origin". The Atmospheres of the Earth and Planets, Kuiper, G. P., ed., Univ. of Chicago Press, chapter 12, 1952, p. 306.

85. Lewis, J. S.: The Clouds of Jupiter and the NH_3-H_2O and NH_3-H_2S Systems. Icarus, vol. 10, no. 3, 1969, p. 365.

86. Margolis, J. S.; and Fox, K.: Studies of Methane Absorption in the Jovian Atmosphere. I. Rotational Temperature from the $3\nu_3$ Band. Astrophys. J., vol. 157, no. 2, 1969, p. 935.

87. Margolis, J. S.; and Fox, K.: Extension of Calculations of Rotational Temperature and Adundance of Methane in the Jovian Atmosphere. J. of the Atmospheric Sciences, vol. 26, no. 5, 1969, p. 863.

88. Margolis, J. S.; and Fox, K.: Studies of Methane Absorption in the Jovian Atmosphere. II. Abundance from the $3\nu_3$ Band. Astrophys. J., vol. 158, no. 3, 1969, p. 1183.

89. Owen, T.: The Spectra of Jupiter and Saturn in the Photographic Infrared. Icarus, vol. 10, no. 3, 1969, p. 355.

90. Wrixon, G. T.: Microwave Absorption in the Jovian Atmosphere. Space Sci. Lab. Series 10, Issue 26, Univ. of Calif., Berkeley, 1969.

91. Hogan, J. S.; Rasool, S. I.; and Encrenaz, T.: The Thermal Structure of the Jovian Atmosphere. J. of the Atmospheric Sciences, vol. 26, no. 5, 1969, p. 898.

92. McGovern, W. E.: Exospheric Temperatures of Jupiter and Saturn. J. Geophys. Research, vol. 73, no. 19, 1968, p. 6361, and vol. 74, no. 14, 1969, p. 3750.

93. Trafton, L. M.: Model Atmospheres of the Major Planets. Astrophys. J., vol. 147, no. 2, 1967, p. 765.

94. Smith, R. E.; and Weidner, D. K.: Space Environment Criteria Guidelines for Use in Space Vehicle Development (1968 Revision). NASA TMX-53798, Marshall Space Flight Center, Huntsville, Ala., 1968, p. VIII-1.

95. Peek, B. M: The Planet Jupiter. Faber & Faber, London, 1958.

96. Solberg, H. G., Jr.: Jupiter's Red Spot in 1967-68. Icarus, vol. 10, no. 3, 1969, p. 412.

97. Solberg, H. G., Jr.: A 3-Month Oscillation in the Longitude of Jupiter's Red Spot. Planetary and Space Sci., vol. 17, no. 9, 1969, p. 1573.

98. Hide, R.: Jupiter's Great Red Spot. Scientific American, vol. 218, 1968, p. 74.

99. Washburn, E. W., ed.: International Critical Tables, vol. 3, McGraw-Hill, New York, 1928.

100. Lange, N. A., ed.: Handbook of Chemistry. Revised Tenth Edition, McGraw-Hill, New York, 1967.

101. Donivan, F. F.; and Carr, T. D.: Jupiter's Decametric Rotation Period. Astrophys. J., vol. 157, no. 1, 1969, p. L65.

102. Chapman, C. R.: Jupiter's Zonal Winds: Variation with Latitude. J. of the Atmospheric Sciences, vol. 26, no. 5, 1969, p. 986.

103. Hide, R.: Dynamics of the Atmospheres of the Major Planets with an Appendix on the Viscous Boundary Layer at the Rigid Bounding Surface of an Electrically-Conducting Rotating Fluid in the Presence of a Magnetic Field. J. of the Atmospheric Sciences, vol. 26, no. 5, 1969, p. 841.

104. Ingersoll, A. P.; and Cuzzi, J. N.: Dynamics of Jupiter's Cloud Bands. J. of the Atmospheric Sciences, vol. 26, no. 5, 1969, p. 981.

105. Teifel, V. G.: Molecular Absorption and the Possible Structure of the Cloud Layers of Jupiter and Saturn. J. of the Atmospheric Sciences, vol. 26, no. 5, 1969, p. 854.

106. Kiess, C. C.; Corliss, C. H.; and Kiess, H. K.: High-Dispersion Spectra of Jupiter. Astrophys. J., vol. 132, no. 1, 1960, p. 221.

107. Forsythe, W. E.: Smithsonian Physical Tables. Ninth Revised Edition, Lord Baltimore Press, 1959.

108. Trafton, L. M.: The Thermal Opacity in the Major Planets. Astrophys. J., vol. 140, no. 3, 1964, p. 1340.

109. Trafton, L. M.: The Pressure-Induced Monochromatic Translational Absorption Coefficients for Homopolar and Non-Polar Gases and Gas Mixtures with Particular Applications to H_2. Astrophys. J., vol. 146, no. 2, 1966, p. 558.

110. Gille, J. C.; and Lee, T.-H.: The Spectrum and Transmission of Ammonia under Jovian Conditions. J. of the Atmospheric Sciences, vol. 26, no. 5, 1969, p. 932.

111. Goodman, G. C.: Models of Jupiter's Atmosphere. Ph. D. Thesis, Univ. of Illinois, 1969.

112. Brown, S. C.: "Conduction of Electricity in Gases". Handbook of Physics. Condon, E. U., and Odishaw, H., eds., McGraw-Hill, New York, 1958, pp. 4-159.

113. Brokaw, R. S.: Alignment Charts for Transport Properties Viscosity, Thermal Conductivity, and Diffusion Coefficients for Nonpolar Gases and Gas Mixtures at Low Density. NASA TR R-81, Lewis Research Center, Cleveland, Ohio, 1961.

114. Weast, R. C.; and Selby, S. M.; editors: Handbook of Chemistry and Physics. Chemical Rubber Co., 1966.

115. DeMarcus, W. C.: The Constitution of Jupiter and Saturn. Astronom. J., vol. 63, no. 1, 1958, p. 2.

116. Peebles, P. J. E.: The Structure and Composition of Jupiter and Saturn. Astrophys. J., vol. 140, no. 1, 1964, p. 328.

117. Smoluchowski, R.: Internal Structure and Energy Emission of Jupiter. Nature, vol. 215, no. 5102, 1967, p. 691.

118. Hubbard, W. B.: Thermal Structure of Jupiter. Astrophys. J., vol. 152, no. 3, 1968, p. 745.

119. Hubbard, W. B.: Thermal Models of Jupiter and Saturn. Astrophys. J., vol. 155, no. 1, 1969, p. 333.

APPENDIX A
SYMBOLS*

A	coefficient in cosmic-ray flux formula (sec 2.7.1)
A	moment of inertia about equatorial axis (sec. 2.1.4)
A_j	parameter of condensible gas j (app. D)
a	semi-major axis of orbit about Jupiter (table V)
B	blue **magnitude** (table IX)
B	magnetic field strength (app. B)
B_R	component of B in radial direction (app. B)
B_ϕ	component of B in latitudinal direction (app. B)
$B_\lambda(T)$	Planck function, per unit wavelength interval (sec. 2.5.2)
$B_\nu(T)$	Planck function, per unit frequency interval (sec. 2.5.2)
C	moment of inertia about polar axis (sec. 2.1.4)
C_p	specific heat at constant pressure (sec. 2.12.2, app. D)
C_v	specific heat at constant volume (sec. 2.12.2, app. D)
c	speed of light, 3×10^{10} cm/sec (sec. 2.7)
c_s	speed of sound (sec. 2.12.2)
D	path length within **synchrotron radiation** volume (sec. 2.5.3.1)
E	charged particle kinetic energy (sec. 2.7)
E_0	local characteristic energy (sec. 2.7.4.2)
E_1	characteristic energy at flux peak (sec. 2.7.4.2)
$\mathcal{E}$	electric field strength, in volts/m (sec. 2.4)
e	absolute value of electron charge, 4.8×10^{-10} e.s.u. (sec. 2.4)
F	integrated **flux** of electromagnetic radiation (sec. 2.5.1.2)
F_λ	**flux** of electromagnetic radiation, per unit wavelength interval (sec. 2.5.1.2)
F_ν	**flux** of electromagnetic radiation, per unit frequency interval (app. C)
G	universal constant of gravitation, 6.668×10^{-8} dyne/cm^2/grams^2 (sec. 2.2)
g	local acceleration of gravity (sec. 2.2.2)

*Words in bold face are defined in Glossary (app. E).

H_p local pressure **scale height** (app. D)

H_ρ local density **scale height** (app. D)

I_λ **intensity** per unit wavelength interval (sec. 2.5.1.2)

I_ν **intensity** per unit frequency interval (sec. 2.5.1.2 and app. C)

J_2 coefficient in gravitational potential (sec. 2.2.1)

J_4 coefficient in gravitational potential (sec. 2.2.1)

K_1 parameter of **adiabatic** gradient (app. D)

K_2 parameter of **adiabatic** gradient (app. D)

k Boltzmann's constant, 1.38×10^{-16} erg/°K (app. C)

L magnetic shell parameter (app. B)

L_0 L evaluated at inner boundary of radiation belts (sec. 2.7.4.1 b)

L_1 L evaluated at peak of radiation belts (sec. 2.7.4.1 b)

L_2 L evaluated at **magnetopause** (sec. 2.7.4.1 b)

M meteoroid mass, in grams (sec. 2.6.3)

M_1 magnetic dipole moment (app. B)

M_J mass of Jupiter, excluding satellites (sec. 2.1.1)

M_{JS} mass of Jupiter system, including satellites (sec. 2.1.1)

M_n mass of satellite n (sec. 2.6.3)

$M_\odot$ mass of the Sun, 1.989×10^{33} grams (sec. 2.1.1)

m_0 absolute **magnitude** (sec. 2.5.1.3)

m_0 rest mass of cosmic ray particle (sec. 2.7.1)

m_p rest mass of proton, 1.67×10^{-24} gram (sec. 2.7.4.4)

m_v apparent visual **magnitude** (sec. 2.5.1.3)

N charged particle concentration, in cm^{-3} (sec. 2.7.5)

N_0 local radiation belt concentration parameter (sec. 2.7.4.1 b)

N_1 N_0 evaluated at flux peak (sec. 2.7.4.1 a)

N_5 N evaluated for electrons with $E > 5$ MeV (sec. 2.7.4.2)

N_E N evaluated for particles with kinetic energy $> E$ (sec. 2.7.4.2)

N_e electron concentration in the **ionosphere**, in cm^{-3} (sec. 2.8.2)

N_M concentration of meteoroids of mass $>$ M (sec. 2.6.3)

n index of refraction (secs. 2.8.2 and 2.12.1)

n_s n evaluated at standard temperature and pressure (sec. 2.12.1)

P local gas pressure in the atmosphere (app. D)

P_2 Legendre polynominal (sec. 2.2)

P_4 Legendre polynominal (sec. 2.2)

P_A P evaluated at some specific atmospheric level (app. D)

P_{js} saturation vapor pressure of condensible gas j (app. D)

P_s standard pressure, 1 atm = 1.013×10^6 dynes/cm^2 (sec. 2.12.1)

P_λ solar spectral irradiance (sec. 2.5.1.1 and ref. 1)

p **geometric albedo**, function of wavelength (sec. 2.5.1.2)

p_b **bolometric geometric albedo** (sec. 2.5.1.2)

R separation from center of Jupiter (sec. 2.2)

R_g universal gas constant (app. D)

R_J equatorial radius of Jupiter's visible disk (sec. 2.1.2)

R_n characteristic semi-diameter of satellite n (sec. 2.6.3)

R_s R evaluated for Jupiter's visible disk (sec. 2.1.2)

r distance from the Sun, in AU (sec. 2.5.1.2)

S solar constant, 1.353×10^6 erg/cm^2 sec (sec. 2.5.1.2)

T period of Jupiter's revolution about the Sun (table IV)

T local temperature in atmosphere or **ionosphere** (app. D)

T_0 period of rotation of Jupiter's core and magnetic field (sec. 2.11.1)

T_1 period of rotation of **System I** (sec. 2.11.1)

T_2 period of rotation of **System II** (sec. 2.11.1)

T_3 period of rotation of **System III** (sec. 2.11.1)

T_A T evaluated at some specific atmospheric level (app. D)

T_a period of revolution in orbit about Jupiter (table V)

T_B **brightness temperature** (app. C)

T_{BD} T_B evaluated for Jupiter's disk (sec. 2.5.2)

T_{BS} T_B evaluated for Jupiter's **synchrotron radiation** source (sec. 2.5.3.1)

T_e **effective temperature** of Jupiter (sec. 2.5.2)

T_s standard temperature, 273.16 °K (sec. 2.12.1)

U ultraviolet **magnitude** (table IX)

u mean molecular weight, grams/mole (app. D)

u_j molecular weight of condensible gas j (app. D)

V visual **magnitude** (table IX)

v meteoroid speed relative to spacecraft (sec. 2.6.3)

v_s spacecraft speed relative to Jupiter (sec. 2.6.3)

W **bandwidth** of Jupiter's **synchrotron radiation** (sec. 2.7.4.2)

w representative cloud mass, per unit volume of gas (app. D)

w_j w evaluated for condensible gas j (app. D)

z altitude above Jupiter's visible disk (sec. 2.2.2)

z_0 z evaluated at base of Jupiter's **ionosphere** (sec. 2.7.6)

z_A z evaluated at some specific atmospheric level (app. D)

α phase angle (sec. 2.5.1.3)

α_R **right ascension** of Jupiter's north rotational pole (sec. 2.1.4)

β **adiabatic** gradient, d*log*T/d*log*P (app. D)

β_0 parameter of **adiabatic** gradient (app. D)

γ ratio of specific heats, C_p/C_v (app. D)

Δ distance from reflecting surface to observer, in AU (sec. 2.5.1.3)

$(\Delta\Phi)_E$ Φ evaluated for energies between E and E+ΔE (sec. 3.7.2)

δ_R **declination** of Jupiter's north rotational pole (sec. 2.1.4)

ϵ **flattening** of Jupiter's disk (sec. 2.1.2)

η coefficient of **viscosity**, in micropoise (sec. 2.12.2)

η_1 angle of equatorward deflection of gravity (sec. 2.2.2)

θ **pitch angle** of electron trajectory (sec. 2.7.4.2)

θ angle between propagation and magnetic field directions (sec. 2.8.2)

κ **opacity** in Jupiter's atmosphere (table XVIII)

κ_R κ evaluated for **Rayleigh scattering** (sec. 2.12.1)

λ wavelength of electromagnetic radiation (sec. 2.5)

λ_j parameter of condensible gas j (app. D)

λ_t thermal **conductivity** (sec. 2.12.2)

ν frequency of electromagnetic radiation (sec. 2.8.2)

ν_B electron **gyrofrequency** (sec. 2.8.2)

ν_P plasma frequency (sec. 2.8.2)

ρ local gas density in the atmosphere (app. D)

$\bar{\rho}$ mean density of Jupiter (sec. 2.1.3)

σ coefficient of rotation term in Ψ (sec. 2.2)

σ_R σ evaluated for rotation with Jupiter (secs. 2.1.4 and 2.2.2)

τ **optical depth** (app. E)

Φ **flux** of charged particles (sec. 2.7)

Φ_E Φ evaluated for particles with kinetic energy $> E$ [$E \neq 0$] (sec. 2.7)

Φ_0 local radiation belt flux parameter (sec. 2.7.4.2)

ϕ latitude, with respect to Jupiter's rotational equator (sec. 2.1.2)

ϕ_0 parameter of radiation belt latitude distribution (sec. 2.7.4.1 c)

Ψ gravitational potential function (sec. 2.2)

Ω solid angle of radio source (app. C)

ω_0 angular velocity of Jupiter's core and magnetic field (sec. 2.1.4)

APPENDIX B
DIPOLE MAGNETIC FIELD

At distance R from Jupiter's center and latitude ϕ, the components of the magnetic field of the dipole whose magnetic moment is M_1 are

$$B_R = \frac{2M_1}{R^3} \sin \phi \tag{B1}$$

and

$$B_\phi = -\frac{M_1}{R^3} \cos \phi. \tag{B2}$$

The magnetic field has the magnitude

$$B = \frac{M_1}{R^3} [1 + 3 (\sin \phi)^2]^{1/2}. \tag{B3}$$

It is directed along field lines in that plane which contains both the dipole and the point of interest; the shape of these field lines is specified by

$$R = L R_J (\cos \phi)^2 \tag{B4}$$

where the quantity L, the magnetic shell parameter, represents the distance from the magnetic dipole at which the magnetic line of force (on which the test point lies) crosses the magnetic equator, in units of R_J.

APPENDIX C
RELATIONSHIPS AMONG RADIO ASTRONOMY QUANTITIES

At UHF (microwave) frequencies, corresponding to wavelengths from a few cm to a few meters, the results of radio astronomical observations are expressed in terms of either flux F_ν or brightness temperature T_B (app. E) which can be related by a form of the Rayleigh-Jeans law

$$F_\nu = 2k\, T_B\, \Omega/\lambda^2 \qquad \text{(C1)}$$

where k is Boltzmann's constant, 1.38×10^{-23} joule/°K, λ is the wavelength of observation, and Ω is the solid angle of the source in steradians ($\Omega \ll \pi$ is required). The flux density F_ν is commonly expressed in flux units FU where 1 FU $= 10^{-26}$ watt/m^2 Hz. The intensity I_ν is then correctly given by F_ν/Ω for all values of Ω and is independent of distance from the source.

APPENDIX D
ATMOSPHERE AND CLOUD RELATIONSHIPS

In terms of the symbols defined in appendix A, the model atmospheres of sections 2.9 and 3.9 are governed, for each atmospheric region, by

(1) hydrostatic equilibrium $$\frac{dP}{dz} = -\rho g \tag{D1}$$

(2) the perfect gas law $$\rho = uP/R_g T, \text{ and} \tag{D2}$$

(3) a temperature-dependent gradient $$\frac{d\, log\, T}{d\, log\, P} = \beta = \beta_0 \frac{T + K_1}{T + K_2} \tag{D3}$$

where values of the constants K_1 and K_2 are restricted by $K_2 \geq 0$ in general, by $K_1 = K_2 > 0$ for regions of constant $\beta = \beta_0 \neq 0$, and by $K_1 = -T_A$ and $K_2 = 0$ for regions of $\beta = 0$, which implies constant temperature $T = T_A$. Values of K_1 and K_2 can be chosen to ensure that β approximates the adiabatic value $(\gamma - 1)/\gamma$ for a real gas mixture whose specific heats are related by $\gamma = C_p/C_v$. The inequality $K_1 > K_2 > 0$ results if C_p and C_v increase with temperature.

The solution of equations D1 through D3 requires that T and z at any value of P be related to those at T_A, z_A, and P_A in the same region by

$$\left(\frac{P}{P_A}\right)^{\beta_0} = \left(\frac{T}{T_A}\right)^{K_2/K_1} \left(\frac{T + K_1}{T_A + K_1}\right)^{(K_1 - K_2)/K_1} \tag{D4}$$

and

$$z = z_A - \frac{R_g}{ug}\left(\frac{T - T_A}{\beta_0} - K_1 \ln\frac{P}{P_A} + \frac{K_2}{\beta_0} \ln\frac{T}{T_A}\right). \tag{D5}$$

The lapse rate and scale heights are given by

$$dT/dz = -\beta ug/R_g \tag{D6}$$

$$H_p = R_g T/ug \tag{D7}$$

and

$$H_\rho = H_p/(1 - \beta). \tag{D8}$$

It is assumed that clouds are formed by condensation of a species j in convective regions moving upward to lower temperature and pressure when the saturation vapor pressure P_{js}.

would be exceeded by the partial pressure (both for the condensible constituent) if condensation were not to occur. P_{js} is conventionally described by a form of the Clausius-Clapeyron equation

$$P_{js} = exp\,[A_j - (\lambda_j/R_g T)]. \tag{D9}$$

Here A_j and λ_j are constants, and λ_j is the latent heat of condensation. In this case P_{js} also specifies the partial pressure of the condensible gas in the cloud region above the lowest level of condensation, and the mass of the cloud per unit volume of gas is approximated by

$$w_j = \frac{u_j P_{js}}{R_g T}\left(\frac{\beta\lambda_j - R_g T}{\beta\lambda_j}\right) \tag{D10}$$

where β is given by equation D3 and u_j is the mean molecular weight of the condensate.

Table D-1 lists the three species actually used in computing cloud properties and the appropriate constants; for NH_3-H_2O solutions as dilute as those likely, the liquid water constants were considered satisfactory approximations.

TABLE D-1

PARAMETERS OF CONDENSATES

Parameter	Liquid H_2O	Solid H_2O Ice	Solid NH_3 Ice
u_j (grams/mole)	18	18	17
A_j (for P_{js} in mm Hg)	20.592	24.055	23.744
λ_j (cal/mole)	10 350.67	12 230.27	7 740.64

APPENDIX E
GLOSSARY*

Adiabatic – Characteristic of processes in which heat is not transferred across system boundaries; in an atmosphere such a system is a hypothetically rising or falling parcel of gas, and the adiabatic requirement must be satisfied when the parcel achieves the local pressure and density.

Astronomical Unit (AU) – A unit of length approximately equal to the semi-major-axis of the Earth's orbit about the Sun. A modern value cited by Melbourne et al. (ref. 4) is 1 AU = $1.49597893 \times 10^8 \pm 5$ km.

Bandwidth (W) – The range of frequencies (or wavelengths) within which electromagnetic radiation is emitted or detected; the power or response distributions need not be uniform within this range.

Bolometric – Characteristic of an infinite **bandwidth**, and including electromagnetic radiation at all frequencies (or wavelengths) and polarizations.

Brightness Temperature (T_B) – The temperature at which a blackbody would radiate an intensity of electromagnetic radiation identical to that of the source for the **bandwidth** and polarization considered.

Color – For a given light source, the difference in **magnitude** for two **bandwidths** centered on different wavelengths.

Conductivity, Electrical – The ratio of current density to the impressed electric field strength. In the presence of both electric and magnetic fields, the direct conductivity is the ratio of the current to the electric field component parallel to the magnetic field; in the plane perpendicular to the magnetic field, the Pederson conductivity is the ratio of the current component, parallel to the electric field component, to that electric field component; and the Hall conductivity is the ratio of the current component, perpendicular to both fields, to the electric field component in the plane perpendicular to the magnetic field.

Conductivity, Thermal (λ_t) – The ratio of the thermal power per unit area crossing an imaginary plane surface perpendicular to a temperature gradient, to that gradient.

Decametric – Characteristic of electromagnetic radiation at those radio wavelengths between 10 and 100 meters; used here synonymously with **high frequency** (HF) to cover a broader range extending to about 7 meters.

Decimetric – Characteristic of electromagnetic radiation at those microwave wavelengths between 10 and 100 cm; used here synonymously with **ultra high frequency** (UHF) to cover a broader range extending to about 1 cm.

Declination – The celestial coordinate equal to the angle (north taken positive) between the direction of the item considered and the plane of the Earth's equator; the **precession** of the latter implies a slow variation of the declination even of fixed directions.

*Cross references within the glossary are indicated by bold face.

Effective Temperature (T_e) – The temperature at which a blackbody would radiate a **bolometric** intensity of electromagnetic radiation identical to that of the source.

Flattening (ϵ) – The positive difference between unity and the ratio of the polar to the equatorial diameter of a planetary disk (optical), or the value for the same quantity which would be derived on the basis of hydrodynamic theory and the gravitational potential inferred from observed satellite motions (dynamical).

Flux, of Electromagnetic Radiation (F, F_ν, or F_λ) – The power per unit area crossing an imaginary plane surface from one side to the other, either per unit **bandwidth** or integrated over all frequencies.

Flux, of Particles (Φ or Φ_E) – The number of particles per unit area and per unit time crossing an imaginery plane surface with positive or negative (but not both) velocity components perpendicular to the surface.

Geometric Albedo (p) – The ratio of the reflected electromagnetic **flux** from an astronomical object (observed at distance Δ, zero **phase angle**, and zero **optical depth**) to the quotient of the solar power intercepted by the object divided by $\pi\Delta^2$, in the **bandwidth** considered. Here the **flux**, the power, and Δ must be expressed in consistent units, and Δ must be large compared to the dimensions of the object.

Gyrofrequency – The frequency of circling of a charged particle (mass m, charge e) in a uniform magnetic field B, given by $eB/2\pi m$ in general, and by (2.8 MHz)B for electrons when B is given in gauss.

Hall Conductivity – See conductivity, electrical.

High Frequency (HF) – Characteristic of electromagnetic radiation at those radio frequencies between 3 and 30 **MHz**, used here synonymously with **decametric** to cover a broader range extending to about 40 **MHz**.

Inertial Coördinates – Any system of coördinates characterized by zero or constant vector velocity with respect to the "fixed stars".

Intensity (I_ν or I_λ) – The **flux** of electromagnetic radiation per unit solid angle of the source for a defining imaginary surface whose normal intersects the source; intensity is independent of the source-surface separation.

Ionosphere – The atmospheric layer which includes the major maxima of electron and ion concentration.

Magnetopause – The **magnetosphere's** outer boundary, where a planet's field interacts with external magnetic field and charged particle environments, particularly the solar wind.

Magnetosphere – The region surrounding a planet in which the local magnetic field is dominated by planet-associated fields rather than by external environments.

Magnitude (m, m_0) – Five-halves times the common logarithm (base ten) of the ratio of the power received per unit area within some **bandwidth** for a standard object to that for an astronomical object of interest. The base of this logarithmic scale is $x = 2.512$ so that an increase of one magnitude corresponds to a decrease in power by a factor x^{-1} or an increase in distance by a factor $x^{1/2}$. Apparent magnitudes (m) are those observed. Absolute magnitudes (m_0) are those for which absorption and scattering effects have

been removed, and observation is assumed to occur in a standard geometrical configuration. For solar system objects, the standard configuration is sun-object distance r = 1 AU, object-observer distance Δ = 1 AU, and **phase angle** α = 0.

Megahertz (MHz) – The frequency unit 10^6 cycles per second.

Opacity (κ) – The cross-section area per unit mass of absorber or scatterer.

Optical Depth (τ) – The integral of the **opacity** κ and the mass density ρ along the absorption or scattering path length ds. The ratio of the **intensity** of a source after to that before absorption is $e^{-\tau}$ where $\tau = \int \kappa\rho \, ds$.

Pederson Conductivity – See conductivity, electrical.

Phase Angle (α) – The angle formed by the Sun, the point of reflection, and the observer.

Pitch Angle (θ) – The angle between the particle velocity vector and the external magnetic field vector evaluated at the position of the particle.

Plasma – A gas in which the concentration of charged particles has more than negligible effects on the properties of the gas.

Position Angle – The angle which describes the direction from one point to another on the sky. It is conventionally taken as zero when the direction of the line between the points is north; the angle increases as the line's direction moves east.

Precession – The change in the directions of the Earth's rotational axis and **vernal equinox** with respect to the "fixed stars". It is approximately periodic with period of 26 000 years.

Prograde – The direction of rotation and revolution common in the solar system in which the motion is counter-clockwise as viewed from the north.

Rayleigh Scattering – Scattering of electromagnetic radiation by particles (in Jupiter's case H_2 molecules) whose characteristic size is small compared to the wavelength λ. The scattering center may be approximated by an oscillating electric dipole whose scattering cross-section and **opacity** are proportional to λ^{-4}.

Relativistic – Characteristic of a particle whose kinetic energy is comparable to or greater than its rest energy and whose speed is only slightly less than that of light.

Right Ascension – The celestial coördinate equal to the angle (east taken postive) between the projection of the direction of the item considered on the plane of the Earth's equator and that of the **vernal equinox**, expressed as fractions of 24 hours rather than 360°; the **precession** of the Earth's rotation axis implies a slow variation of the right ascension even of fixed directions.

Scale Height (H_p, H_ρ) – A measure of the vertical gradient of a quantity x, e.g., pressure, electron concentration, such that if $H = -x(dx/dz)^{-1}$ is constant with altitude z, the quantity x changes by a factor e within the altitude interval H.

Stratopause – The upper boundary of the **stratosphere**, characterized by a near-discontinuity in the temperature gradient.

Stratosphere – The atmospheric layer directly above the **troposphere**, within which the temperature is constant or increases with altitude.

Synchrotron Radiation – Electromagnetic radiation emitted by a **relativistic** charged particle as it is accelerated, i.e., follows a curved path, in a magnetic field.

System I – The artificial Jupiter longitude measurement system in which the meridian at $47^{\circ}31$ is directed toward the Earth at 0^{h} Universal Time on 14 July 1897 and has **prograde** rotation with angular velocity of 877.90 degrees/day. It is applied to the analysis of optical observations at equatorial latitudes.

System II – The artificial Jupiter longitude measurement system in which the meridian at $96^{\circ}58$ is directed toward the Earth at 0^{h} Universal Time on 14 July 1897 and has **prograde** rotation with angular velocity of 870.27 degrees/day. It is applied to the analysis of optical observations at mid-latitudes.

System III (1957.0) – The artificial Jupiter longitude measurement system in which the meridian at $108^{\circ}02$ is directed toward the Earth at 0^{h} Universal Time on 1 January 1957 and has **prograde** rotation with period of $9^{h}\ 55^{m}\ 29^{s}.37$. It is applied to the analysis of radio observations.

Trapped Radiation – Energetic charged particles whose trajectories in a planetary magnetic field are confined within certain boundaries. A particle travels nearly along the field lines, "mirrors" at equal north and south magnetic latitudes, and drifts in longitude.

Tropopause – The upper boundary of the **troposphere** and the lower boundary of the **stratosphere**, characterized by a near-discontinuity in the temperature gradient.

Troposphere – The atmospheric layer within which major weather phenomena occur, characterized by temperatures which decrease as altitude increases.

Ultra High Frequency (UHF) – Characteristic of electromagnetic radiation at those microwave frequencies between 300 and 3000 **megahertz (MHz)**; used here synonymously with **decimetric** to cover a broader range extending perhaps to 30 000 **MHz**.

Vernal Equinox – The direction from the center of the Earth to the center of the Sun at the time when the latter lies in the plane of the Earth's equator in March of each year.

Viscosity (η) – The ratio of the tangential component (perpendicular to the velocity gradient) of the force per unit area to the velocity gradient in a moving fluid.

Zenith – The direction opposite to that of the local acceleration of gravity (including the centrifugal terms) and perpendicular to the local horizon.

Zenith Angle – The angle between the directions to the **zenith** and to an object observed.

LIST OF NASA SPACE VEHICLE DESIGN CRITERIA MONOGRAPHS

SP-8001	(Structures)	Buffeting During Atmospheric Ascent, Revised November 1970
SP-8002	(Structures)	Flight-Loads Measurements During Launch and Exit, December 1964
SP-8003	(Structures)	Flutter, Buzz, and Divergence, July 1964
SP-8004	(Structures)	Panel Flutter, July 1964
SP-8005	(Environment)	Solar Electromagnetic Radiation, Revised, May 1971
SP-8006	(Structures)	Local Steady Aerodynamic Loads During Launch and Exit, May 1965
SP-8007	(Structures)	Buckling of Thin-Walled Circular Cylinders, revised August 1968
SP-8008	(Structures)	Prelaunch Ground Wind Loads, November 1965
SP-8009	(Structures)	Propellant Slosh Loads, August 1968
SP-8010	(Environment)	Models of Mars Atmosphere (1967), May 1968
SP-8011	(Environment)	Models of Venus Atmosphere (1968), December 1968
SP-8012	(Structures)	Natural Vibration Modal Analyses, September 1968
SP-8013	(Environment)	Meteoroid Environment Model – 1969 (Near-Earth to Lunar Surface), March 1969
SP-8014	(Structures)	Entry Thermal Protection, August 1968
SP-8015	(Guidance and Control)	Guidance and Navigation for Entry Vehicles, November 1968
SP-8016	(Guidance and Control)	Effects of Structural Flexibility on Spacecraft Control Systems, April 1969
SP-8017	(Environment)	Magnetic Fields – Earth and Extraterrestrial, March 1969
SP-8018	(Guidance and Control)	Spacecraft Magnetic Torques, March 1969
SP-8019	(Structures)	Buckling of Thin-Walled Truncated Cones, September 1968
SP-8020	(Environment)	Mars Surface Models (1968), May 1969
SP-8021	(Environment)	Models of Earth's Atmosphere (120 to 1000 km), May 1969
SP-8022	(Structures)	Staging Loads, February 1969
SP-8023	(Environment)	Lunar Surface Models, May 1969

SP-8024	(Guidance and Control)	Spacecraft Gravitational Torques, May 1969
SP-8025	(Chemical Propulsion)	Solid Rocket Motor Metal Cases, April 1970
SP-8026	(Guidance and Control)	Spacecraft Star Trackers, July 1970
SP-8027	(Guidance and Control)	Spacecraft Radiation Torques, October 1969
SP-8028	(Guidance and Control)	Entry Vehicle Control, November 1969
SP-8029	(Structures)	Aerodynamic and Rocket-Exhaust Heating During Launch and Ascent, May 1969
SP-8030	(Structures)	Transient Loads From Thrust Excitation, February 1969
SP-8031	(Structures)	Slosh Suppression, May 1969
SP-8032	(Structures)	Buckling of Thin-Walled Doubly Curved Shells, August 1969
SP-8033	(Guidance and Control)	Spacecraft Earth Horizon Sensors, December 1969
SP-8034	(Guidance and Control)	Spacecraft Mass Expulsion Torques, December 1969
SP-8035	(Structures)	Wind Loads During Ascent, June 1970
SP-8036	(Guidance and Control)	Effects of Structural Flexibility on Launch Vehicle Control Systems, February 1970
SP-8037	(Environment)	Assessment and Control of Spacecraft Magnetic Fields, September 1970
SP-8038	(Environment)	Meteoroid Environment Model – 1970 (Interplanetary and Planetary), October 1970
SP-8040	(Structures)	Fracture Control of Metallic Pressure Vessels, May 1970
SP-8042	(Structures)	Meteoroid Damage Assessment, May 1970
SP-8043	(Structures)	Design-Development Testing, May 1970
SP-8044	(Structures)	Qualification Testing, May 1970
SP-8045	(Structures)	Acceptance Testing, April 1970
SP-8046	(Structures)	Landing Impact Attenuation For Non-Surface-Planing Landers, April 1970

SP-8047	(Guidance and Control)	Spacecraft Sun Sensors, June 1970
SP-8048	(Chemical Propulsion)	Liquid Rocket Engine Turbopump Bearings, March 1971
SP-8049	(Environment)	The Earth's Ionosphere, March 1971
SP-8050	(Structures)	Structural Vibration Prediction, June 1970
SP-8051	(Chemical Propulsion)	Solid Rocket Motor Igniters, March 1971
SP-8052	(Chemical Propulsion)	Liquid Rocket Engine Turbopump Inducers, May 1971
SP-8053	(Structures)	Nuclear and Space Radiation Effects on Materials, June 1970
SP-8054	(Structures)	Space Radiation Protection, June 1970
SP-8055	(Structures)	Prevention of Coupled Structure-Propulsion Instability (Pogo), October 1970
SP-8056	(Structures)	Flight Separation Mechanisms, October 1970
SP-8057	(Structures)	Structural Design Criteria Applicable to a Space Shuttle, January 1971
SP-8058	(Guidance and Control)	Spacecraft Aerodynamic Torques, January 1971
SP-8059	(Guidance and Control)	Spacecraft Attitude Control During Thrusting Maneuvers, February 1971
SP-8060	(Structures)	Compartment Venting, November 1970
SP-8061	(Structures)	Interaction With Umbilicals and Launch Stand, August 1970
SP-8062	(Structures)	Entry Gasdynamic Heating, January 1971
SP-8063	(Structures)	Lubrication, Friction, and Wear June 1971

SP-8065	(Guidance and Control)	Tubular Spacecraft Booms (Extendible, Reel Stored), February 1971
SP-8066	(Structures)	Deployable Aerodynamic Deceleration Systems, June 1971
SP-8067	(Environment)	Earth Albedo and Emitted Radiation, July 1971
SP-8068	(Structures)	Buckling Strength of Structural Plates, June 1971
SP-8070	(Guidance and Control)	Spaceborne Digital Computer Systems, March 1971
SP-8071	(Guidance and Control)	Passive Gravity-Gradient Libration Dampers, February 1971
SP-8072	(Structures)	Acoustic Loads Generated by the Propulsion System, June 1971
SP-8074	(Guidance and Control)	Spacecraft Solar Cell Arrays, May 1971

NASA-Langley, 1972